A mouse model for genetic deletion of presynaptic BDNF from adult hippocampal mossy fiber terminals

Mausmodell für genetische Deletion von präsynaptischem BDNF aus adulten hippokampalen Moosfaserterminalen

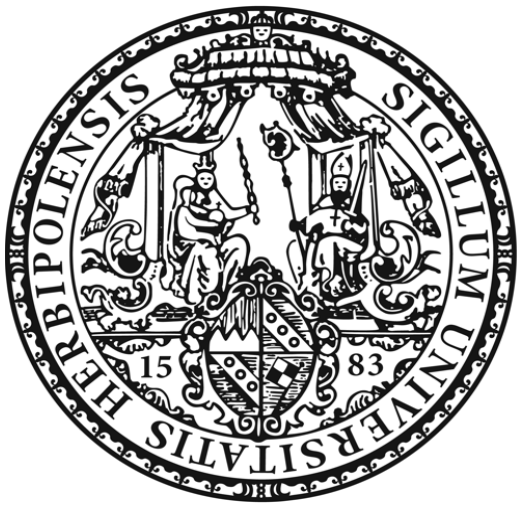

Doctoral thesis for a doctoral degree
at the Graduate School of Life Sciences,
Julius-Maximilians-Universität Würzburg,
Section Neuroscience
submitted by

Manju Sasi
from
Coimbatore, India

Würzburg, 2019

Submitted on:

……..……..

Members of the *Promotionskomitee*:

Chairperson: Prof. Dr. Thomas Dandekar

Primary Supervisor: PD Dr. Robert Blum

Supervisor (Second): Prof. Dr. Michael Sendtner

Supervisor (Third): Prof. Dr. Dieter Chichung Lie

Supervisor (Fourth): PD Dr. Angelika Schmitt

Date of Public Defence: ……..……

Date of Receipt of Certificates:……..

Affidavit

I hereby confirm that my thesis entitled " **A mouse model for genetic deletion of presynaptic BDNF from adult hippocampal mossy fiber terminals** " is the result of my own work. I did not receive any help or support from commercial consultants. All sources and / or materials applied are listed and specified in the thesis.

Furthermore, I confirm that this thesis has not yet been submitted as part of another examination process neither in identical nor in similar form.

Place, Date **Signature**

Eidesstattliche Erklärung

Hiermit erkläre ich an Eides statt, die Dissertation "**Mausmodell für genetische Deletion von präsynaptischem BDNF aus adulten hippokampalen Moosfaserterminalen**" eigenständig, d.h. insbesondere selbständig und ohne Hilfe eines kommerziellen Promotionsberaters, angefertigt und keine anderen als die von mir angegebenen Quellen und Hilfsmittel verwendet zu haben.

Ich erkläre außerdem, dass die Dissertation weder in gleicher noch in ähnlicher Form bereits in einem anderen Prüfungsverfahren vorgelegen hat.

Ort, Datum **Unterschrift**

TABLE OF CONTENTS

ABSTRACT

Brain-derived neurotrophic factor (BDNF) is a modulator and mediator of structural and functional plasticity at synapses in the central nervous system. Despite our profound knowledge about the synaptic function of BDNF at synapses, it is still controversially discussed whether synaptic BDNF acts primarily from pre- or postsynaptic sites.

In the central nervous system, several studies show that mossy fiber (MF) projections formed by hippocampal granule neurons store the highest amount of BDNF. However, immunofluorescence and RNA labelling studies suggest that MF BDNF is primarily produced by granule neurons. Multiple other studies prefer the view that BDNF is primarily produced by postsynaptic neurons such as CA3 pyramidal neurons.

Here, we question whether the BDNF, which is stored in the mossy fiber synapse, is primarily produced by granule neurons or whether by other cells in the MF-CA3 microcircuit. After standardization of immunolabelling of BDNF, confocal imaging confirmed the localization of BDNF in presynaptic MF terminals. This anterograde location of synaptic BDNF was also found in distinct regions of the fear and anxiety circuit, namely in the oval nucleus of the *bed nucleus stria terminals* (ovBNST) and in the central amygdala.

To find out whether the presynaptic BDNF location is due to protein translation in the corresponding presynaptic dentate gyrus (DG) granule neuron, we developed and characterized a mouse model that exhibits BDNF deletion specifically from adult DG granule neurons. In this mouse model, loss of presynaptic BDNF immunoreactivity correlated with the specific Cre-activity in granule neurons, thus confirming that MF BDNF is principally released by granule neurons. After BDNF deletion from granule neurons, we observed more immature neurons with widely arborized dendritic trees. This indicated that local BDNF deletion also affects the local adult neurogenesis, albeit Cre-mediated BDNF deletion only occur in adult granule neurons.

Since BDNF is a master regulator of structural synaptic plasticity, it was questioned whether it is possible to visualize presynaptic, synapse-specific, structural plasticity in mossy fiber synapses. It was established that a combination of Cre-techniques together with targeting of GFP to membranes with the help of palmitoylation / myristoylation anchors was able to distinctly outline the synaptic structure of the BDNF-containing MF synapse.

In summary, the mouse model characterized in here is suited to investigate the synaptic signalling function of presynaptic BDNF at the mossy fiber terminal, a model synapse to investigate microcircuit information processing from molecule to behaviour.

ZUSAMMENFASSUNG:

Der neurotrophe Wachstumsfaktor BDNF (brain-derived neurotrophic factor) ist ein Regulator und Vermittler von struktureller und funktionaler Plastizität in Synapsen des zentralen Nervensystems. Trotz des umfassenden Wissens über die synaptische Funktion von BDNF an Synapsen wird immer noch kontrovers diskutiert, ob synaptisches BDNF vorrangig von der prä- oder von der postsynaptischen Seite her agiert. Zahlreiche Studien zeigen, dass die größten BDNF Mengen des Zentralnervensystems in den Projektionen der hippocampalen Körnerzellen, den sogenannten Moosfasern (MF), enthalten sind. Während manche Studien basierend auf der Markierung von RNA und Immunofloureszenz nahelegen, dass MF BDNF in erster Linie von Körnerzellen produziert wird, bevorzugen zahlreiche andere Studien wiederum die Sicht, dass BDNF primär von postsynaptischen Neuronen wie beispielsweise den CA3 Pyramidenneuronen gebildet wird.

In dieser Arbeit wurde die Fragestellung untersucht, ob das BDNF, welches in den Moosfasersynapsen enthalten ist, in erster Linie von Körnerzellen hergestellt wird, oder ob es hauptsächlich von anderen Zellen aus dem MF-CA3 Mikronetzwerk gebildet wird. Nachdem eine Standardisierung der Immunfluoreszenzmarkierung von BDNF etabliert wurde, konnte anhand von konfokaler Bildgebung die Lokalisierung von BDNF in den präsynaptischen MF Terminalen bestätiget werden. Diese anterograde Lokalisierung synaptischen BDNFs konnte außerdem in zwei weiteren Regionen des Furcht- und Angstnetzwerkes, genauer gesagt im ovalen Kern des bed nucleus stria terminalis (ovBNST) und in der zentralen Amygdala, nachgewiesen werden.

Um Herauszufinden, ob die präsynaptische Lokalisation von BDNF von der Proteintranslation in den zugehörigen präsynaptischen Körnerzellen des Gyrus Dentatus abhängig ist, entwickelten und charakterisierten wir ein Mausmodel , welches die spezifische Deletion von BDNF aus den ausgereiften Körnerzellen des Gyrus Dentatus ermöglicht. In diesem Mausmodell korrelierte der Verlust präsynaptischer BDNF Immunreaktivität mit der spezifischen Cre-Aktivität in Körnerzellen, was bestätigt, dass MF BDNF hauptsächlich von den Körnerzellen ausgeschüttet wird.

Nach BDNF Deletion aus den Körnerzellen konnten mehr unreife Neurone mit sich weit verzweigenden, dendritischen Strukturen beobachtet werden. Dies weist darauf hin, dass die lokale Deletion von BDNF auch die lokale adulte Neurogenese beeinflusst, obwohl die Cre-vermittelte BDNF Deletion nur in adulten Körnerzellen stattfindet.

Da BDNF ein Hauptregulator von struktureller synaptischer Plastizität ist, kam die Frage auf, ob es möglich ist, diese präsynaptische, synapsenspezifische strukturelle Plastizität in Moosfasersynapsen zu visualisieren. Es wurde festgestellt, dass eine Kombination aus der Cre-Technik zusammen mit der gezielten Verankerung von GFP in der Zellmembran durch Palmitoylierungs-/Myristoylierungsmotive in der Lage ist, die synaptische Struktur von BDNF enthaltenden MF Synapsen darzustellen.

Zusammenfassend konnte gezeigt werden, dass das hier entwickelte und charakterisierte Mausmodell dafür geeignet ist, die synaptische Signalfunktion präsynaptischen BDNFs in der Moosfaserterminale, einer Modellsynapse für die Erforschung der Informationsverarbeitung in Mikronetzwerken vom Molekül bis hin zum Verhalten, zu untersuchen.

1 Introduction

Neurotrophins are a family of secreted proteins, fundamental for survival, differentiation, and growth. Nerve growth factor (NGF), brain-derived neurotrophic factor (BDNF), neurotrophin 3 (NT3), and NT-4) comprise of this highly conserved family of neuronal growth factors. Neurotrophins mediate their function in autocrine or paracrine mechanisms and were originally thought to act primarily as target-derived factors (Barde et al., 1982; Cohen et al., 1954; Lewin and Barde, 1996; Yan et al., 1997). However, at least one of the Neurotrophins, BDNF, was shown to regulate neurotransmitter release, synaptic plasticity and long-term potentiation, indicating that these factors can also act in fast communication between neurons (Blum and Konnerth, 2005; Cohen et al., 1954; Thoenen, 1995). In 1954, nerve growth factor was first discovered as a survival and growth factor for sensory neurons (Levi-Montalcini et al., 1954). Since then there has been tremendous work in the field of growth factors, to better understand their cellular and molecular mechanisms in neural development and in neurodegenerative and neurological disorders (Chao, 2003; Lee et al., 2001; Park and Poo, 2012).

1.1 Brain-derived neurotrophic factor

In 1982, in the group of Hans Thoenen in Munich, they reported a second neurotrophic factor purified from pig brain that supported the survival and fiber outgrowth of embryonic chick sensory neurons (Barde et al., 1982). It was later termed as brain-derived neurotrophic factor. Subsequent analysis by many laboratories showed independently that BDNF is directly involved in synaptic communication and that it may act as modulator or mediator of synaptic plasticity events such as long-term potentiation (Blum et al., 2002; Figurov et al., 1996; Kafitz et al., 2001; Korte et al., 1995; Kovalchuk et al., 2002; Lohof et al., 1993; Pang et al., 2004). BDNF is an activity-dependent modulator; the expression and secretion of the factor is regulated by neuronal activity and could be elicited by high frequency or theta-burst stimulation (TBS) (Gärtner and Staiger, 2002; Park and Poo, 2013).

BDNF mediates its activities by binding to its high affinity receptor, Tropomyosin kinase B (TrkB). *In vitro* and *in vivo* BDNF facilitates or is even essential for survival and differentiation of certain subsets of neurons (Barde, 1994; Barde, 2002; Barde et al., 1982; Sendtner et al., 1992). However, in contrast to earlier expectations, BDNF is not a major cell survival factor in the central nervous system (Rauskolb et al., 2010). BDNF exerts a significant role in synaptic modulation including amplifying synaptic transmission, LTP induction during learning and memory processing and synapse stability (Chen et al., 2018; Feng et al., 2017; Lang et al., 2007; Lohof et al., 1993; Wang et al., 2018).

The BDNF protein is the most abundant factor among the neurotrophic family and is highly expressed in the neocortex, hippocampus, amygdala and cerebellum (Altar et al., 1997; Conner et al., 1997). As most secretory proteins, BDNF carries a translocation signal peptide. BDNF is initially synthesized as a precursor protein. The prodomain is 129 amino acids long (aa), the mature, cleaved BDNF is 118 aa long. The uncleaved BDNF isoform is called pro-BDNF. BDNF transport includes the endoplasmic reticulum (ER), the Golgi network and is finally

transported into the secretory granules such as dense core vesicles (Lessmann and Brigadski, 2009). In the cellular trafficking pathway, proconvertases cleave the prodomain from the pro-BDNF at a conserved RVRR sequence to form a mature BDNF. The mature BDNF is a 27 kDa protein dimer (Lessmann and Brigadski, 2009) which can be stored in secretory dense core vesicles of neurons (Dieni et al., 2012).

The expression of BDNF is a complex and tightly regulated process and engages both epigenetic and transcriptional factors (Park and Poo, 2013). The *Bdnf* gene sequence in mammals, from rodents to humans is highly conserved and controlled by activity and cell specificity (Park and Poo, 2013). The *Bdnf* gene consists of eight 5' exons (I-VIII), each have their respective promoters and a 3' exon (IX) which encodes the BDNF protein. In humans, there are different protein start sites (5' Exon I, VII, VIII) yielding in several pre-proBDNF sequences with varied amino acids lengths at the amino terminal end (Pruunsild et al., 2007). The mRNA transcribed from the exon IX produces a shorter pre-proBDNF and the exon IX also has two poly-A site sequences to produce either a short or longer 3' untranslated region (Aid et al., 2007; Pruunsild et al., 2007). The expression of these different transcripts of BDNF are either tissue or brain region-specific. The expression of BDNF is also controlled by complex splicing mechanisms (Park and Poo, 2013). Hence, the transcriptional regulation of the BDNF gene is quite complex and is even differentially decoded between single neurons (Maynard et al., 2017).

Multiple experiments show that pro-forms of BDNF are functionally secreted and participate in relevant biological mechanisms (Bergami et al., 2008; Matsumoto et al., 2008; Yang et al., 2014). The secreted pro-BDNF is cleaved in the extracellular region to produce mature BDNF that's involved in late phase LTP in hippocampus (Pang et al., 2004). Pro-BDNF binds with high affinity to the p75 receptor and plays an opposing role to BDNF in synaptic plasticity including synaptic depression (Yang et al., 2014). The prodomain is also released in an activity-dependent manner and was shown to attenuate growth cone elongation (Anastasia et al., 2013).

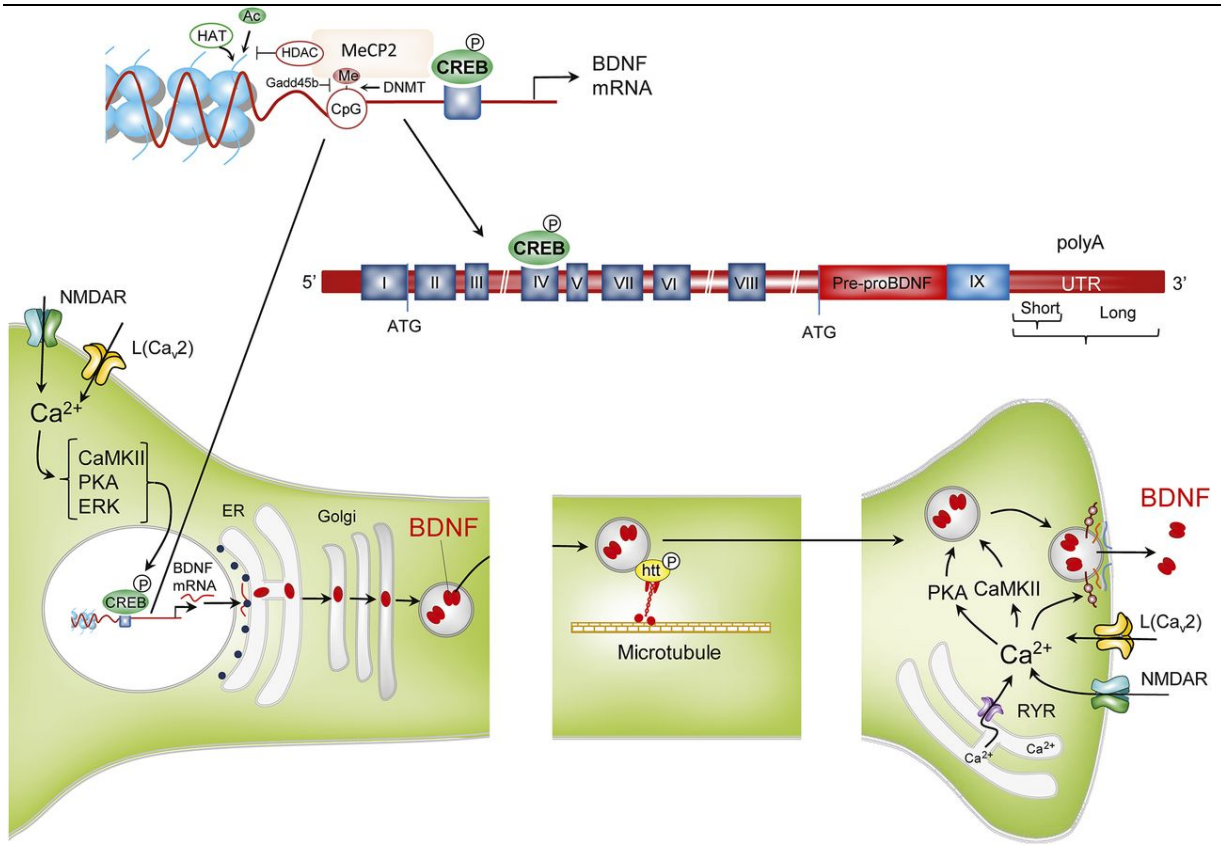

Figure 1 BDNF transcription, translation, transport and release.
The BDNF gene consists of multiple 5' non-coding exons and one 3' exon for encoding the BDNF protein. The synthesis of BDNF is highly regulated by transcriptional and epigenetic factors (CpG islands). The transcription of BDNF is either regulated by glutamate release or neuronal activity. The synthesis of pro-BDNF occurs during ER import, before the protein is transferred to the trans-Golgi. Here, the protein is converted to BDNF and sorted into dense core vesicles (DCVs). The secretion of BDNF occurs upon neuronal depolarization and can be regulated by cytoplasmic calcium ions (Benarroch, 2015).

1.2 BDNF secretion

The release of BDNF is a highly regulated signalling pathway (Blum and Konnerth, 2005; Park and Poo, 2013). As mentioned above, the protein is sorted into a secretory pathway and packaged into dense core vesicles. Secretion occurs in response to neuronal activity. The sorting of the freshly synthesized BDNF is a precise mechanism that involves the binding of carboxypeptidase to the BDNF prodomain which in turn interacts with sortilin, a VSP10 domain protein (Chen et al., 2005). The activity-dependent vesicular release of BDNF at the pre-synapse is mediated by synaptotagmin-IV and SNAREs, Syb2, SNAP25 and SNAP47 (Shimojo et al., 2015).

There is an ongoing and passionate discussion of whether BDNF acts primarily as an anterograde or a retrograde plasticity mediator . BDNF protein is considered to be transported anterogradely in the brain (Altar et al., 1997; Dieni et al., 2012). In the peripheral nervous system, BDNF, as well as the homolog NGF, is thought to be a retrograde factor, meaning the direction of action comes from the target and acts retrogradely to the effector neuron (Conner

et al., 1997). However, there are still no conclusive experiments in the literature regarding the localization of BDNF. Some studies suggest pre-synaptic synthesis and release while others suggest post-synaptic synthesis and release of BDNF. In addition, TrkB, the BDNF receptor, is expressed in both pre- and postsynaptic sites and this then further adds to the discrepancies.

1.2.1 Tropomyosin receptor kinase B

TrkB belongs to the family of receptor tyrosine kinases and is the receptor for BDNF (Sasi et al., 2017). Upon BDNF binding, TrkB activates downstream pathways that are involved in neuronal survival, differentiation and synaptic plasticity (Barde, 1994; Blum and Konnerth, 2005; Park and Poo, 2012; Patapoutian and Reichardt, 2001; Sasi et al., 2017; Sendtner et al., 1992). There are two forms of the TrkB receptors: the full length TrkB and the truncated TrkBs, TrkB-T1 and TrkB-T2 (Middlemas et al., 1991). The plasticity effects of neurons are mainly believed to be facilitated by TrkB-kinase (full length), whereas the TrkB-T1 is preferentially located in astrocytes (Rose et al., 2003). There is no evidence yet for a functional TrkB-T2 protein in the brain. The TrkB kinase receptors dimerize upon BDNF binding and in turn activate intrinsic kinase functions. This kinase activity instigates autophosporylation of the tyrosine receptor and forms specific phosphorylation-dependent binding sites for the intracellular target proteins (Sasi et al., 2017). This activates three main cascades (Fig. 2):

1) Via the Shc-adapter site, Ras activation links TrkB to the MEK/ERK pathway to facilitate functions such as synaptic transmission and synaptic protein translation.

2) PI_3K activation in the Akt pathway can regulate apoptosis to support neuronal survival.

3) PLCγ activation signals to PKC and IP_3 thereby initiating calcium release from intracellular calcium stores (Chao, 2003; Huang and Reichardt, 2003; Patapoutian and Reichardt, 2001).

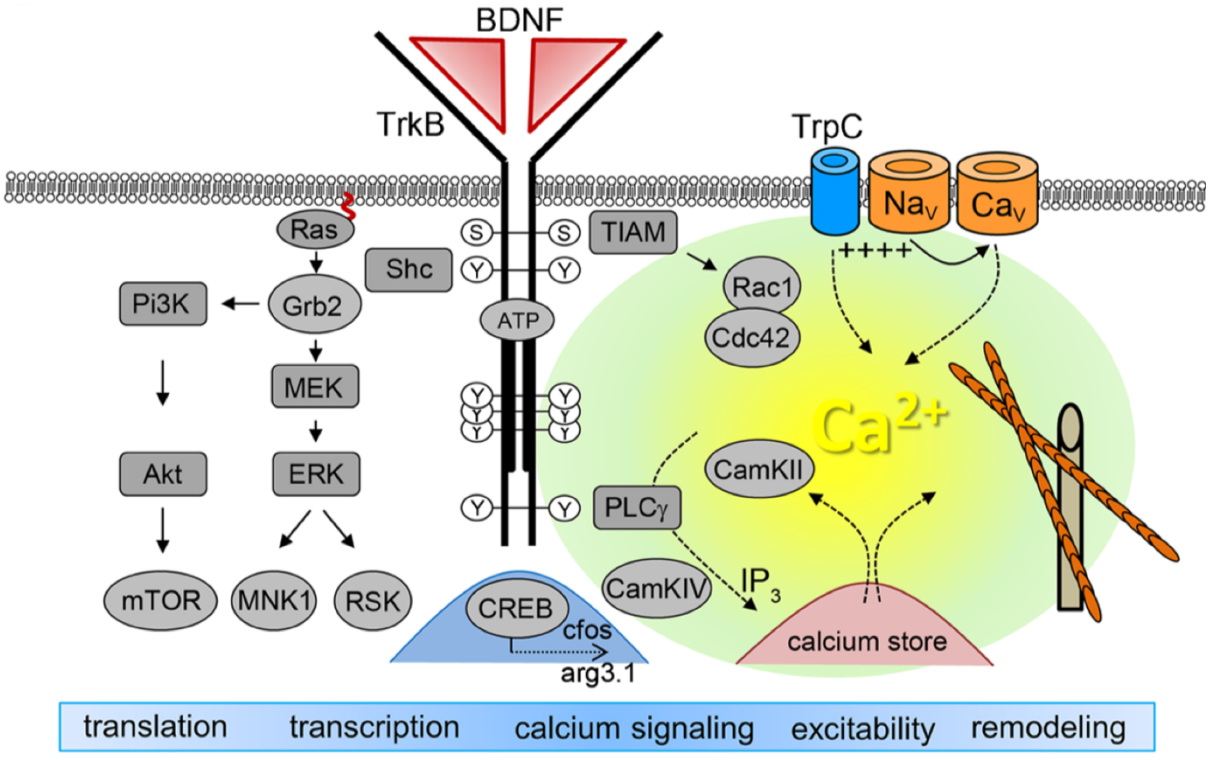

Figure 2 BDNF/TrkB signalling.

BDNF binds with high affinity to its receptor TrkB.TrkB activation leads to dimerization and autophosphorylation of TrkB which initiates three main intercellular downstream pathways. 1) Ras-MEK/ERK pathway that leads to translation of synaptic proteins by downregulating FMPR1, a translation inhibitor. 2) PI_3K/Akt pathway that negatively influences apoptosis and thereby promotes survival and maintenance of neurons. 3) The PLCγ / PKC / IP_3 pathway links BDNF to fast intracellular calcium release and subsequent regulation of ion fluxes over the plasma membrane. BDNF/TrkB signalling elicits dendritic spine plasticity via the TIAM-Rac1 pathway (Sasi et al., 2017). Abbreviations: Akt (protein kinase B), arg3.1 activity-regulated gene 3.1 protein homolog(Arc), CamK Ca2+/calmodulindependentprotein kinase, CaV voltage-gated calcium channel, Cdc42GTPase cell division control protein 42, cfos transcription factor cFos, CREB transcription factor cAMP response element-binding protein, ERK extracellular signal regulated kinase, Grb 2 growth factor receptor bound protein 2, IP3 inositol 1,4,5-trisphosphate, MEK mitogen-activated proteinkinase kinase, MNK mitogen-activated protein kinase-interacting kinase, mTOR mechanistic target of rapamycin, NaV voltage-gated sodium channel, Pi3K phosphatidyl inositol3-kinase, PLC phospholipase C, Rac GTPase RasrelatedC3 botulinum toxin substrate, Ras GTPase rat sarcoma, RSK ribosomal S6 kinase, Shc Src homologous and collagen-like protein, TIAM T celllymphoma invasion and metastasis-inducing protein, TrpC canonical transient receptor potential channel, Zn2+ zinc ions.

1.3 Postsynaptic BDNF secretion

BDNF levels are low in neuronal cultures, thus overexpression of recombinant BDNF became the method of choice to support localization analyses for BDNF (Adachi et al., 2005; Brigadski et al., 2005; Canossa et al., 2001; Chen et al., 2004; Cheng et al., 2011b; Dean et al., 2009; Gärtner and Staiger, 2002; Hartmann et al., 2001; Kohara et al., 2001; Matsuda et al., 2009; Petoukhov et al., 2013; Santi et al., 2006; Shimojo et al., 2015). Data obtained with GFP-tagged versions of BDNF suggested that postsynaptic secretory granules are a preferential site of BDNF release (Brigadski et al., 2005; Hartmann et al., 2001; Lessmann and Brigadski, 2009). An increase in BDNF expression upon activity has been shown by *in situ* hybridization techniques. In some of the studies BDNF mRNA was found in neuronal dendrites close to the cell body of cultured neurons as well as in brain sections (Tongiorgi, 2008; Tongiorgi et al., 1997). The *Bdnf* gene encodes a number of different transcript isoforms (see section 1.1), however all transcripts encode an identical functional BDNF protein. However, the different transcripts seem to differentially localize in neurons. Some transcripts are preferentially found in the cell body and in proximal dendrites (Exon I and IV) while other transcripts are enriched in distal dendrites (Exon II and VI) (Maynard et al., 2017). Specific deletion or silencing of each of these exons have an impact on dendrite morphology (Chiaruttini et al., 2008; Wang et al., 2015). Additionally, the BDNF transcripts with the long and short 3'UTR also show distinct localization in cell body and dendrites and local protein translation from different transcript isoforms seem to play a role in local regulation of spine morphology and synaptic plasticity, at least in hippocampal CA1 neurons (An et al., 2008). In a study exploiting FRET (fluorescence resonance energy transfer) combined with 2-photon fluorescence live imaging, local glutamate uncaging could induce postsynaptic BDNF release from single dendritic spine. This locally

released, postsynaptic BDNF could stimulate structural plasticity in an autocrine action onto the postsynaptic compartment (Harward et al., 2016; Hedrick et al., 2016).

However, electron microscopy combined with immunodetection of BDNF was not able to find immunoreactivity of BDNF in postsynaptic structures such as dendrites of spines (Dieni et al., 2012). Therefore, it was speculated whether immunolabelling is a suitable method to ultimately detect low amounts of BDNF in postsynaptic spines (Edelmann et al., 2015; Edelmann et al., 2014).

1.4 Presynaptic storage of BDNF

Immunohistochemical studies support the view that BDNF is synthetized preferentially in the cell body and is then anterogradely delivered to the presynaptic compartment (Altar et al., 1997; Conner et al., 1997; Dieni et al., 2012; Sasi et al., 2017). In vivo, presynaptic storage of BDNF was shown with the help of electron microscopy techniques followed by a quantitative analysis of anti-BDNF immunoreactivity (Dieni et al., 2012). Super-resolution microscopy localized endogenous, but not overexpressed BDNF to presynaptic glutamatergic synapses of mature cultured hippocampal neurons (Andreska et al., 2014). In this study, at a resolution of about 20 nm, it was shown that up to 90% of the synaptic immunoreactivity can be found within single glutamatergic presynapses (Andreska et al., 2014; Sasi et al., 2017).

Synaptic release of BDNF occurs either in an activity-dependent manner or after intracellular calcium release or can be stimulated by BDNF itself (Canossa et al., 2001; Gärtner and Staiger, 2002). Presynaptic localization of BDNF is in accordance with regulated BDNF release triggered by the activity of high-voltage activated presynaptic calcium channels (Balkowiec and Katz, 2002).

Due to a lack of synapse-specific BDNF-deficient mouse models, it is still not clear where BDNF primarily localizes. However, multiple lines of evidence point to the hippocampus as a model structure suited to find out whether presynaptic BDNF localization is due to BDNF synthesis in the same cell or whether it reflects presynaptic uptake from other structures. For instance, it is well verified that partial or complete deletion of BDNF causes deficits in LTP at hippocampal CA1 synapses. Furthermore, treatment with recombinant BDNF is able to rescue genetic BDNF deficiency in LTP measurements and is also able to increase basal synaptic transmission (Korte et al., 1995; Patterson et al., 1996). In the hippocampus, BDNF immunoreactivity is preferentially found in the mossy fiber terminal (Conner et al., 1997; Dieni et al., 2012; Sasi et al., 2017; Will et al., 2013).This indicates that investigating BDNF abundance in the mossy fiber of dentate gyrus granule neurons and mossy fiber terminals may be suited to investigate the origin and function of presynaptic BDNF.

1.5 Hippocampal BDNF

1.5.1 Hippocampus

The hippocampus is a part of the limbic system and is located in the medial temporal lobe. The dorsal hippocampus is responsible for processing of spatial information, while the ventral part is critical for processing of fear and anxiety memory (Bannerman et al., 2004; Kjelstrup et al.,

2002; Sahay and Hen, 2007). The anatomical structure of hippocampus consists of the infra-/supra-pyramidal blades of the dentate gyrus (DG) and a "C" structure called the Cornu Ammonis (CA1, CA2 and CA3). The CA region is primarily composed of the pyramidal cell layer and the DG is composed of the subgranular zone and the granule cell layer (Amaral et al., 2007).

The granule neurons of the DG project glutamatergic synapses to the hilus and as well with a diverse set of local inhibitory interneurons (Bischofberger et al., 2006b; Wiera and Mozrzymas, 2015). The hilus is the region formed between the supra- and infra- pyramidal blades of the dentate gyrus and consists of mossy cells. The granule neurons form prominent connections with the mossy fiber synapse (Bischofberger et al., 2006a). This synapse carries several large boutons of ~3–5-μm diameter which raise from a single mossy fiber axon. The mossy fiber bouton forms a presynaptic connection with the CA3 pyramidal neuron (Chicurel and Harris, 1992). They either form en passant boutons or they are attached to the main axon via a short perpendicular axonal branch (Bischofberger et al., 2006a; Galimberti et al., 2006; Gogolla et al., 2007). Here, the granule cells form bouton-like synapses with mossy neurons as well. The hippocampal sulcus or fissure is the region that separates the CA1 region and the dentate gyrus (Martin et al., 2017).

A trisynaptic glutamatergic circuit runs along the hippocampus. The first projection is the entorhinal cortex projection to the dendrites of the granule cells of the DG (perforant path). Second, the granule cells of the DG project to the pyramidal neurons of the CA3 through the mossy fiber. Third, the CA3 pyramidal neurons project to CA1 pyramidal neurons via the Schaffer collateral system. This circuit carries out all the crucial hippocampal functions such as spatial learning, episodic memory, and contextual elements of emotional processing. The long-term potentiation, long-term depression, synaptic transmission and plasticity of the cellular population of this circuit is extensively investigated (Bliss and Collingridge, 1993; Bliss and Lomo, 1973; Collingridge and Bliss, 1995; Ji and Maren, 2005; Morris et al., 1982; Nicoll and Malenka, 1995; Scoville and Milner, 1957; Teng and Squire, 1999).

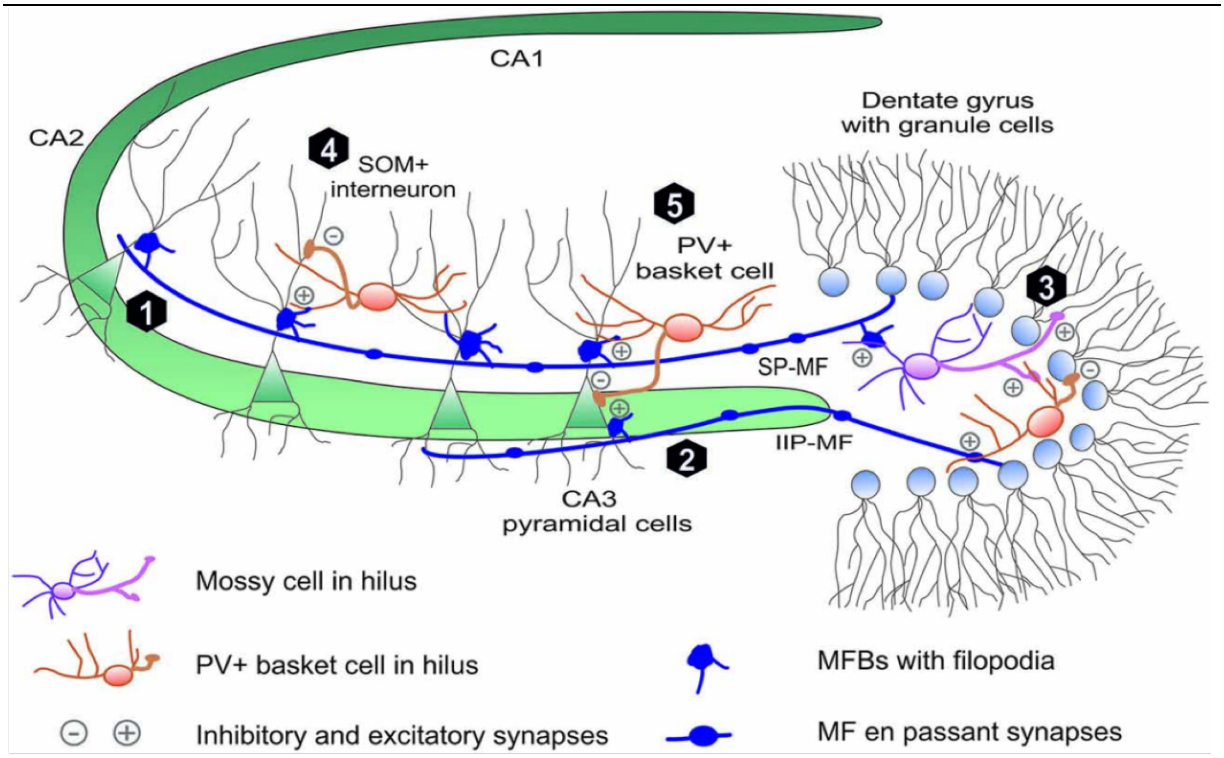

Figure 3 Hippocampal mossy fiber synapses.
The DG granule neurons (light blue) form glutamatergic synapses with the mossy cells (pink) in the hilus and a prominent excitatory synaptic connection with CA3 pyramidal neurons (green) via large mossy fiber boutons. They also project to the local parvalbumin+ and somatostatin+ interneuron population (orange) in the hilus via en passant boutons (Wiera and Mozrzymas, 2015).

1.5.2 BDNF at the mossy fiber terminal

The mossy fiber terminal forms a prominent synaptic connection with the thorny spines on CA3 pyramidal neurons. It also forms *en passant* boutons and filopodial connections with the local inhibitory neurons (Martin et al., 2017). The glutamatergic boutons carry a high amount of BDNF. In this microcircuit, there is an activity-dependent increase in the expression and release of BDNF that is suited to improve the synaptic plasticity of the DG granule neurons (Gooney et al., 2004; Kramar et al., 2012). The filopodial connection upon the interneurons are vital for memory precision as they control feedforward inhibition upon experience- and learning-dependent structural plasticity (Danzer and McNamara, 2004; Ruediger et al., 2011). Furthermore, voluntary exercise and enriched environment has also been shown to evoke increase of BDNF expression at this terminal. Increased BDNF levels correlate with improved learning behaviour in rodents (Fan et al., 2016; Jha et al., 2016). LTP at the mossy fiber terminal (MFT) is not dependent on NMDA receptor expression on the postsynaptic side, but seems to depend on increased presynaptic transmitter release (Nicoll and Schmitz, 2005). The mossy fiber terminal undergoes experience-dependent plasticity which is accompanied by an increase in local BDNF expression (Gomez-Palacio-Schjetnan and Escobar, 2008; Vaynman et al., 2004). Furthermore, there is pre-synaptic structural plasticity in the MFT upon high frequency stimulation (Schjetnan and Escobar, 2012). The terminal mossy fiber boutons also undergo

constant structural rearrangements, for instance by the addition of the new axonal connections from the adult born granule neurons and also by experience-dependent synaptic plasticity (Caroni et al., 2012; Galimberti et al., 2006; Toni et al., 2008). This all indicates that BDNF may contributes to local plasticity events in the MFT-CA3 microcircuit. The latter causes a tremendous increase in the size and number of these large mossy fiber boutons (Galimberti et al., 2006).

Albeit there is strong evidence for functional BDNF release from presynaptic sites, there is also genetic evidence that the BDNF comes originally from the postsynapse, not only in the mossy fiber microcircuit, but also in the CA3 region (Figurov et al., 1996; Harward et al., 2016; Hedrick et al., 2016; Winnubst and Lohmann, 2017).

1.6 Synaptic BDNF – instructor or mediator?

BDNF has emerged as key regulator of synaptic plasticity, a biological process describing the regulation of synaptic strength by neuronal activity. Many neuromodulatory factors affect neuronal plasticity, but in contrast to many molecules involved in synapse function, BDNF may serve as a real mediator rather than a modulator of synaptic plasticity (Park and Poo, 2013; Sasi et al., 2017) (Fig. 4a). Furthermore, BDNF and neurotransmitter signalling seem to act together in a close temporal context to show immediate and instructive functions on synaptic plasticity (Fig. 4b). Therefore, much attention has been given to BDNF because specific interference with BDNF-related signalling is regarded as a leading strategy to stimulate neuronal and synaptic plasticity for potential protective and functionally restorative treatments for neurological and psychiatric disorders (Autry and Monteggia, 2012; Martinowich et al., 2007; Sasi et al., 2017). As BDNF is highly abundant in mossy fiber terminals of the hippocampus, a leading model structure for fundamental research on how synaptic plasticity contributes to learning, memory and memory-associated diseases, specific deletion of BDNF from mossy fiber terminals might be suited to better understand how BDNF signalling contributes to synaptic plasticity.

BDNF acts as mediator both on pre- and post-synaptic sites in different manner (locally, autocrine and paracrine fashion) and it exerts fast and slow effects on these synapses. At the pre-synaptic end, the role of BDNF on LTP is dependent on glutamate and GABA release. These modifications induce LTP, increase in synaptic strength and increase in excitability that in turn aids in processing of learning and memory (Lisman et al., 2018). Whereas at the post-synaptic site, from reported studies, the BDNF modulates the glutamatergic receptors and there is also an increase in AMPA receptors that is directly correlated to LTP and decline in surface AMPA receptors to LTD (Aarse et al., 2016; Edelmann et al., 2015; Hedrick et al., 2016; Leal et al., 2017; Lu et al., 2014; Penn et al., 2017) (Kowianski et al., 2018). BDNF is functionally shown to be localized in pre- and post-synaptic manner yet there has not been a clear understanding of how BDNF is transported and localized within the neuronal system (Song et al., 2017). As well the balance in fast and slow signalling cascades exerted by BDNF is not clear and also the related factors involved in the BDNF downstream signalling. Taken together, there is a need to study the BDNF/TrkB signalling at a molecular level, more specifically at a synaptic level to get better insight on its fundamental mechanisms (Sasi et al., 2017).

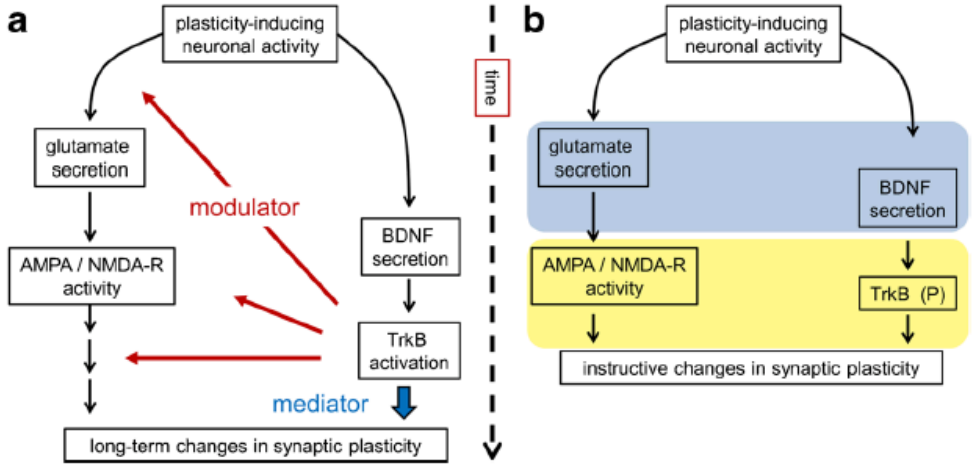

Figure 4 BDNF – a learning modulator.

The schematic depicts the BDNF signalling at the pre-and post-synaptic compartment. Principal glutamatergic neurons carry high amount of BDNF. BDNF release from these synapses regulates synaptic plasticity, learning and memory. A) At the pre-synapse, there is a simultaneous release of BDNF and glutamate. BDNF activates TrkB thereby initiating downstream signaling cascades at the post-synapse. B) BDNF also acts in an autocrine manner and induce neurotransmitter release at the pre-synapse. BDNF as well acts as an instructor upon release along with glutamate within a certain time point (blue window) and signals for associative post-synaptic LTP (yellow window) (Sasi et al., 2017).

1.7 Aim of the thesis

In this study, we thus focussed to investigating the localization and effect of BDNF at synaptic level. We developed mouse model, lenti-viral tracing systems and utilized high resolution microscopy to visualize effect of hippocampal BDNF at individual mossy fiber synapses. During the first part of the study, we optimized the BDNF immunoreactivity method to confirm the anterograde transportation of BDNF. Secondly, we characterized a new conditional BDNF knock-out mouse model (cBdnf ko) that carried out a Cre mediated deletion of the bdnf gene, on the base of the initially verified conditional bdnf mouse model (Rauskolb et al., 2010). We aimed to reduce BDNF levels exclusively at mossy fiber synapses of the hippocampal circuit, enabled by this Cre model, which was under the control of the intrinsic Ciliary Neurotrophic Factor promoter (heterozygous CNTF knockin, termed CNTF::Cre). The effect of cBdnf ko on functionality of the hippocampus on a cellular and network level in this synapse-specific deletion of BDNF was investigated. Finally, due to the structural complexity of the DG-CA3 network, structural tracing systems were developed to study the change in the number and volume of large mossy fiber boutons, filopodial connections and as well dendritic spines of granule neurons upon BDNF deletion.

2 Materials & Methods

2.1 Materials:

2.1.1 Chemicals

Product	Company	Catalogue Nr.
Agar	Merck	101615
Agarose	Biozym	840004
B27 Supplement 50X	Gibco/Life technologies	17504044
Bovine Serum Albumin – fatty acid free, low endotoxin (BSA)	Merck	A8806-5G
Bromophenol blue	Sigma-Aldrich	B8026
Cetrimide	Sigma-Aldrich	1102974
Chloroform	Sigma-Aldrich	32211
DAPI (4',6-diamidino-2-phenylindol)	Sigma-Aldrich	D9542
Di-potassium hydrogen phosphate	Sigma-Aldrich	P9666
Di-sodium hydrogen phosphate	Merck	106580
DMEM, high glucose, GlutaMAX™ Supplement, pyruvate	Thermofisher	31966
Dulbecco's PBS	Gibco/Life technologies	14040133
EDTA (Ethylenediaminetetraacetic acid)	Sigma-Aldrich	E-6511
Ethanol	Sigma-Aldrich	32205
Ethyleneglycol	Merck	100949
Glucose	Merck	108342
GlutaMax	Gibco/Life technologies	35050061
Glycerol	Merck	104093
Hank's Balanced Salt Solution (HBSS)	Gibco/Life technologies	14170-088
Heparin-sodium 25000	Ratiopharm	
HEPES	Roth	6763.2
Isopropanol	Sigma-Aldrich	33539
Lipofectamine 2000	Thermofisher Scientific	11668019
Magnesium chloride	Merck	5833.1
Magnesium sulphate	Merck	105886
Methyl butane	Sigma-Aldrich	M32631
Neurobasal medium	Gibco/ThermoFisherScientific	21103049
Opti-MEM	Gibco/ThermoFisherScientific	31985047
Paraformaldehyde	Merck	104005
Poly-L-lysine hydrobromide	Sigma-Aldrich	P2636-100MG

Potassium chloride	Sigma-Aldrich	P-5405
Potassium dihydrogen phosphate	Merck	104873
SDS (sodium dodecyl sulphate)	PanReac Applichem	A2572,1000
Sodium chloride	Sigma-Aldrich	31434
Sodium dihydrogen phosphate	Merck	106342
Sodium hydroxide	Sigma-Aldrich	30620
Sodium pyruvate	Sigma-Aldrich	P2256
Sucrose	Merck	107687
Tris Base	PanReac Applichem	A2264.1000
Tris HCl	PanReac Applichem	A3452.1000
Triton X100	Carl Roth	3051.2
Trypsin inhibitor	Gibco/Life technologies	R007100
Tryptone	Merck	110859
Tween 20	PanReac Applichem	A7932,0500
Xylene cyanol	Fulka	95600
Yeast extract	Merck	103753

2.1.2 Antibiotics, cells and other substances

Product	**Company**	**Catalogue Nr.**
5× Taq enhancer	5-Prime	2201250
Ampicillin	Carl Roth	K029.1
Aquapolymount	Polyscienes Inc.	18606
dNTP set	Fermentas	R0182(1ml)
E.coli competent cells	Self-made from TOP10 competent cells (Life technologies)	C3019H
E.coli stable competent cells	Self-made from NEB Stable competent *E. coli* (high efficiency)	C3040H
GelStar GEL STAIN	Lonza	50535
Horse serum	Linaris	SHD3250KYA
Midori green	Nippon Genetics	MG04
O.C.T compound tissue tek	Sakura	4583
Penicillin-Streptomycin (5,000 U/mL)	Gibco/Life technologies	15070-063
Sterile water	Ampuwa	10333412

2.1.3 DNA ladders

Product	**Company**	**Catalogue Nr.**
1 kb gene ladder	Fermentas	SM0311

1 kb -100 bp gene ladder	Fermentas	SM0242

2.1.4 Enzymes

Product	Company	Catalogue Nr.
*Bam*HI	NEB	R0136S
*Cla*I	NEB	R0197S
*Eco*RI	Fermentas	ER0271
*Eco*RV	Fermentas	ER0305
FastAP thermosensitive alkaline phosphatase	Thermo Scientific	EF0651
Lysozyme	Merck	L6876
*Nde*I	Fermentas	ER0581
*Nhe*I	NEB	R0131S
Pfu DNA polymerase	Self-made	
Proteinase K	PanReac Applichem	A3830
Rnase A	Applichem	A2760.0100
T4 DNA Polymerase	NEB	M0203S
T4 DNALigase	Thermofisher	EL0011
Taq DNA polymerase	5-Prime	2200020
Trypsin	Worthington	TRL3 3707
TrypLE™ Express enzyme (1×), phenol red	Gibco/Life technologies	12605-010
*Xba*I	NEB	R0145S
*Xho*I	NEB	R0146S
*Xho*I	Fermentas	ER0695

All enzymes were used with their appropriate buffers. The 10× *Pfu* reaction buffer for *Pfu* DNA polymerase was self-made.

2.1.5 Kits

Product	Company	Catalogue Nr.
EndoFree Plasmid Maxi Kit	QIAGEN	12362
Genopure Plasmid Midi Kit	Roche Life Sciences	3143414001
Monarch PCR & DNA Cleanup Kit	NEB	T1030S
NucleoBond Xtra Maxi	Macherey-Nagel	740414.50
QIA quick gel extraction kit	QIAGEN	28704
Quick Blunting™ Kit	NEB	E1201S

2.1.6 Antibodies

Primary Antibodies	Dilution	Company	Catalogue Nr.
Chicken anti-GFP	1/1000	Abcam	ab13970
Chicken anti-Neurofilament, Heavychain	1/400	Millipore	ab5539

Goat anti-TrkB	1/500	R&D Systems	AF1494
Guinea pig anti-vGLUT	1/400	Synaptic Systems	135304
Guinea pig anti-NeuN	1/400	Synaptic Systems	266004
Mouse anti (human)-BDNF	1/500	Icosagen	329-100
Mouse anti-BDNF (mAB9)	1/400-1/1000	Developmental studies hybridoma bank	BDNF-#9
Mouse anti-Cre	1/500	Covance	PRB-106P
Rabbit anti-Doublecortin	1/400	Cell Signalling Tech.	4604S
Rabbit anti-Parvalbumin	1/400	Swant	PV28
Rabbit anti-RFP	1/1000	Rockland	600-401-379
Rat anti-BrdU	1/100	Abcam	ab6326

Secondary Antibodies	**Concentration**	**Dye Label**	**Company**	**Catalogue Nr.**
Donkey anti-guinea pig IgG affiniPure	1/800 (0.44µg/µl)	Alexa 488	Jackson	706-545-148
Goat anti-chicken IgG (H+L)	1/800 (0.5µg/µl)	Alexa 488	Invitrogen	A11039
Donkey anti-chicken (IgG)	1/800 0.75mg/ml	Cy3-550	Jackson	703-165-155
Donkey anti-goat	1/800 (0.55µg/µl)	Cy3-550	Jackson	705-165-147
Donkey anti-guinea pig IgG (H+L)	1/800 (0.5µg/µl)	Cy3-550	Jackson	706-165-148
Donkey anti-rat IgG affiniPure (H+L)	1/800 (0.5µg/µl)	Cy3-550	Jackson	712-165-150
Donkey anti-mouse IgG affi-pure (H+L)	1/800 (0.222µg/µl)	DyL-550	Thermo Scientific	SA5-10167
Donkey anti-rabbit IgG affi-pure (H+L)	1/800 (0,5µg/µl)	Cy3-550	Jackson	711-165-152
Donkey anti-goat affiniPure	1/800 (0.5µg/µl)	Alexa647	Jackson	705-605-003
Donkey anti-guinea pig IgG (H+L) affiniPure	1/600 (0.44µg/µl)	Cy5-650	Jackson	706-175-148
Donkey anti-rabbit IgG affiniPure (H+L)	1/600 (0.44µg/µl)	DyL-649	Jackson	711-495-152
Goat anti-mouse IgG affiniPure (H+L)	1/800 (0.5µg/µl)	Cy5-650	Jackson	115-175-146

2.1.7 Plasmids

AG Blum Vector Database Nr.	Plasmid description
586	IRES NLS-Cre
725	FuVal-MyrGFP
726	pcDNA3MyrGFP
852	pLV-CAG (EcoRV)
882	pEX-k4-MyrTdTomato
893	pLV-CAG-MyrTdTomato
915	pLV-CAG-MyrTdTomato-MyrGFP
957	pLV-CAG-MyrGFP
971	pLV-CAG-MyrGFP-IRESCre
985	pLV-CAG-FLEx (flox-MyrTdTomato-MyrGFP-flox)

2.1.8 Primers

The primers used for PCR, genotyping and sequencing are given in the tables below. These primers were tested for the optimal annealing temperature by setting up gradient PCRs.

Table 1 DNA primers for sequencing

Name	for/rev	Sequence (5´-3´)
MyrGFP	for	CCTGGGCAACGTGCTGGTTATT
EGFP	for	TCCTGGTCGAGCTGGACGGCGACG
EGFP	rev	CACGAACTCCAGCAGGACCATG
pEGFPN1	for	GTCGTAACAACTCCGCCC
pEGFPN1	rev	GTCCAGCTCGACCAGGATG
WPREADD	rev	TGTTGCTCCTTTTACGCTATG

Table 2 DNA primers for genotyping

Mouse Line	Name	Sequence (5´-3´)	Annealing (°C)	Extension (s)	Product size (bp)
CNTF-Cre	Wt	TGATGGTTAAGAGT TGGGCTAGAAG	60	60	~ 250 (wt) ~ 500 (tg/tg)
	laksocreas	GCATAACCAGTGAA ACAGCATTGCTG			
	Cntfp1	GACTAGTGAAGACA GAAGCAAACCAG			
BDNF$^{fl/fl}$	309U21	CCCATAGCTTGTGT TGCGTAA	57	45	674 (wt), ~840 (floxed)
	962L21	ATTCAAGTCAGGAT CAATGCC			
CAG eGFP	AG-2	CTGCTAACCATGTT CATGCC	55	60	350
	CAT-2	GGTACATTGAGCAA CTGACTG			

Table 3 DNA primers for Cloning

Name	for/rev	Sequence (5´-3´)	Annealing (°C)	Extension (s)	Product size (bp)
MyrGFP	768	GAATTCTTAGCTAGC CTTGTACAGC	57	60	774
	6f	CGCACCATGGGCTGT GTCTGC			
Cre	F2	CAGAATTCACTAGTG GATCCGCCCCTCTC	58	120	~1600
	R	TAGAATTCCTAATCG CCATCTTCCAGAAG			

2.1.9 Buffers, solutions and media

	Composition/ Concentration
0.5M EDTA	380.2g in 1 litre dH_2O, pH 8.0
100mM Tris base	121.4g in 1 litre dH_2O, pH 8
100mM Tris HCl	157.6g in 1 litre dH_2O, pH 7.5
10× Phosphate buffer saline	80g NaCl, 2g KCl, 2g KH_2PO_4, 11.75g $Na_2HPO_4x2H_2O$ in 1 litre dH_2O
1M HEPES	23.8g in 100ml sterile dH20, pH7.3, sterile filter.
1M Phosphate buffer	13.61g KH_2PO_4, 17.42g K_2HPO_4 in 100ml dH_2O, pH 7.4
1M Sodium chloride	58.44g in 1 litre of dH_2O
20% Sucrose	20g Sucrose in 100ml 1X PBS
20% Triton X100	10ml Triton X100 in 40ml dH_2O. Stir for 30 min.
20% Tween 20	50ml Tween 20 in 250ml dH_2O. Stir for 5 min.
4% Paraformaldehyde	40g Paraformaldehyde in 500ml dH_2O with few drops of 5M NaOH, stir for 20-30 min at 60°C till paraformaldehyde dissolves. Pass it through a filter paper and add 410ml of Buffer A (0.2M $Na_2PO_4x2H_2O$ in dH_2O) and 90ml Buffer B (0.2M $NaH_2PO_4x2H_2O$ in dH_2O). pH 7.4
5% SDS	2.5g in 50ml dH_2O
50X TAE buffer	242g Tris base, 292g EDTA in 1 litre dH_2O, pH 8.0
5M Sodium hydroxide	99.99g in 500ml dH_2O
6X Gel loading dye	40% Glycerin, 0.02% Bromophenol blue, 0.06% Xylene-cyanol, 1X TAE in dH_2O
Ampicillin	518mg in 5ml dH_2O. Concentration - 100mg/ml
Blocking solution	0.3% Triton X100 (from 20% Triton X100 stock), 0.1% Tween 20 (from 20% Tween 20 stock), 10% Horse serum in 1X PBS
Cryoprotectant solution	30% Ethyleneglycol, 25% Glycerine, 0.4M Phosphate buffer in dH_2O
CTAB	5% CTAB in sterile dH20.
Dissociation medium	500ml HBSS, 1x Na-Pyruvate, 0.1% Glucose, 10mM HEPES (pH7.3)
HEK cell culture medium	450ml DMEM with GlutaMax, 10%FCS, 1% Pen/Strep
LB agar	LB medium + 15g/l Agar, autoclaved
LB medium	10g Yeast extract, 20g Trypton water, 20g NaCl in 2 litre dH_2O, pH 7.4, autoclaved

LB/Amp agar	1ml 50mg/ml Ampicillin in 1 litre autoclaved LB agar. Final concentration of ampicillin 1µg/ml.
LB/Amp medium	1ml 50mg/ml Ampicillin in 1 litre autoclaved LB medium. Final concentration of ampicillin 1µg/ml.
Lysis buffer	10mM Tris HCl (pH 7.5), 100mM EDTA (pH 8.0), 150mM NaCl, 0.5% SDS in dH_2O
Lysozyme	50mg/ml in sterile dH20
Maintenance medium	500ml Neurobasal, 1x B27, 1x Glutamax, 1x Pen/Strep
PBS/Heparin	0.4% Heparin in 1X PBS
SOC Medium	2g Tryptone, 0.5g Yeast extract, 58.44 mg NaCl, 18.5g KCl in 100ml dH_2O, pH 7.2 and autoclaved. Then filter sterilized 1ml 1M MgCl2, 1ml 1M $MgSO_4$, 2ml 1M Glucose were added.
STET	8% Sucrose, 0.15 Triton X-100, 50mM EDTA, 50mM Tris pH8.0
Tris EDTA (TE) buffer	10mM Tris (pH 8.0) and 1mM EDTA (pH 8.0) in dH_2O
Washing solution	0.1% Triton X100 (from 20% Triton X100 stock), 0.1% Tween 20 (from 20% Tween 20 stock) in 1X PBS

2.1.10 Equipment

Equipment	**Company**
All in one Fluorescence microscope BZ-8100	Keyence
Centrifuge-5424R	Eppendorf
FluoView FV1000 Confocal microscope	Olympus
Gel documentation system	peqlab Biotechnology
Cell culture CO_2 Incubator	Binder
Incubator shaker series	New Brunswick Scientific
Lauda Eco-line water bath	Lab Commerce
Nanodrop Spectrophotometer ND-1000	peqlab Biotechnology
PCR-Mastercycler	Eppendorf
PCR-Mastercycler Gradient	Eppendorf
Rocking platform -Duomax 1030	Heidolph
Thermomixer comfort	Eppendorf
Vibratome-VT1000S	Leica Microsystems
Zeiss ELYRA S1 SIM microscope	Carl Zeiss

2.1.11 Other materials

Product	Company
10 mm Deckgläser	Hartenstein
12-well/24-well plates – 128 × 86 mm	Thermo Scientific
Coulter counter container	
Cover glass – 24 × 40 mm, 24 × 50 mm	R. Langenbrick
Dow Cronning High vacuum grease (Z273554-1EA)	Sigma Aldrich
Gel comb – 20 well, 1.5mm thickness	peqlab Biotechnologie
Object slides – 70 × 26 mm	R. Langenbrick
Immersion oil IMMOIL-F30CC	Olympus
Roti coll 1, cyanoacrylate basis one component-instant glue	ROTH
T25 Filter Cap Flasks	Greiner Bio-one
Venofix Safety winged IV needle 25Gx3/4" (0.5 × 19 mm)	B Braun
Vibratome injector blades – single edges	Leica Microsystems

2.1.12 Software

ApE 3.0 (A plasmid editor)
BZ-II Analyzer 1.42 (Keyence)
Fluoview, version 4.1.a (Olympus).
ImageJ (WS Rasband, ImageJ, US NIH, Bethesda, Maryland, USA)
IMARIS x64 7.7.2 (BitPlane)
Photoshop CS5 (Adobe)
Prism 6 (GraphPad)
Rolera-XR camera (Qimaging)
StreamPix 4 software (Norpix)
Upright epifluorescence microscope (BXWI,Olympus)
ZEN Imaging software (Zeiss)

2.2 Methods

2.2.1 Animals

All experiments and study protocols were performed in accordance with the European Union guidelines and were approved by our institutional Animal Care and Utilization Committee and the Regierung von Unterfranken,Würzburg, Germany (licence numbers: 55.2-2531.01-95/13, 55.2.2-2532-2-558).

Mice were bred in the animal facility of the Institute of Clinical Neurobiology, University Hospital of Würzburg. Mice were housed in groups of 3 to 5 animals under standard laboratory conditions (12h/12h light/dark cycle, food and water *ad libitum*). All mice were healthy and pathogen-free, with no obvious behavioral phenotypes. Mice were quarterly tested according to the Harlan 51M profile (Harlan Laboratories, Netherlands). Yearly pathogen-screening was performed according to the Harlan 52M profile. Animals were randomly allocated to experimental groups.

For this study, we used the following transgenic mouse lines:

- C57BL/6J-BDNF$^{flox/Msd}$ (Rauskolb et al., 2010)
- C57BL/6 J -Tg(CNTF-Cre)TM^{Msd} (unpublished)
- C57BL/6 J -Tg(CAG-CAT-eGFP) reporter mice (Nakamura et al., 2006)
- Control – C57Bl/6J (Jackson, in-house breeding)

To characterize the expression of the Cre recombinase driven by the CNTF promoter, the line CNTF::Cre and CAG-CAT-EGFP were crossed to generate CNTF-Cre reporter mice.

The mouse lines *bdnf$^{fl/fl}$* and CNTF::Cre were crossed to produce conditional *Bdnf* knockout mice.

2.2.2 Cell Biology

2.2.2.1 Coating cover glass

Cover glass (10 mm, Marienfeld) was either placed in 4-wells or in 24-well plates. 100 µl of 0.1% PLL was added to each cover glass and incubated at 4°C overnight. The PLL was removed and the cover glasses were washed thrice with HBSS. In case of transfection or lentiviral transduction of HEK293 cells, the cells were added immediately upon HBSS removal. In case of primary hippocampal neurons, the HBSS was replaced with maintenance medium and equilibrated for few hours in a cell culture incubator (37°C, 5% CO_2).

2.2.2.2 Primary hippocampal neurons

Hippocampi from both hemispheres were prepared from five E19 C57Bl/6J mice or CD1 mice. The hippocampi were washed twice with dissection medium and 500 µl 2.5% trypsin was added and incubated at 37°C, 5% CO_2 for 20 min. 500 µl DNase was added to the trypsinated hippocampal cells and incubated at 37°C, 5% CO_2 for 5 min. The cells were washed twice with dissection medium. 500 µl trypsin-inhibitor (TI) was added to stop the trypsinization. The cells in dissection medium with TI were triturated with a 1ml pipette tip and were pelleted by centrifugation at 1400 × g for 3 min. The trituration step was repeated once more. The pelleted

cells were re-suspended in maintenance medium (with 1% serum) and were triturated with yellow pipette tip. Cells were counted using a Neubauer chamber and 20,000 cells per cover glass were plated on 0.1% PLL-coated cover glasses. The cells were flooded with maintenance medium (with 1% serum) to a final volume of 2 ml. Cells were cultured at 37°C, 5% CO_2. Half of the medium was exchanged on day in vitro (DIV) 5 and once more on DIV 10 with serum-free maintenance medium.

2.2.2.3 HEK293T cell culture

293T is the mutant line of the human embryonic kidney 293 cell line series that expresses the SV40 T-antigen. The cells were kindly provided by Prof. Dr. Uwe Maskos, Pasteur Institute, Paris. Confluent HEK cells were washed twice with HBSS medium and trypsinized with TrypLE Express, diluted 1/5 in 1× PBS. The trypsinization was stopped with DMEM cell culture medium*. The desired ratio of cells was seeded to fresh DMEM medium* in a new culture flask. In case of transfection, 200,000 cells were seeded on PLL-coated cover glasses. After attachment of the cells, the dishes were flooded with fresh cell culture medium. Cells were cultured at 37°C, 5% CO_2.

2.2.2.4 Transfection

HEK293T cells were plated approximately 8 hours before transfection. 2 µg of plasmid DNA was added to 200 µl OptiMEM in a 1.5 ml reaction tube and 4 µl Lipofectamine 2000 was added to 200 µl of OptiMEM in a separate 1.5 ml reaction tube: both were incubated at RT for 5 min. Then, both mixes were pooled together and incubated at RT for 30 min. The transfection mix was added dropwise to the HEK293T cells and incubated overnight. The cells were washed with fresh DMEM medium* and the expression of the plasmid DNA was tested by immunofluorescence labelling after 48 - 72 hours at 37°C, 5% CO_2. . DNA-free transfection mixtures served as negative controls.

2.2.2.5 Tittering of lentiviral particles by limiting dilution colony counting

The viral production was routinely performed by Hildegard Troll (viral facility, Institute of Clinical Neurobiology). Lentiviral particles were separated from the supernatant by ultracentrifugation and stored at -80°C in (mM) 50 Tris–HCl, pH 7.8, 130 NaCl, 10 KCl, 5 $MgCl_2$ in 10 µl aliquots. The number of transducing units in the viral pellet preparation was determined by tittering on HEK293T cells.

For this, 200,000 HEK293T cells / per well were seeded on PLL-coated cover glasses in a 24-well in a volume of 500 µl DMEM medium*. 1 µl of the viral suspension was mixed into the first well. 50 µl of the viral suspension in the first well was transferred to the consecutive well as shown in the scheme below. The expression of the virus was tested after cultivation at 37°C, 5% CO_2 for 72 hours by immunofluorescence labelling. The transducing units were determined after counting of label-positive colonies (or cells) and documented as transducing particles per µl ($TD_{Hek293T}$).

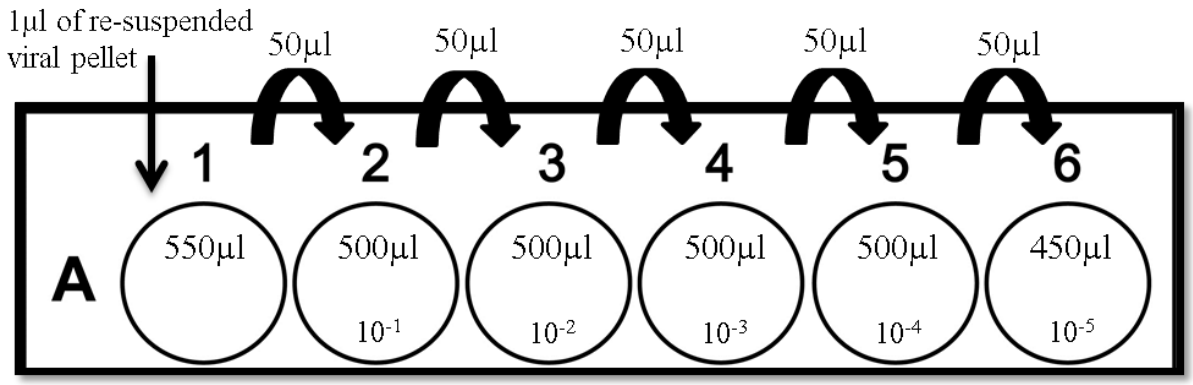

Figure 5 Pipetting scheme for limiting dilution colony counting. Lentiviral transduction

1 µl of the lentiviral volume containing 1.2 - 1.4 x 10^8 TU/ml was added to the culture medium of freshly seeded HEK293T cells or freshly settled hippocampal cells. Alternatively, hippocampal neurons were transduced at DIV 14. Here, a typical mixing strategy was used (3× cross, round cycles). The transduction was tested at DIV 3 for HEK cells and 5-7 days post-infection (dpi) for hippocampal cells.

	Transduction efficiency
pLV-CAG-MyrTdTomato-MyrGFP	1.4 x 10^8 TU/ml
pLV-CAG-MyrGFP-IRESCre	1.2 x 10^8 TU/ml

2.2.3 Molecular biology

2.2.3.1 Genotyping

Ear punches were used to prepare genomic DNA for mouse genotyping. 0.5 ml lysis buffer and 20 µl of proteinase K were added to the samples and incubated at 60°C overnight at 600 rpm in a thermomixer. 450 µl of 5% SDS and 150 µl of 3M NaCl were added and vortexed for 15 sec. 750 µl of chloroform was added and vortexed till the solution became whitish. The samples were centrifuged at 14,000rpm for 7 min, at 4°C and the upper phase was transferred to fresh 2 ml reaction tube. 700 µl of isopropanol was added, mixed by inversion and centrifuged at 14,000rpm for 5 min at 4°C and the supernatant was discarded. The pellet was washed with 70% ethanol and air dried for 10 min at RT. The pellet was dissolved in 100 µl of TE buffer and incubated at 65°C for 10 min in a thermomixer. The DNA samples were run on a 1% agarose gel to verify the presence of DNA. DNA samples were stored at -20°C. The DNA samples were used as template in PCR reactions. The PCR conditions are given above (Section **2.1.8**).

2.2.3.2 Cloning

The Cre-dependent and Cre-independent tracing vectors were prepared by blunt cloning. The myristoylated and palmitoylated TdTomato sequence was designed *in silico* and the sequence was synthesized by the company Eurofins. All the purified vectors and blunted inserts were ligated using T4 DNA ligase.

Table 4 Cloning Strategies

Expected Clone	Backbone	Preparation	Insert	Preparation	Verification
pLV-CAG-MyrTdTomato (893)	pLV-CAG (852)	• XhoI&EcoRI digestion • Gel separation • Blunting • Dephosphorylation	pEX-k4-MyrTdTomato (882)	• XhoI digestion • Gel separation • Blunting & Kinasing	• XbaI digestion • Sequencing (LGC Genomics)
pLV-CAG-MyrTdTomato-MyrGFP (915)	pLV-CAG-MyrTdTomato (893)	• EcoRV digestion • Dephosphorylation	pcDNA3MyrGFP (726)	• MyrGFP amplification • Gel separation • Blunting & Kinasing	• NdeI & EcoRI digestion • Sequencing (LGC Genomics)
pLV-CAG-MyrGFP (957)	pLV-CAG (852)	• EcoRV digestion • Dephosphorylation	pcDNA3MyrGFP (726)	• EcoRI&BamHI digestion • Gel separation • Blunting & Kinasing	• NdeI & NheI digestion • Sequencing (LGC Genomics)
pLV-CAG-MyrGFP-IRESCre (971)	pLV-CAG-MyrGFP (957)	• XhoI digestion • Blunting • Dephosphorylation	IRES NLS-Cre (586)	• IRES NLS-Cre amplification • Gel separation • Blunting & Kinasing	• ClaI & NheI digestion • Sequencing (LGC Genomics)
Expected Clone	**Backbone**	**Preparation**	**Insert**	**Preparation**	**Verification**

pLV-CAG-FLEx (985)	pLV-CAG (852)	• XhoI digestion • Dephosphorylation	pGH-FLEx (Eurofins)	• XhoI digestion • Gel separation	• XhoI and NheI digestion • LGC Genomics

2.2.3.3 Restriction digestion

Restriction reactions were set with 10× reaction buffer, restriction enzyme, and sample DNA. The reaction was gently mixed and was incubated at 37°C for 2 – 4 hours. The restriction digestion of the samples was verified by agarose gel electrophoresis.

2.2.3.4 Polymerase chain reaction (PCR)

Polymerase Chain Reaction is a technique employed for amplifying DNA fragments. It has three main steps, denaturation of the DNA double strand, annealing of the primers and the extension step where the new DNA strand is synthesized.

Table 5 PCR reaction mix

Components	*Volume (µl)*	*Concentration*
10× reaction buffer	5	1×
5× Taq enhancer	5	0.5×
dNTPs (2 mM of each)	5	0.2 mM of each
20pmol/µl Forward primer	0.5	0.2 pmol
20pmol/µl Reverse primer	0.5	0.2 pmol
5 U/µl *Taq* / *Pfu* DNA polymerase	0.4 / 0.5	0.04 U *Taq*
Sterile water	ad volume of 49µl	-

The mix was added to 1 µl of the template DNA and the mixture was set in a PCR mastercycler with corresponding PCR conditions. A representative PCR cycle is given below.

Table 6 Typical PCR cycle

PCR conditions	*Temperature (ºC)*	*Time*
Initial denaturation	94	5 min
Denaturation	94	30 s
Annealing	primer-specific	45 s
Extension	72	1 min per 1 kbp
Final extension	72	7 min
	15	∞

Primers used and their respective amplification conditions are given in Material section. The PCR product was analysed by agarose gel electrophoresis.

2.2.3.5 Gel purification of PCR product

For isolating specific DNA bands for DNA cloning, a single DNA band was excised from the agarose gel labelled with Gelstain (3 µl / 50 ml) on a blue light table to avoid damage to the DNA fragment. The gel portion with the DNA was weighed and the DNA was extracted using the QIA

quick Gel Extraction Kit. The DNA was eluted using 50µl elution buffer. The purified DNA fragment was quantified with Nanodrop Spectrophotometer ND-1000 and was stored at -20°C.

2.2.3.6 Blunting

Quick Blunting Kit was used to convert DNA with 5' and /or 3' incompatible overhangs to 5' phosphorylated, blunt-end fragments.

Table 7 Reaction mix

Components	*Volume (µl)*
10× blunting buffer	2.5
T4 DNA polymerase	1
1mM dNTPs	2.5
Purified DNA (up to 5 µg)	1-19
Sterile water	ad final volume of to 25

The reaction mix was incubated at 25°C for 30 min and the enzyme was inactivated by heating at 70°C for 10 min.

2.2.3.7 Kinasing

T4 Polynucleotide kinase reaction was used to phosphorylate 5'-ends of corresponding DNA-fragments.

Table 8 Reaction mix

Components	*Volume (µl)*
10× Ligase buffer (contains ATP)	5
PNK	2
Amplicon	43

The reaction mix was incubated at 37°C for 30 min and the enzyme was inactivated at 65°C for 20 min.

2.2.3.8 Dephosophorylation

To remove the 5'phosphate groups from the vector backbone, Fast Alkaline Phosphatase was used.

Table 9 Reaction mix

Components	*Volume (µl)*
10× Reaction buffer	6
FastAP	4
Digested vector backbone	50

The reaction mix was incubated at 37°C for 15 min and the enzyme was inactivated by heating at 75°C for 5 min.

2.2.3.9 Ligation

T4 DNA ligase catalyzes the formation of a phosphodiester bond between adjacent 5'-phosphate and 3'-hydroxyl chain ends in duplex DNA and RNA, respectively.

Table 10 Reaction mix

Components	*Volume (µl)*
10× Ligation buffer	1
T4 DNA Ligase	1
Blunted insert	x (100 - 300ng)
Purified vector	x (30 - 60ng)
Sterile water	ad final volume of 10

The reaction mix was incubated at 16°C overnight.

2.2.3.10 Transformation of chemical competent E. coli

5 µl of the ligation mix was mixed with 50 µl of competent cells and incubated on ice for 30 min. The cells were given heat-shock for 30 seconds at 42°C in a water bath and were immediately placed on ice. 250 µl of SOC medium was added and incubated at 37°C for one hour in the shaker series at 150 rpm at 37°C. The culture was pelleted and re-suspended in 50 µl SOC and was spread on a LB/Amp plate and incubated at 37°C overnight in an incubator.

2.2.3.11 Plasmid isolation

Colonies in the LB/Amp plate were inoculated in LB/Amp medium and incubated overnight at 37°C, at 250 rpm. Mini preparation of plasmid was done using 3 ml LB-culture. In brief, the 3 ml culture was pelleted and re-suspended in 400 µl STET. 5 µl of 50 mg/ml lysozyme was added and incubated at RT for 5 min. Samples were boiled at 99°C for a min and cooled down for 2 min. The samples were centrifuged at max. speed for 15 min and the debris was discarded with a toothpick. 8 µl of CTAB was added, mixed and centrifuged at full speed for 5 min. The supernatant was discarded and 200 µl of 1.2 M NaCl was added to the pellet. 700 µl of ice cold 100% ethanol was added to the re-suspended sample and incubated on ice for 10 min. Then the samples were centrifuged, and the resulting pellets were washed with 70% ethanol, air-dried and re-suspended in 50 µl 10 mM Tris (pH 8.0) along with RNaseA. The DNA samples were visually verified by running on a gel and stored at -20°C

Midi and maxi preparation of plasmid was done using Genopure Midi kit, Endofree Maxi kit and Nucleobond Xtra Maxi kit. The kit protocol was strictly followed, and the plasmid DNA was eluted with the respective elution buffer and stored at -20°C. The plasmid DNA isolated was quantified with Nanodrop Spectrophotometer ND-1000.

2.2.4 Histology

2.2.4.1 Tissue preparation for immunohistochemistry

Mice were sacrificed using carbon dioxide inhalation. For transcardial perfusion the animal was placed on a foil covered thermocool platform in a tray, the limbs were pinned down with needles and the ventral skin surface was sprayed with 70% ethanol. An incision along the chest was made

and the skin was removed to expose the ribcage. The sternum was carefully held, and the tissue below was cut to open up to the liver and diaphragm. The diaphragm was excised to expose the heart and lung. The ribcage was cut along the distal ends, lifted up and fixed back to reveal the heart and lungs. A perforation into the left ventricle was done using a winged infusion set and the right atrium was cut open. The animal was transcardially perfused with 0.4% heparin in 1× phosphate buffered saline (PBS) followed by 4% paraformaldehyde (PFA). The pump speed, volume of buffer, fixative and time were noted down. During perfusion, the liver lost its colour and became pale, and when perfused spasms along the thigh muscle, involuntary lifting up of tail was observed. Following perfusion, the skull was removed, and the brain was taken out. The brain was rinsed once with 1× PBS and post-fixed in 4% PFA. Brains of adult mice were post-fixed overnight ; brains of postnatal mice for up to 2 days. After post - fixation, the brain was transferred to 1× PBS and stored at 4°C until it was sectioned.

Table 11 Parameters recorded during transcardial perfusion of mouse

Parameters	**P-1 – P- 14**	**P-14 – P-21**	**P21- Adult**
PBS / heparin volume	5 ml	5 ml	5 ml
Duration of PBS / heparin perfusion	5 min	5 min	5 min
4% PFA volume	15 ml	15 ml	25 ml
Duration of PBS / heparin perfusion	10 min	10 min	10 - 12 min
Pump speed (arbitrary units)	12	15	20 - 25

2.2.4.2 Vibratome Sectioning

Coronal brain slices were obtained with Leica VT 1000S vibratome. For vibratome sectioning, the fixed brain was placed in a mold pre-filled with melted 6% agarose in 1× PBS. The brain was completely immersed with agarose. After the agarose was fully cured, the brain in the mold was fixed on a magnetic holder using super glue. The tank containing the magnetic holder was fixed and filled with 1× PBS. Coronal brain sections of 40µm were cut at moderate speed. The sections were either stored in 1× PBS at 4°C until labelling or were put in cryoprotectant solution for long-term storage.

2.2.4.3 Indirect immunofluorescence – free floating sections

Free floating brain sections were washed once with 1× PBS for 10 min. Sections were permeabilized and blocked by incubating in 500 µl blocking solution for 90 min at RT. Primary antibody incubation was performed overnight at 4°C with 400 µl blocking solution per 4 slices (100 µl / slice). Slices were washed thrice with washing solution, 10 min each and incubated for 1 hour with secondary antibody in 400µl blocking solution at RT. Sections were washed thrice, 10 min each and one time with 1× PBS for 5 min at RT. Finally, sections were stained with DAPI (2 mg / ml; 1/5000 in 1× PBS) for 5 min at RT and washed two times with 1× PBS for 5 min respectively. The sections were mounted on object slides, embedded with Aquapolymount and

covered with cover glass. All the incubation steps were performed on a rocking platform. The corresponding primary and secondary antibodies are listed in the Material section above.

2.2.4.4 Indirect immunofluorescence labelling of BrDU – free floating sections

Free floating brain sections were washed with 1× TBS once for 10 min. Sections were permeabilized and blocked by incubating in 500 µl blocking solution (1× TBS, 5% goat serum, 0.25% Triton X-100), 2% BSA) for 3 h at RT. Followed by incubation overnight at 4°C with the primary antibody in 400 µl blocking solution. Slices were washed thrice with washing solution (1× TBS, 0.1% Triton X-100, 0.1% Tween 20), 10 min each and incubated overnight at 4°C with secondary antibody in 400 µl blocking solution. Sections were washed thrice for 10 min with washing solution. The sections were post-fixed with 4% PFA (pH 7.4) for 15 min at RT and washed thrice with 1× TBS, 10 min each. Then, the section were treated with 2 N HCl for 15 min at 37°C and neutralized with 100 mM sodium borate buffer (pH 8.5). The sections were washed thrice with 1× TBS, 5 min each. Sections were again permeabilized and blocked by incubating in 500 µl blocking solution for 1 h at RT. Rat anti-BrdU antibody (1/100 dilution) in blocking solution was added and incubated overnight at 4°C. Slices were washed thrice with washing solution, 10 min each and incubated overnight at 4°C with secondary antibody in 400 µl blocking solution. Sections were washed thrice, 10 min each with washing solution. DAPI (2 mg/ml; 1/5000 in 1× TBS) staining was performed at RT for 15 min and washed twice with 1× TBS. The sections were embedded in Aquapolymount. All the incubation steps were performed on a rocking platform. Primary and secondary antibodies used are given in the Material section above.

2.2.4.5 Indirect immunofluorescence – cell culture

The cells were fixed with 4% PFA at 37°C for 15 min and washed twice with 1× PBS for 10 min each. Cells were permeabilized and incubated in blocking solution for 1 h at RT. The primary antibody in blocking solution was added and incubated at RT for 3 h. Cells were eight times washed with washing solution and secondary antibody labelling was performed at RT for 2 h. The cover glasses were washed again in washing solution (8×). Cells were washed once with 1× PBS and were subsequently stained with DAPI (2 mg / ml; 1/5000 in 1× PBS) for 5 min at RT. Finally, cells were washed twice with 1× PBS. The cover glass was dipped in sterile dH_20 once. The cover glasses were mounted on to object slides and were embedded with Aquapolymount. All the primary and secondary antibodies used are given in the Material section above.

2.2.4.6 Fluorescence Microscopy

2.2.4.6.1 Epifluorescence Microscopy

Overview images were taken with a Keyence BZ-8100 microscope and a Nikon PlanApo objective (2 ×, numerical aperture 0.10) with a colour camera. The microscope was equipped with standard filter sets for visualization of DAPI, GFP and TexasRed. Images of 1360 x 1024 pixels were stored in the .bmp file format and were subsequently analysed with Image J. For overview of whole brain sections, images were combined using the BZ-II analyser program (Keyence).

2.2.4.6.2 Confocal Microscopy

Immuno-labelled brain sections and cells were imaged with an inverted IX81 microscope equipped with an Olympus FV1000 confocal laser scanning system, a FVD10 SPD spectral detector and diode lasers of 405 nm, 473 nm, 559 nm, and 635 nm. The different objectives and their numerical apertures are listed below. For confocal scanning a pinhole setting representing one Airy disc was used. In case of high-resolution confocal microscopy, settings were chosen to meet an optimum resolution of at least 3 pixels per feature in x-y direction. In z-direction, 300 nm – 700 nm steps were used. 12-bit Z-stack images were processed by maximum intensity projection and were adjusted in brightness and contrast using Image J software. Final figure preparation was performed in Adobe Photoshop CS5. Images are shown as RGB images (8-bit per colour channel).

Table 12 FluoView FV1000 Confocal Microscope

Objectives	Numerical Apertures	Air/Oil
10× UPlan SAPO	0.4	Air
20× UPlan SAPO	0.75	Air
40× UPlanFLN	1.30	Oil
60× UPlanFLN	1.25	Oil

2.2.4.6.3 Structured Illumination Microscopy (SIM)

For structured illumination microscopy (SIM) analysis, cells and brain slices were labeled by indirect immunofluorescence using secondary antibodies labeled with Alexa Fluor 488. The microscopy samples were imaged with a SIM Zeiss ELYRA S.1 microscope system with a Plan-Apochromat 63 × /1.4 Oil Dic M27 objective in x–y–z stacks. Raw images (16 bit) were processed to reconstruct high-resolution information using the provided commercial software package (Zeiss). One-colour images were aligned using a transformation matrix and were later processed with ImageJ. Shown are maximum-intensity projections of eight to fifteen z-stacks of 100 nm distance.z-stacks.

2.2.4.7 Quantification and Image Processing

2.2.4.7.1 DCX counting / staging of new-born neurons

Coronal sections were selected according to stereotactic coordinates.. The hippocampus was defined according to (Franklin and Paxinos, 2008)

- Dorsal hippocampus, fig. 40 - 50. Bregma: -1.06mm - - 2.30mm
- Ventral hippocampus, fig. 55 - 58. Bregma: -2.92mm - - 3.28mm

40 µm sections of the dorsal and ventral hippocampus were made, with the chosen Bregma coordinates thus obtaining 30 dorsal and 9 ventral sections for every animal. Every 10^{th} section from the dorsal hippocampus and every 3rd section from the ventral area (3 sections per region per animal) were taken. The anti-Doublecortin labelling was performed according to standardized criteria. Confocal imaging was performed as described above at a resolution of

1024 × 1024 pixels per 635.9 µm² with an UPlan SAPO objective (20x, 0.75 NA). Z-stacks of 1 µm for 9 images were acquired and analysed for DCX-positive neuron staging. The images of the immuno-labelled coronal hippocampal sections were processed with ImageJ and the final RGB-tif files were used for the stereological quantification of cells. The quantification of cells was carried out manually using the 8-bit RGB image with ImageJ software. Pre-defined features of the cells to be counted and the cells that have to be unaccounted were devised. A uniform sized grid with a frame of 700 pixels^2 (~ 270 µm^2) was imposed on the sections and all the cells of pre-defined features were counted within the grid.

2.2.4.7.2 Dendritic measurement / branching

The immuno-labelled sections from the counting of DCX-positive immature neurons were used and were re-imaged by confocal microscopy with an Olympus UPlanFLN objective (40 ×, oil, 1.3 NA) objective and a resolution of 1024 × 1024 to cover 211,97 x 211,97 µm. Z-stacks were taken by scanning the entire volume of the 40 µm section. For every animal, twenty neurons were imaged. The raw image stacks were analyzed with the IMARIS x64 7.7.2 software and viewed as surpass in 3D. The autopath method of the filament tracer plugin in the IMARIS system was used to trace and reconstruct the dendritic tree of DCX neurons and to determine the primary & total dendritic length and the tertiary branching. DCX+ neurons were classified in three maturation stages (I early; II intermediate; III late) within the dorsal supra- and infrapyramidal blades of the hippocampus as described in (Deusser et al., 2015)

2.2.4.7.3 Counting of BrDU-positive cells in the dentate gyrus

2 sections from the dorsal hippocampus and 2 from ventral region were used. The anti-GFP and anti-BrDU labelling was performed according to the method explained. The quantification of BrDU cells was carried out manually using the 8-bit RGB image obtained from immuno-labelled sections. Using the plug-in in ImageJ software, all GFP+ cells and the BrdU+ cells along the dorsal supra- and infrapyramidal blades of the hippocampus were counted and as well screened for cells with co-labelling of GFP and RFP. The area of the molecular layer of the dentate gyrus was calculated along which the cells were counted.

2.2.4.7.4 Counting of Parvalbumin-positive neurons in the hippocampus

Every 10th section from the dorsal hippocampus and every 3rd section from the ventral area (3 sections per region per animal) were taken. The anti-parvalbumin labelling was performed according to standardized criteria. The quantification of cells with somata positive for anti-Parvalbumin was carried out manually using the 8-bit RGB image obtained from immuno-labelled sections. Using the plug-in in ImageJ software, the mossy fiber terminal and the MFT connection with CA3 region was lined out. All Parv+ somata within this enclosure of the hippocampus were counted.

2.2.4.7.5 Mossy fiber area measurement

Every 10th section from the dorsal hippocampus was stained for ZnT3. The ZnT3 labels the complete field with mossy fiber synapses. The ZnT3 label-positive area was marked in ImageJ software and the area positive for ZnT3 immunoreactivity was measured.

2.2.4.7.6 Statistical analysis

GraphPad Prism 6 software was employed to perform the statistical tests and to create the graphical representation of the data. Grubb's test was used to identify statistical outliers. All the values were considered to be normal distributed and were analyzed with parametric unpaired t-test. To compare, the DCX+ cells over age and genotype two-way ANOVA followed by Bonferroni's multiple comparison tests was performed. All the data in the figures are shown as mean ± SEM (standard error of the mean).

3 Results:

In this project attributed to the SFB-TRR58-A09/A10 our group focusses on hippocampal BDNF in contextual fear regulation. Here, BDNF is regarded as both an instructive molecule and a synaptic mediator that regulates synaptic plasticity under fear memory processing at the mossy fiber synapse (Sasi et al., 2017). BDNF is highly expressed in mossy fiber synapses (MF) of the DG granule neurons and it is thought to be crucial for regulating the hippocampal function by affecting the anterograde signalling to CA3 pyramidal neurons and local interneurons (Danzer and McNamara, 2004; Huang et al., 2008; Sasi et al., 2017). However, there is an ongoing controversial discussion about the directionality of BDNF signalling. While some studies prefer the view that hippocampal neurons synthesize BDNF and release it via their dendrites onto presynaptic terminals (Edelmann et al., 2014; Figurov et al., 1996; Harward et al., 2016; Park and Poo, 2013; Winnubst and Lohmann, 2017), other studies suggest an anterograde or autocrine action of BDNF to regulate local microcircuit function (Conner et al., 1997; Dieni et al., 2012; Sasi et al., 2017).

The focus of this study was to work out whether dentate granule neurons are the source of BDNF in the mossy fiber synapses. A second aim was to establish and verify a mouse model for anterograde BDNF action at the mossy fiber synapse. As local, synapse-specific deletion of BDNF might affect the overall functionality of the hippocampus it was also aimed to investigate whether local, mossy-fiber specific deletion of BDNF also affects the biological integrity of the neural circuit. As the neuroanatomical situation in the dentate gyrus circuit is highly complex, methodological strategies for local structure tracing were established in order to find out whether mossy fiber-specific deletion of BDNF has consequences on typical morphological attributes in the circuit.

As a first step in analysing local BDNF function in the DG-CA3 microcircuit, it was essential to find out the natural localization of steady-state BDNF in the hippocampus.

3.1 Standardization of BDNF immunofluorescent labelling (IF)

Early studies already showed BDNF protein localization in the mossy fiber band of the hippocampus (Conner et al., 1997; Yang et al., 2009). However, these studies were not controlled by BDNF KO models and therefore it was not fully clear whether the observed BDNF localization data were ultimately true, or not. Furthermore, the antibody used in the corresponding study was no longer available to the research community. A recent study confirmed that BDNF immunoreactivity (IR) in the mossy fiber was lost when BDNF was specifically deleted from neurons (Dieni et al., 2012), however, the study could not exclude the possibility that steady-state anti-BDNF-IR is a function of retrograde uptake of BDNF into MF synapses. In this study, the antibody anti-BDNF mab#9 was used (Kolbeck et al., 1999). As this antibody is available as a hybridoma cell culture (http://dshb.biology.uiowa.edu/BDNF-9_2) and

was also tested to be BDNF specific in our own studies (Andreska et al., 2014), I initially focused on this antibody for BDNF localization in the hippocampal circuit.

As BDNF is a highly basic dimeric protein of 27 kDa (Barde et al., 1982; Kolbeck et al., 1999; Leibrock et al., 1989), I first tested anti-BDNF immunoreactivity under different pH-conditions. As BDNF carries a high isoelectric point (pI - ~ 11-12), it could be that the accessibility of antigenic epitopes of the protein is different at different pH conditions (Hempstead, 2015). The following perfusion conditions were tested and adapted for successfully localizing BDNF (Fig. 6).

Conc. of PFA	**PFA's pH**	**Post-fixation**	**Results / Comments**
4%	pH 7	O/N	No anti-BDNF IR
2%	pH 6	No post-fixation was performed	Fragile tissue, brain could not be sectioned
2%	pH 6	2 hours	BDNF labelling very fragile vibratome sections
2%	pH 6	2 hours + *sections underwent quenching with 0.1% glycine*	BDNF labelling fragile vibratome sections
4%	pH 6	2 hours + *sections underwent Quenching with 0.1% glycine*	BDNF labelling better stability of vibratome sections

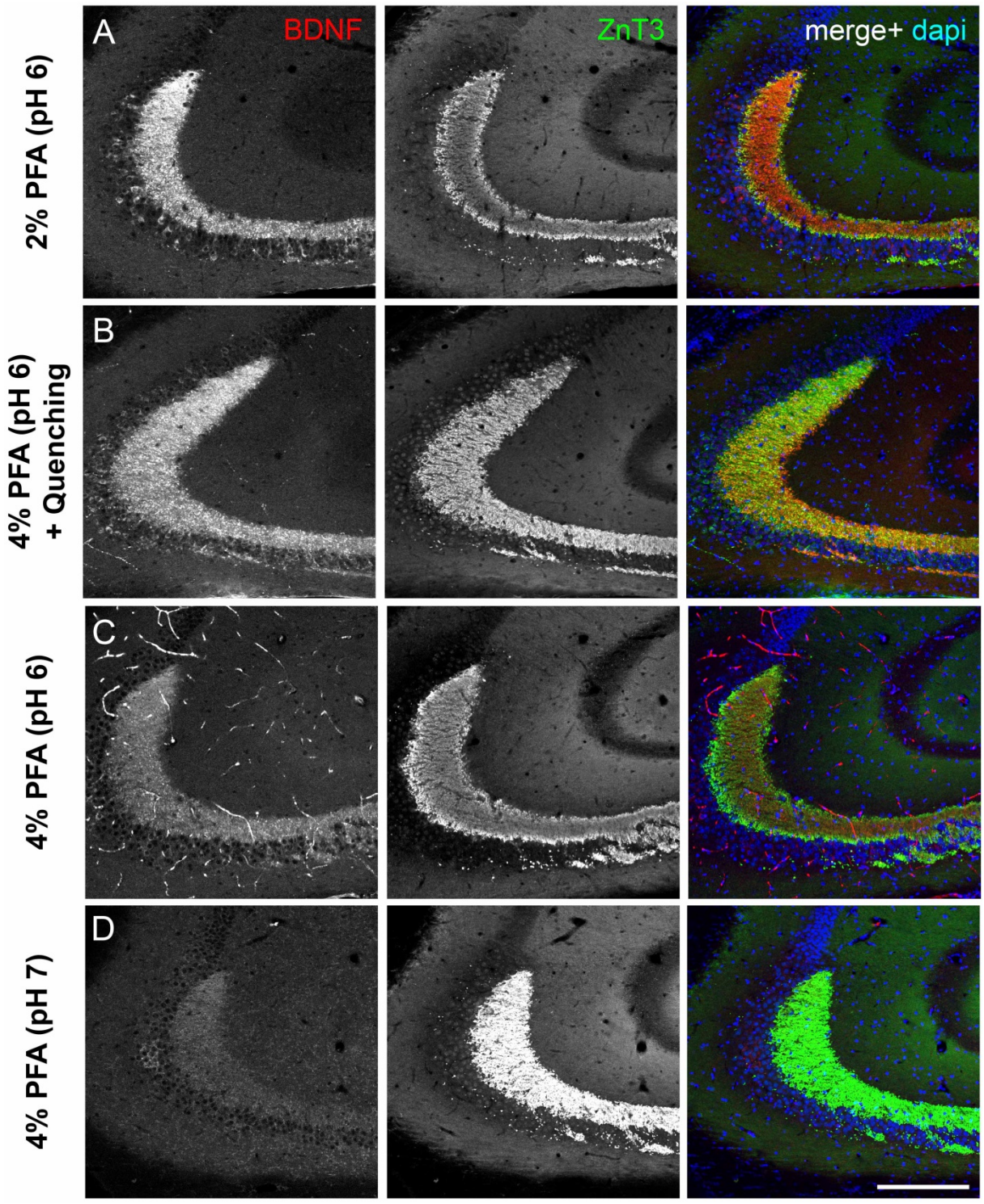

Figure 6 BDNF immunolabelling under different fixation conditions. Certain fixation conditions are needed to allow BDNF localization to presynaptic mossy fiber terminals in the hippocampus.

All the mice were ~ 8 weeks old. Coronal sections of the dorsal hippocampus were labelled with anti-BDNF (mab#9) and anti-ZnT3. A) Tissue fixed with 2% PFA with pH 6.0, followed by 2 hours of post-fixation. B) Tissue fixed with 4% PFA with pH 6.0, followed by 2 hours of post-fixation. Sections were treated with 0.1M TRIS-buffered glycine before immunolabelling. C) Tissue fixed with 4% PFA

with pH 6.0, followed by 2 hours post-fixation. D) Tissue fixed with 4% PFA (pH 7.4), followed by 2 hours post-fixation. Scale bar 200µm.

For efficient BDNF labelling, perfusion conditions with 4% PFA (buffered at pH 6.0), followed by 2 hours of post-fixation was best suited to maintain anti-BDNF immunoreactivity. Subsequent quenching of free aldehyde-groups with buffered glycine solution was most suitable to establish a balance between brain section stability and immunolabelling. After testing a series of antibodies, the most suitable antibodies for this method were found to be anti-BDNF mab#9 and anti-human BDNF (clone) 3B2 (Icosagen). With this protocol, the further BDNF localization experiments were performed.

3.2 Colocalization of BDNF and TrkB at hippocampal mossy fiber terminals

In order to find out the localization of BDNF in relation to its receptor TrkB, double-immunolabelling was performed. For this, a goat anti-TrkB antibody (RD systems), raised against the extracellular domain of TrkB was used. This antibody was tested against TrkBKO vibratome slices (data by D. Segebarth, our research group), harvested from early postnatal TrkB full knockouts (Rohrer et al., 1999). The antibody detects the TrkB kinase as well as the truncated TrkB-T1 receptor. Double immunolabelling followed by high-resolution confocal microscopy revealed the high abundance of BDNF in the MFT and as well in the somatic compartment of a subset of CA3 pyramidal neurons (arrows in Fig. 7). The label against TrkB, the receptor of BDNF showed the global expression of the protein in the Stratum lucidum, the region with highest abundance of mossy fiber terminals, as well as in the CA3 pyramidal cell layer, thus indicating a pre- and post-synaptic distribution of TrkB in the DG-CA3 microcircuit. To see whether TrkB is localized to glutamatergic presynapses of the DG neurons, the labelling was combined with a staining for the vesicular glutamate transporter (vGLUT), a well-established marker for presynaptic glutamatergic terminals (Fig. 7-8). The labelling showed a close proximity of BDNF, vGlut and TrkB in the synaptic region of the *Stratum lucidum*, indicating a high abundance of TrkB in glutamatergic MFTs (Fig. 8). The localization of BDNF to be in close proximity with vGLUT (Fig. 7-8) was in accordance with BDNF being expressed in excitatory neurons in the MFT region (Dieni et al., 2012) and in mature cultured hippocampal neurons (Andreska et al., 2014).

Next, it was asked whether BDNF immunoreactivity is also seen in fast-spiking Parvalbumin-positive interneurons in the DG-to-CA3 microcircuit. Early studies suggested that BDNF is preferentially found in glutamatergic, but not GABAergic neurons (Andreska et al., 2014; Dieni et al., 2012). Anti-Parvalbumin labelling, the most prominent interneuron population in the MFT, showed that the Parvalbumin-positive interneurons do not carry a somatic BDNF label (Fig. 9). Taken together, at the DG-CA3 hippocampal circuit, the BDNF IR is most abundant in the glutamatergic presynaptic terminal of dentate gyrus granule neurons. BDNF is also found in postsynaptic CA3 pyramidal neurons, while we could not see much steady-state anti-BDNF immunoreactivity in GABAergic Parvalbumin-positive interneurons.

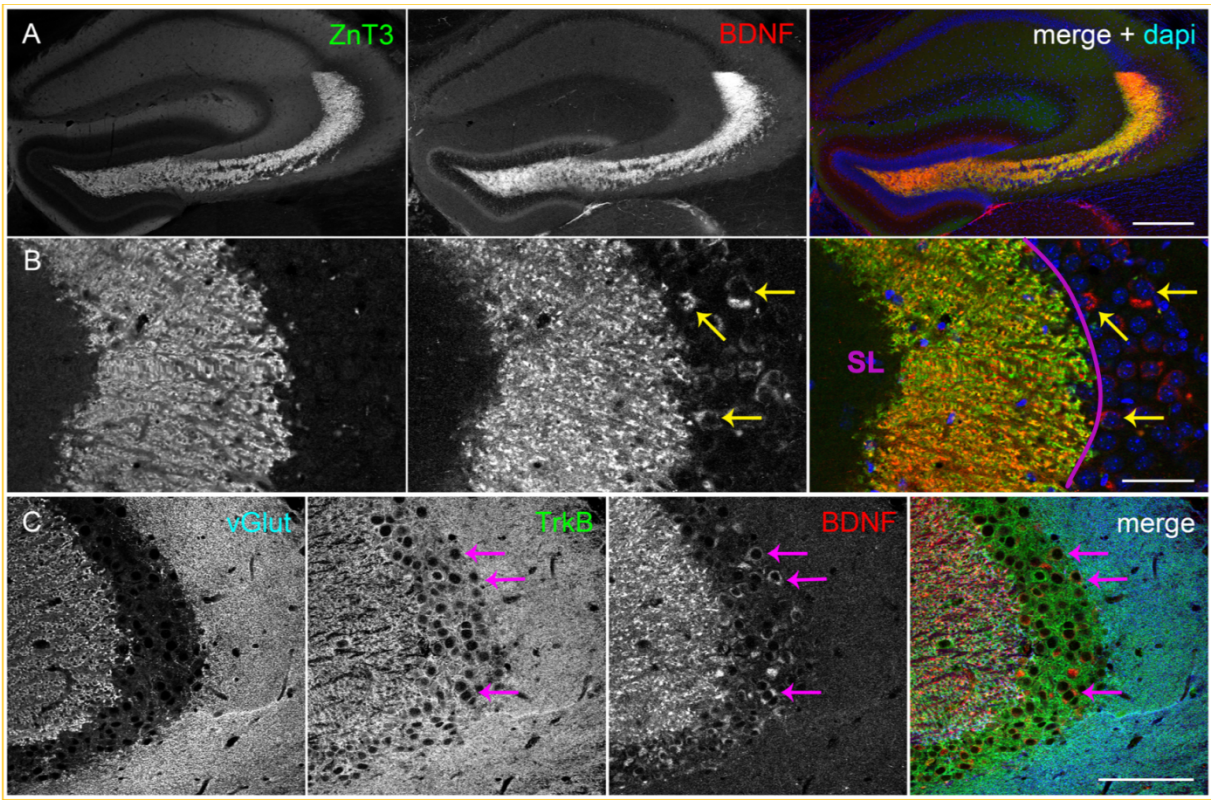

Figure 7 BDNF/TrkB expression at the mossy fiber terminal.All the mice were ~ 8 weeks old. *A) Coronal sections of the dorsal hippocampus, post-labelled with anti-BDNF (mab#9) and anti-ZnT3. Scale bar 200 μm. B) High-resolution image of the Stratum lucidum (SL) shows the localization of BDNF in large boutons of the MFT and a small subset of CA3 pyramidal neurons carrying BDNF protein in their soma. Scale bar 50 μm. C) Staining of BDNF, vGlut and TrkB. Shown is the Stratum lucidum and the CA3 pyramidal neuron band. BDNF expression appeared to be high vGLUT-positive synapses. Anti-TrkB immunoreactivity was observed both in the pre- and post-synaptic terminals at the DG-CA3 terminal. Scale bar 100μm.*

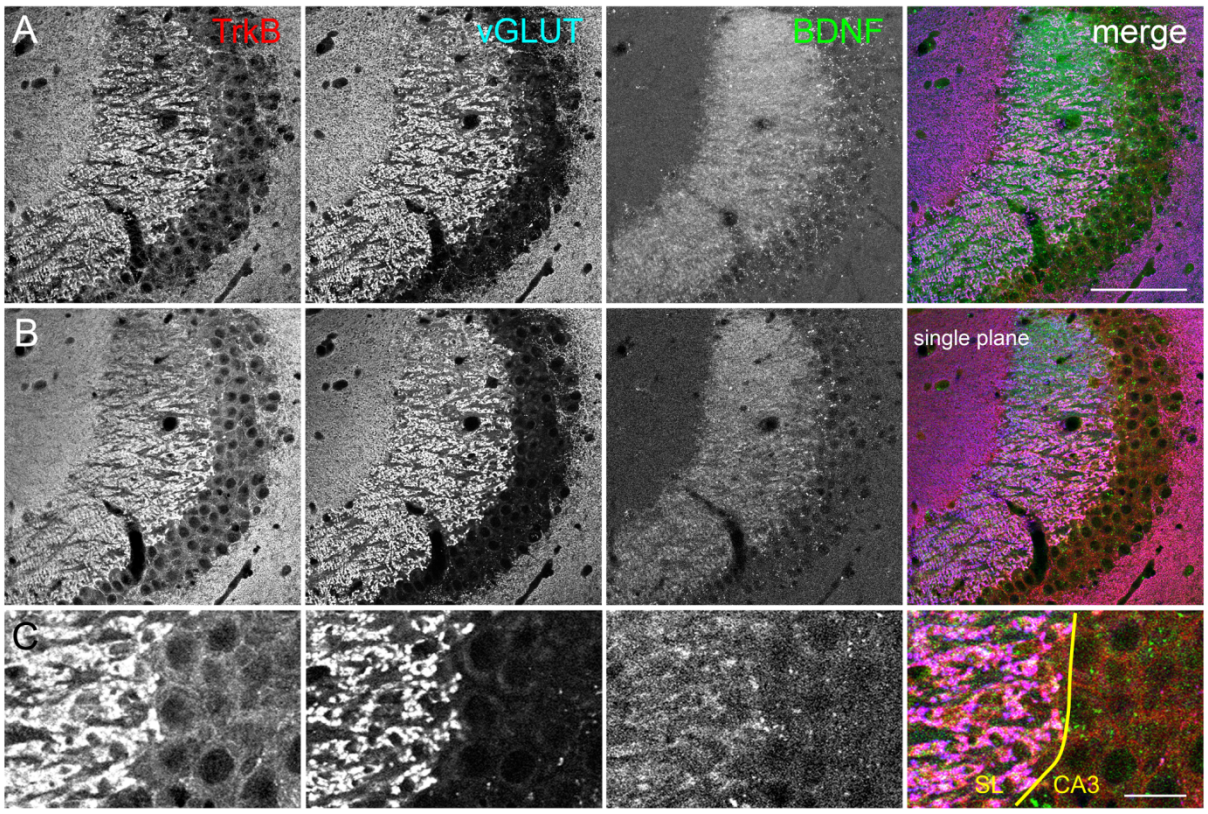

Figure 8 Localization of BDNF and TrkB at the DG-CA3 synapse.

All the mice were at an age of about 8 weeks. A) Coronal sections of the dorsal hippocampus post-labelled with anti-BDNF (mab#9), vGLUT and TrkB. Scale bar 200 μm. B) Single plane confocal image shows the localization of BDNF and vGLUT in mossy fiber terminal and TrkB to be enriched in close proximity of the presynaptic marker vGLUT. C) High-resolution image of the Stratum lucidum with the MFTs. Shown is the overlap of TrkB and vGLUT immunolabels. Scale bar 20 μm.

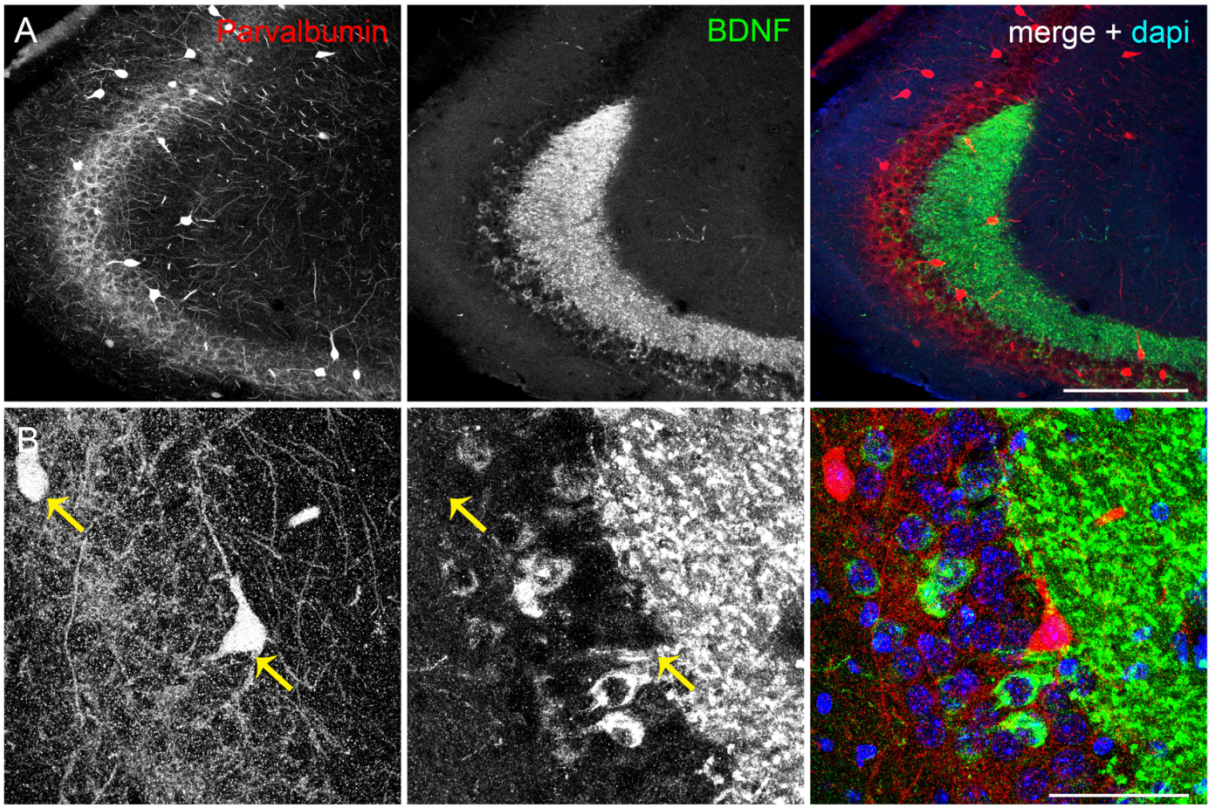

Figure 9 BDNF expression in Parvalbumin+ interneurons at the mossy fiber terminal.
The mice were ~ 8 weeks old. A) Coronal sections of the dorsal hippocampus labelled with anti-BDNF (mab#9) and anti-Parvalbumin. Parvalbumin labelling shows the huge interneurons located at the MFT and along the arc of the CA3 region. Scale bar 200 µm. B) High-resolution image of the MFT, shows the localization of BDNF in the boutons of the MFT and in somata of CA3 pyramidal neurons, but not in the somata of Parv+ interneurons. Scale bar 50 µm.

3.3 Anterograde distribution pattern of BDNF in the fear circuit

To prove whether the prominent labelling of BDNF in presynaptic fibers of glutamatergic projection neurons is a typical pattern for BDNF localization, BDNF immunoreactivity was also tested in two other prominent regions of the fear circuit: the amygdala and the Bed nucleus stria terminalis (BNST) (Lebow and Chen, 2016; Tovote et al., 2015). Early data indicated that the BDNF encoding transcript is not expressed in these two regions, but that BDNF IR in fiber-like structures can be found in the BNST as well as the central amygdala (Conner et al., 1997), thus indicating anterograde axonal transport of BDNF in the fear circuit.
BDNF labelling was performed on coronal vibratome slices and confocal microscopy images were acquired from the indicated regions. Staining for NeuN (Fox3) was used to label for neuronal nuclei and to offer a counterstain to discriminate fiber bundles, such as the anterior commissure, from regions with cell bodies. In the BNST, a strong BDNF staining was observed in the oval nucleus of the BNST (indicated in Fig. 10). Confocal imaging at higher resolution showed that BDNF is preferentially found in fiber-like structures, thus indicating a presynaptic axonal abundance of the protein in this brain region (Fig. 10).

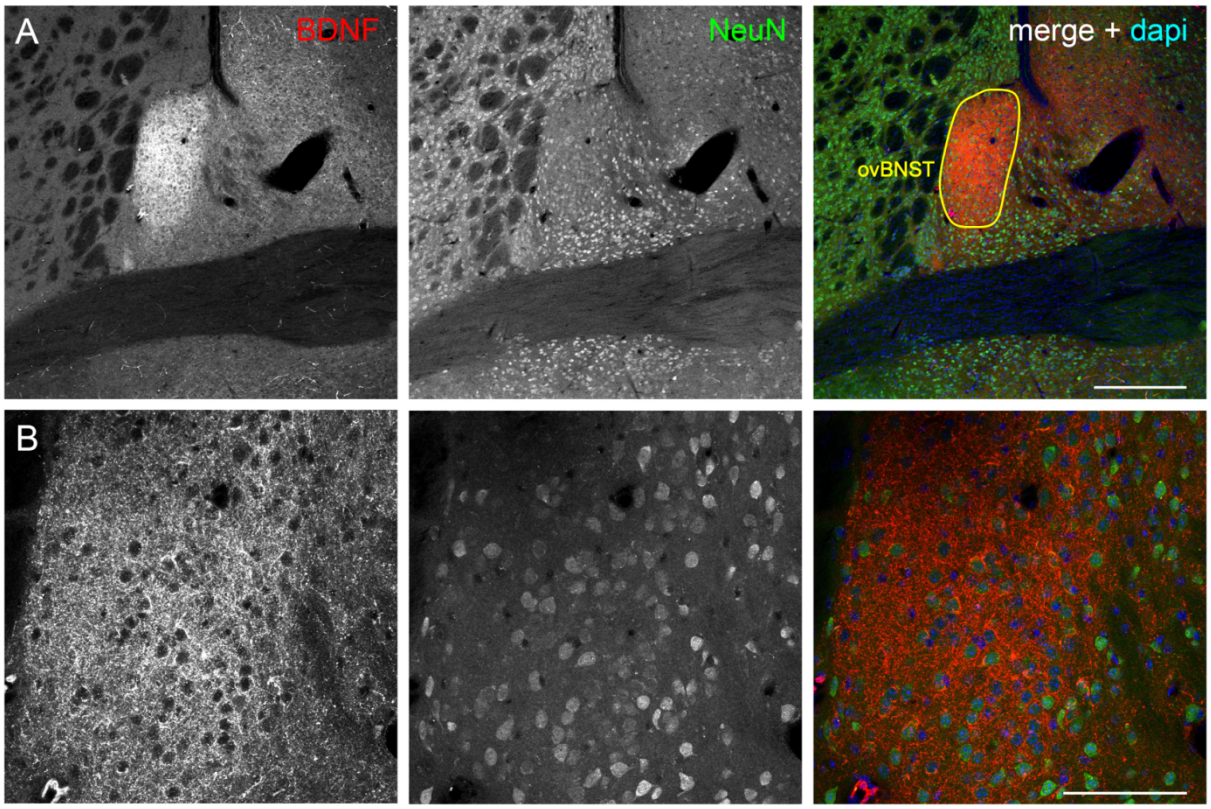

Figure 10 BDNF expression in the bed nucleus of the stria terminalis (BNST).
Coronal section stained for BDNF and NeuN. A) The BDNF labelling shows a high amount of BDNF protein close to NeuN+ neurons in the oval nucleus of the BNST (indicated in yellow). Scale bar 300 μm. B) High-resolution image of the ovBNST shows the localization of BDNF in fiber-like structures, presumably axons. Scale bar 100 μm.

Labelling for BDNF in the amygdala showed a high abundance of BDNF IR in fiber-like structures in the central amygdala, and a moderate labelling of BDNF in single somata of the basolateral amygdala (Fig. 11(I)A). This is in accordance with the finding that BDNF immunoreactivity is high in fiber-like structures in the central, but not basolateral amygdala, while a high amount of BDNF RNA is available in the basolateral amygdala, but not in the central amygdala (Conner et al., 1997). In the striatum, a region which was shown to be significantly affected by global deletion of BDNF, the protein is seen in form of puncta and is almost absent from striasomes (Fig. 11(I)B).

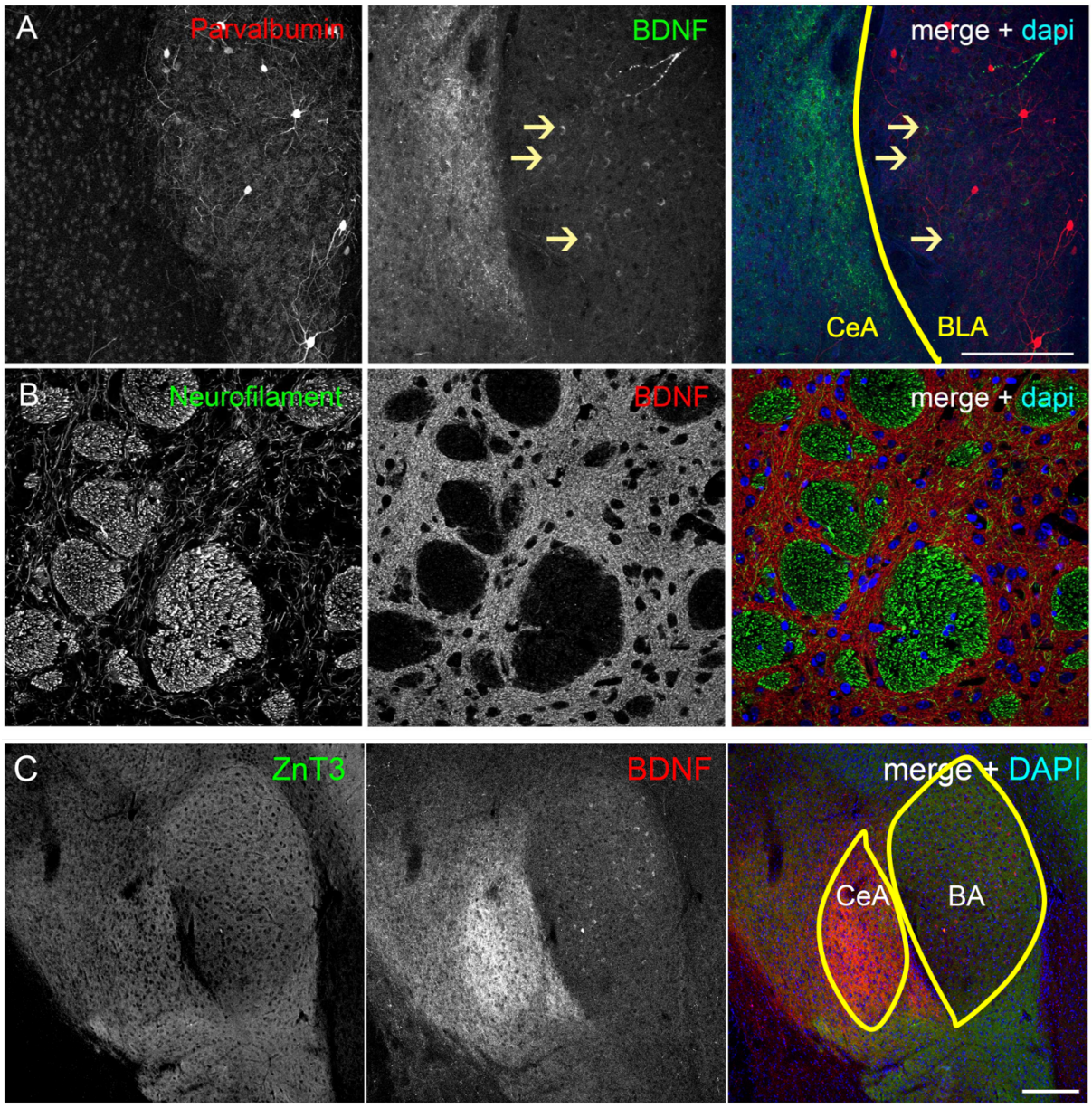

Figure 11 BDNF expression in the amygdala and the striatum.

A) Coronal section of the amygdala labelled with anti-BDNF (mab#9) and anti-Parvalbumin. The BDNF labelling is strong in the central amygdala (CeA). In the basolateral amygdala (BLA), few neurons carry BDNF in their somatic compartment (arrows). Scale bar 200 μm. B) Coronal section of the striatum labelled with anti-BDNF (mab#9) and anti-Neurofilament (heavy chain). BDNF is expressed in the grey matter of the striatum and is almost absent from the axon-rich striasomes. Scale bar 100μm. C) Coronal section of the amygdala labelled with anti-BDNF (mab#9) and anti-ZnT3. The BDNF labelling is strong in the central amygdala (CeA). In the basolateral amygdala (BLA), few neurons carry BDNF in their somatic compartment (arrows). Scale bar 200 μm.

3.4 Conditional deletion of BDNF from dentate gyrus granule neurons

The detailed localization of BDNF in the hippocampus, BNST and amygdala suggested that BDNF is anterogradely delivered to glutamatergic terminals, where it is stored in presynaptic terminals. This concept of anterograde BDNF function suggests that BDNF deletion from the

presynaptic neuron, and not postsynaptic neuron, can be suited for identifying BDNF function at synapses. Thus, site-specific deletion of BDNF from the mossy fiber terminal would provide an ideal situation to understand how BDNF signalling is able to affect neural microcircuits.
For this reason, it was aimed to investigate the potential of a new Cre-deleter mouse model showing Cre-activity specifically in granule neurons of the hippocampus(Meneghetti, 2010/11)

3.5 CNTF-promoter driven Cre recombinase shows age-dependent Cre-activity in adult granule neurons of the dentate gyrus

The CNTF::Cre knock in mouse model (C57BL/6-Tg(CNTF-Cre)TM^{Msd}) was created in our Institute of Clinical Neurobiology, by Dr. Yasuhiro Ito, under the supervision of Prof. M. Sendtner. The identification of the Cre insertion site was based on the characterization of CNTF-promoter expression features in mice (Ito et al., 2006). Genetic mapping of the Cre-insertion site was started in the course of my master thesis (Sasi, 2014)and was finished in the course of this work.
With the help of PCR amplification products and subsequent DNA sequence analysis, the following genomic structure was identified (Fig. 12A). In the CNTF-Cre mice, the C*ntf* Exon1 is replaced by a *Cre* recombinase encoding gene cassette (Acc. Nr. AB449974) followed by a neomycin cassette (Fig.12A, gene map with single-base pair resolution).
In earlier work by E. Meneghetti, B. Wachter and myself in our institute, the CNTF::Cre knock-in mice were crossed with a CAG-CAT-eGFP Cre-reporter mice (Nakamura et al., 2006). The CNTF::Cre reporter mice showed a high GFP expression specifically in the mature neurons of DG of the hippocampus (Fig.13). This was not due to a leaky promoter in the CAG-CAT-eGFP reporter, as the typical GFP expression in granule neurons of the hippocampus was only seen in CNTF::Cre x CAG-CAT-eGFP mice, but not in Cre-deficient CAG-CAT-eGFP littermates (Fig. 13).

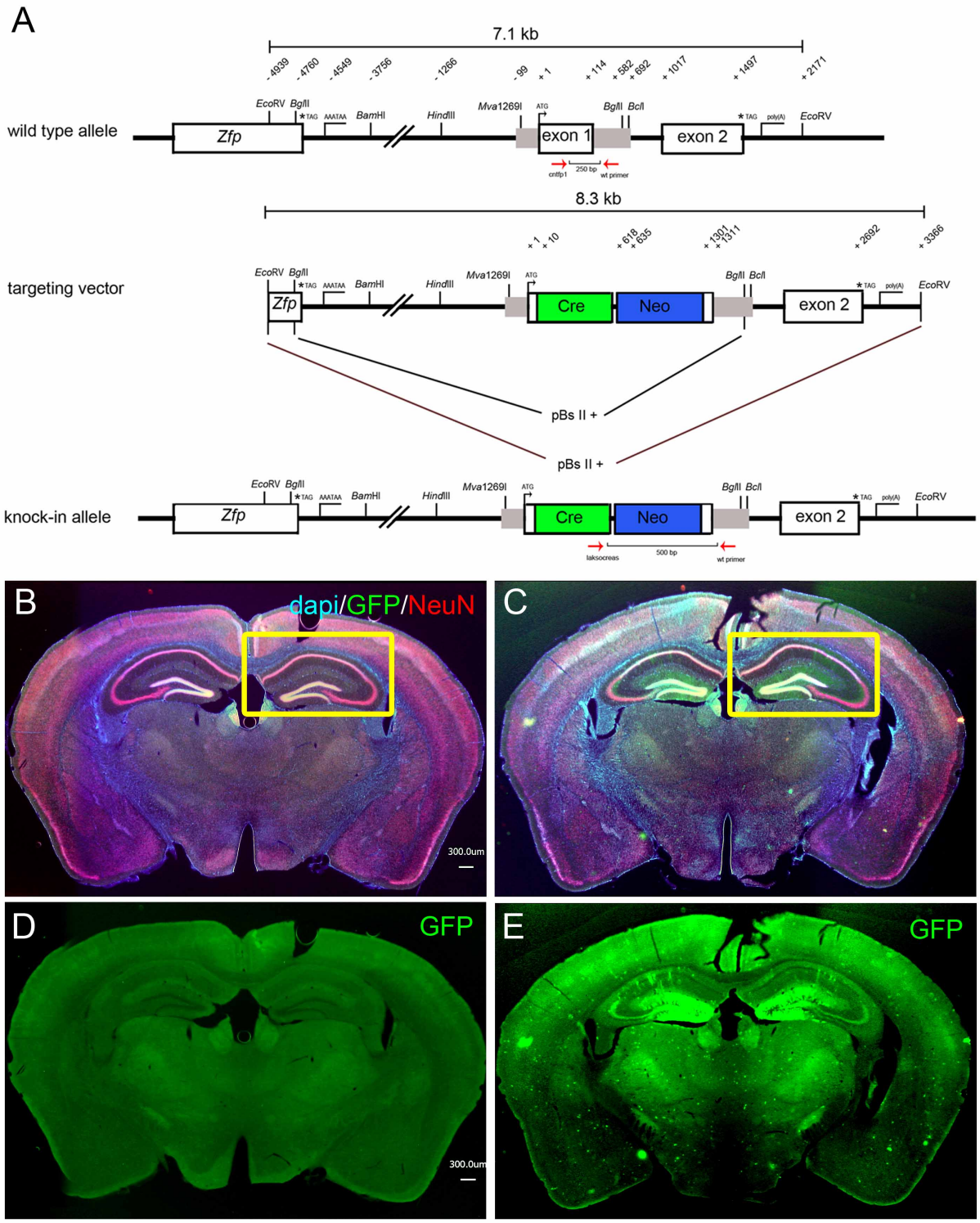

Figure 12 CNTF::Cre knock-in construct.

A) *The targeting vector was a modified version of a 6.5 kb DNA fragment containing the complete Cntf gene including the 4.7 kb 5' flanking region until the coding region of the Zfp gene. The knock in allele contained the complete P1 Cre recombinase coding region and a neomycin resistance gene. The cassette was preceded by the 5'UTR of the Cntf gene start codon and 9 nt of the Cntf gene. The 3'UTR was followed by intron 1, exon 2 and the stop codon of the Cntf open reading frame.* ***B)*** *Overview image of CNTF::Cre +/+ CAG-EGFP tg/+ coronal section labelled with anti-GFP, anti-NeuN and DAPI. The dentate gyrus is highlighted shows the GFP+ granule neurons. Scale bar 300*

µm. ***C)*** *Overview image. Hippocampus of a CNTF::Cre tg/+ CAG-EGFP tg/+ mouse. Section was post-labelled with anti-GFP. The dentate gryus is indicated.* ***D)*** *Overview image. Hippocampus of CNTF::Cre +/+ CAG-EGFP tg/+ coronal section. Green channel only shown (in green). Scale bar 300 µm.* ***E)*** *Overview image. Hippocampus of a CNTF::Cre tg/+ CAG-EGFP tg/+ mouse. Green channel only shown (in green). Section was post-labelled with anti-GFP.*

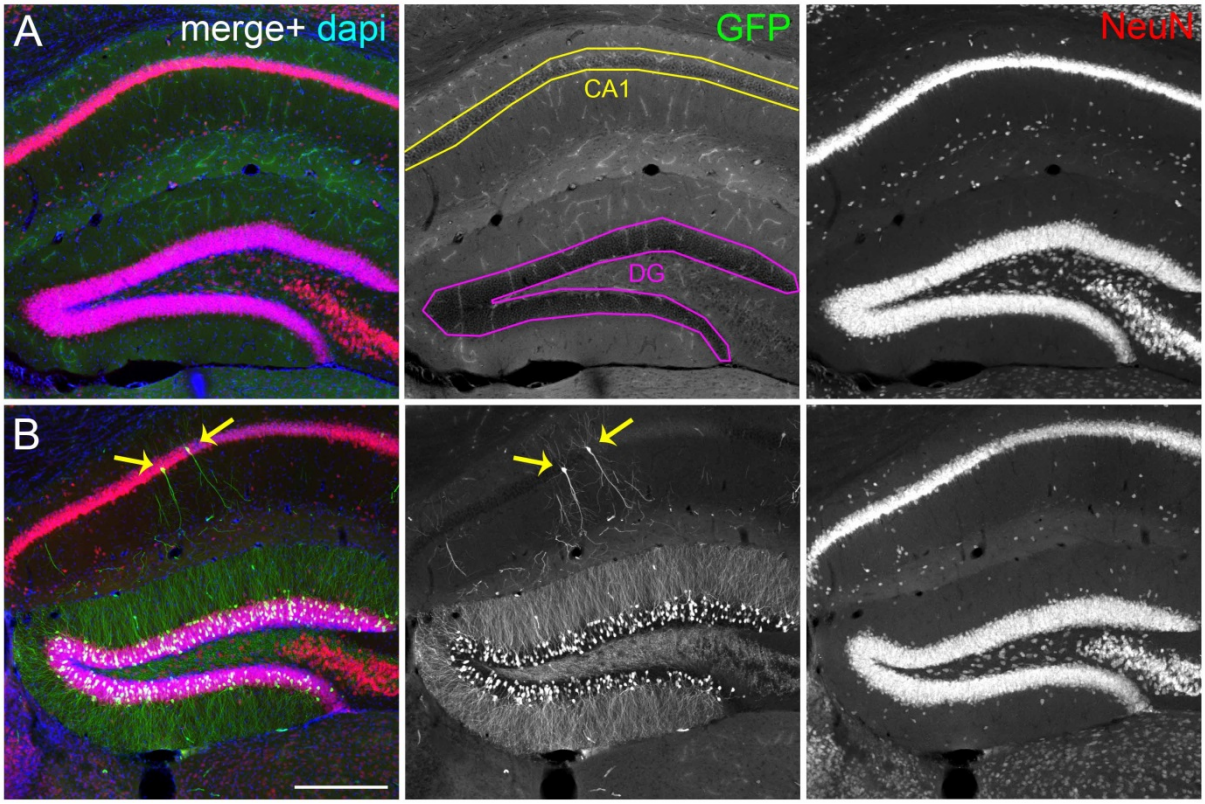

Figure 13 CNTF promoter activity in adult mice.
A) *Coronal section of the dorsal hippocampus of an 8 week old CNTF::Cre +/+ reporter mouse, labeled with anti-GFP and anti-NeuN. In absence of the Cre, no GFP label is seen in the hippocampus. Scale bar 200 µm* ***B)*** *Dorsal hippocampus of an 8 week old CNTF::Cre transgene positive reporter mouse, immunolabeled against GFP and NeuN. GFP expression indicates preceding Cre-activity in dentate gyrus granule neurons and in few CA1 pyramidal neurons (yellow arrows).*

However, as Cre-reporter activity was almost absent in embryonic and early postnatal brain regions, but was highly abundant in adult granule neurons (Sasi, 2014), it was asked to which extent and at which developmental time point the CNTF-Cre mouse model is able to delete floxed genes. It was seen that in one year old reporter mice there was high number of GFP+ cells in the DG than nine week old mice, so we analyzed the number of GFP+cells in the DG of mice ranging from three weeks of age till 54 weeks. One to three animals were chosen per age and up to six high resolution images obtained at 40X were chosen at random. This experiment was done together with Britta Wachter.

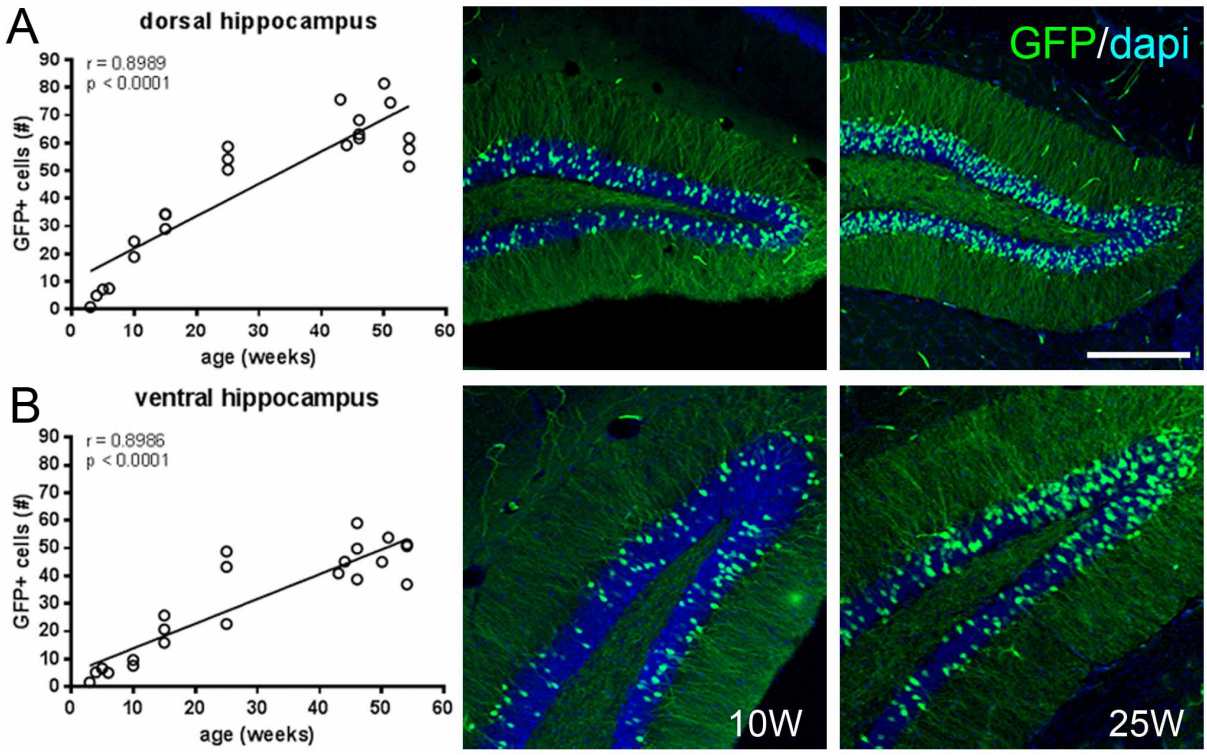

Figure 14 Timeline of GFP expression.

A, B) The number of GFP+ cells was determined in CNTF::Cre tg/+ CAG-EGFP tg/+ mice of different age. The data show a linear correlation (r) between the age (x-axis) and the number of reporter positive granule neurons (GFP+; y-axis)v in individual CNTF-Cre reporter mice (indicated as small circles). In A) left panel: data for the dorsal hippocampus. Right panel: Representative image showing GFP+ cells in the dentate gyrus of a 10-week old (10W) and a 25-week (25W) old reporter mouse. In B) Corresponding data for the ventral hippocampus. Scale bar 200 µm. P-value of less than 0.0001 indicates the significance of the x,y-correlation.

3.6 Cre-activity in CNTF-Cre deleter mice does not occur in adult-born neurons

A linear correlation between age and the number of Cre-positive reporter cells let us assume that CNTF-promoter driven Cre activity occurs specifically in adult-born neurons. Earlier data by our group indicated that the GFP-reporter signal does not appear in immature DCX+ neurons(Meneghetti, 2010/11). As it could not be ruled out that CNTF-Cre activity occurs at late stages of neurogenesis or whether the CAG-driven reporter is promotor inactive in the lineage of adult born neurons, 5'-Bromo-2-deoxyuridine (BrDU)-labelling was performed. BrDU is a structural analogue of the DNA base thymidine and can be incorporated to DNA in the S-phase of the cell cycle. BrDU labelling consists of a pulse or pulses of intraperitoneal BrDU injections followed by a variable survival time allowing for tracking the fate of neural progenitors and their progeny. Here, male mice of an age of 19-20 weeks got 5 pulses of 50 mg/kg BrDU.

Brain sections where cut at 35 days post-BrDU labelling, at a time point, when BrDU in newborn neurons should co-localize with markers for adult born neurons, such as NeuN (Yeh et al., 2012). Slices labelled for NeuN and GFP were treated with HCl and where subsequently labelled with antibodies against BrDU. Finally, image stacks were acquired at a confocal microscope and single z-stack images were used to determine the colocalization of the BrDU signal in NeuN-positive cells and to find out whether BrDU-positive NeuN+ cells were also CNTF-Cre reporter positive.

The data showed surprisingly, that CNTF promoter is restricted to NeuN+ mature granule neurons. Furthermore, not a single BrDU-positive cell was found to be GFP-reporter positive (Fig.15, data in Table 13), thus verifying that CNTF-Cre- reporter is absent from the adult-born neuron lineage.

Table 13 Quantification of GFP+ and BrdU+ cells

Animal No.	Genotype		Region	No. Of GFP+ cells	No. Of BrdU+ cells	No. Of GFP+ & BrdU+ cells
	CNTF::Cre	CAGeGFP				
45	tg+	tg+	Dorsal	215	5	0
45	tg+	tg+	Ventral	145	7	0
46	tg+	tg+	Dorsal	183	3	0
46	tg+	tg+	Ventral	47	5	0
55	tg+	tg+	Dorsal	116	16	0
55	tg+	tg+	Ventral	97	7	0
56	tg+	tg+	Dorsal	278	18	0
56	tg+	tg+	Ventral	207	6	0

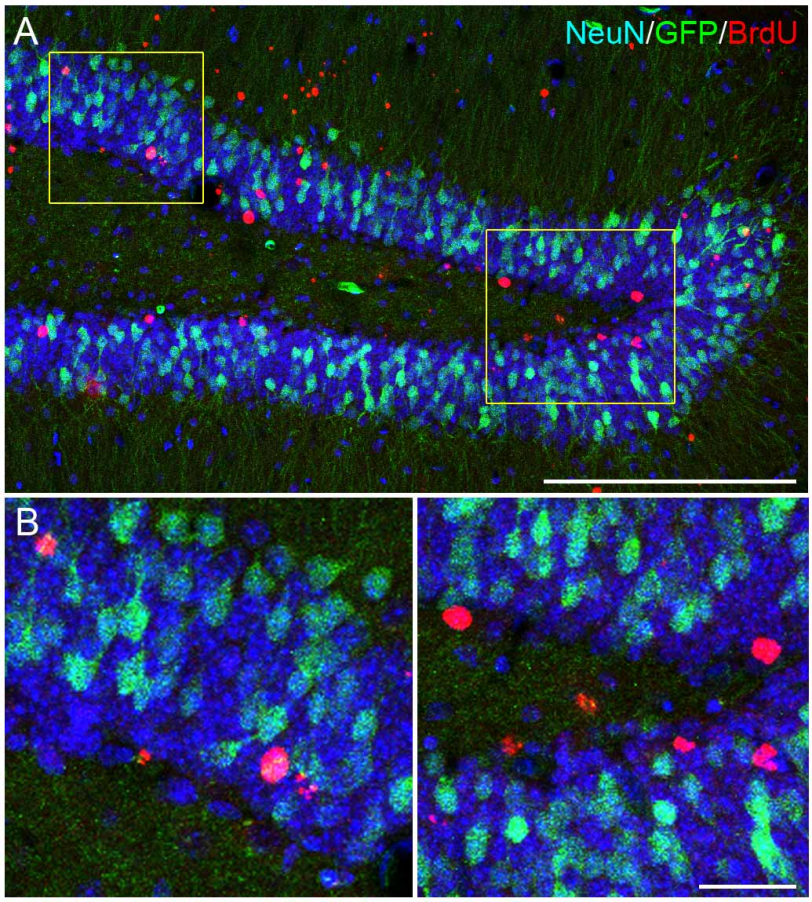

Figure 15 BrdU quantification on the hippocampal section of the CNTF::Cre reporter mice. *A) Overview of the coronal section of dHippo of 10-week-old mice, immunolabeled with GFP, NeuN and BrdU. It showed the co-localization of GFP and NeuN, whereas BrdU+ cells were GFP-. Scale bar 200 µm. B) Higher resolution of the mature granule neurons further confirms that GFP co-localizes only with NeuN and not with BrdU. Scale bar 40 µm.*

3.7 Presynaptic BDNF in mossy fiber terminals is cell-autonomously produced by dentate gyrus granule neurons

Albeit BDNF is stored at high amounts in mossy fiber terminals, this does not exclude the possibility that mossy fiber BDNF originates from other cell types such as CA3 pyramidal neurons or mossy cells in the hilus of the hippocampus; both are known to express BDNF transcripts (Altar et al., 1997). To find out whether the presynaptic BDNF immunoreactivity in mossy fiber terminals is a cell-autonomous BDNF signal, mice with a loxP-site flanked *Bdnf* gene (*Bdnf* $^{fl/fl}$ mice) (Rauskolb et al., 2010) were crossed to delete BDNF from granule neurons of the dentate gyrus. To see to which extent Cre-positive neurons lack BDNF immunoreactivity, we took advantage of GFP-reporter mice that were additionally crossed to CNTF-Cre, BDNF$^{fl/fl}$ mice (Fig. 16A). This would result in a mouse model with BDNF deletion and GFP expression exclusively in the DG granule neurons, thus enabling to see whether GFP+ mossy fiber terminals are BDNF-deficient or not.

In CNTF::Cre tg/+ BDNF fl/fl CAG-CAT-eGFP tg/+ mice, anti-BDNF IR was dramatically reduced, thus indicating that indeed most BDNF in mossy fibers derives from granule neurons (Fig. 16B,C). The origin of a weak residual anti-BDNF signal in the Stratum lucidum may derive from neurons lacking Cre-activity.

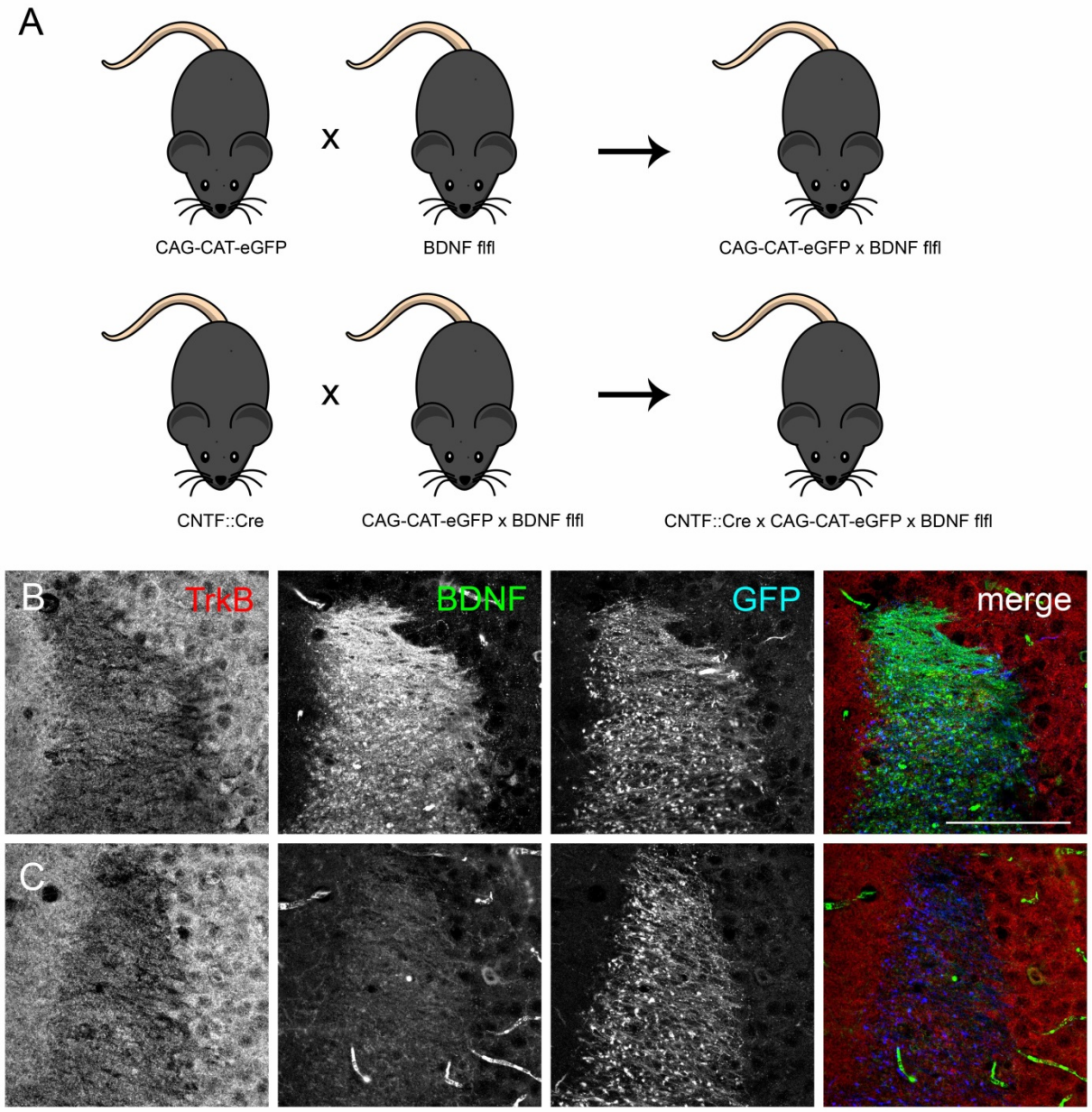

Figure 16 BDNF expression in the Triple transgenic mouse model and validation of the conditional ko model.

A) Schematic of the breeding plan of the triple transgenic cBdnf ko model. Coronal sections post-labelled with GFP, BDNF (mAB9) and TrkB. B) CNTF::Cre tg/+ BDNF +/+ CAGeGFP tg/+ mouse showed GFP labelling at the MFT and the LMT boutons and as well BDNF, TrkB expression was clearly observed in here. Scale bar 100 μm. C) CNTF::Cre tg/+ BDNF fl/fl CAGeGFP tg/+ mouse showed high reduction in the expression of BDNF at the MFT but no change in TrkB expression.

Environmental enrichment with voluntary exercise is a commonly used to induce structural plasticity in the hippocampal circuit (Bergami et al., 2015; Kempermann et al., 1997). Furthermore, it is a suited model to drive enhanced BDNF expression in hippocampal and cortical regions(Fan et al., 2016; Novkovic et al., 2015) Therefore, enriched environment (EE) is suited to test whether the induction of plasticity events in the hippocampus may change the fundamental localization of BDNF. For this reason, mice were put in an enriched environment system (Fig. 17).

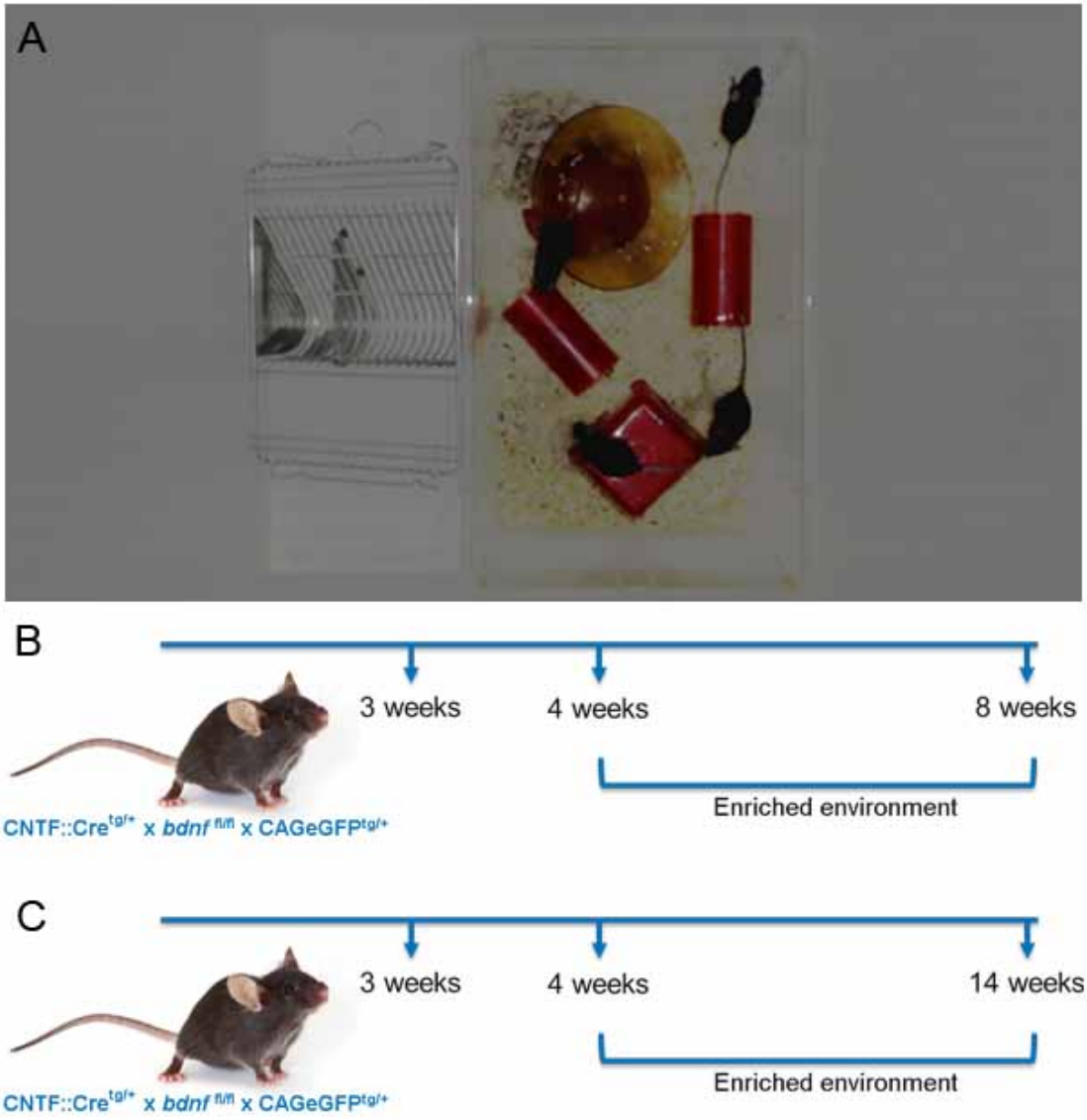

Figure 17 Enriched environment (EE) Set up.

A) In the EE set up, only males were used in the experiment, the mice were housed in groups of 4 to 5 animals under standard laboratory conditions (12h/12h light/dark cycle, food and water ad libitum) in a cage size M with the dimensions 425 x 276 x 153 mm. Every environment had the house equipped with a running wheel, one tunnel and additional two of the following were added: a maze house, a spherical or a rectangular house and an additional tunnel. The toys and houses were re-positioned once a week and they were checked every day for bite marks or wounds. B) One set up was, the mice were put together right after weaning and introduced to the EE at 4W of age and

sacrificed after 4 weeks. C) Second one was, the mice were put together right after weaning and introduced to the EE at 4W of age and sacrificed after 10 weeks.

Five male mice (littermates) were put to an EE cage at the age between 3-4 weeks. Mice were left in the cage for another for 4 weeks. The male animals were controlled daily and did not show signs of aggression behaviour. Then animals were perfused, and brain sections were labelled to visualize the DCX+ neuronal population. EE is known to drive adult neurogenesis and therefore an increase in the number of DCX+ neurons in the dentate gyrus is suited to test whether our EE approach stimulated neurogenesis and cellular plasticity in the hippocampus. DCX+ labelling confirmed that the EE system used in our study could substantially increase DCX+ immunoreactivity in the hippocampus (Fig. 18).

The second cohort of animals were kept in the similar EE for 10 weeks. Then, the animals were perfused and hippocampal sections were stained for BDNF, GFP and vGlut1, a marker to label presynaptic mossy fiber synapses. In these animals, the BDNF labelling was still preferentially observed in mossy fiber terminal, in the dorsal as well as in the ventral hippocampus, indicating that even long periods of environmental enrichment could not change the gross localization of BDNF to mossy fiber terminals (Fig. 19 E,F). In the conditional BDNF KO mice (home cage controls), anti-BDNF immunoreactivity was dramatically reduced in the dorsal as well as ventral hippocampus (Fig. 19 C,D). In mice exposed to EE, a weak, but substantial anti-BDNF immunoreactivity was found (Fig. 19 G,H). Due to the high variability, a quantitative analysis of the amount of local BDNF abundance was not possible. The origin of the EE-dependent BDNF signal was out of scope of this study.

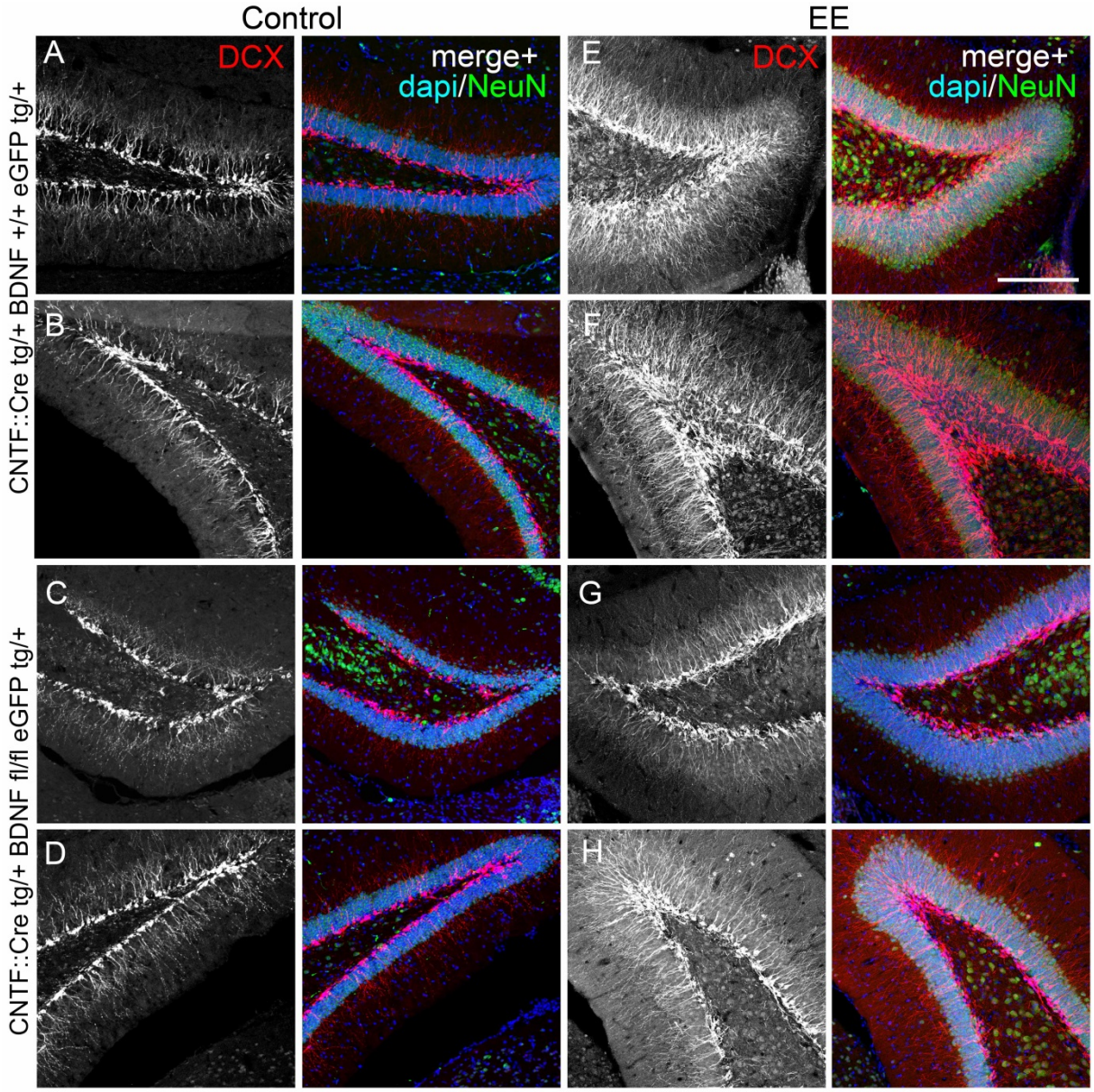

Figure 18 Enriched environment – 'proof of principle'.

Coronal sections post-labelled with DCX and NeuN, CNTF::Cre tg/+ BDNF +/+ CAGeGFP tg/+ - wildtype, CNTF::Cre tg/+ BDNF fl/fl CAGeGFP tg/+ - cBdnf ko. (A) – (D) Mice were housed under normal conditions in individual cages with water and food ad libitum. (E) – (H) Mice were housed in an enriched environment (EE) in a social set up with running wheel and toys from age of 4W until 12W (Fig 19). (A) & (B) Dorsal and ventral region of wildtype (C) &(D) Dorsal and ventral region of cBdnf ko, all showing DCX positive immature neurons. (E) & (F) Dorsal and ventral region of wildtype (G) &(H) Dorsal and ventral region of cBdnf ko, it clearly shows the tremendous increase in the DCX expression, proving the effect of EE on neurogenesis. Scale bar 200 μm.

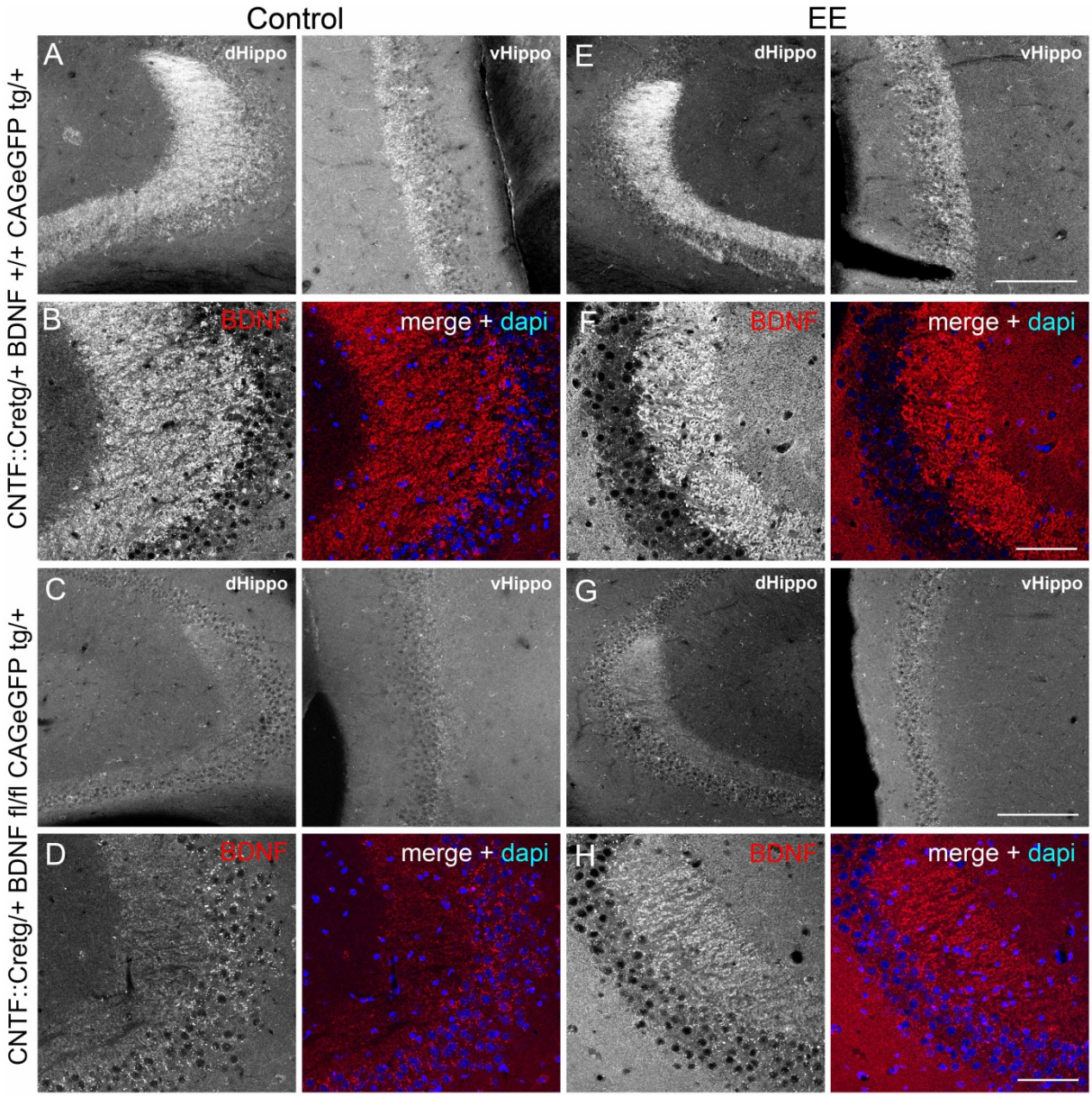

Figure 19 Enriched environment effect on BDNF expression.

Coronal sections post-labelled with BDNF (3B2). CNTF::Cre tg/+ BDNF +/+ CAGeGFP tg/+ - wildtype, CNTF::Cre tg/+ BDNF fl/fl CAGeGFP tg/+ - cBdnf ko. (A) – (D) Mice were housed under normal conditions in individual cages with water and food ad libitum. (E) – (H) Mice were housed in an enriched environment (EE) in a social set up with running wheel and toys from age of 4W until 12W (Fig. 19). (A) & (B) Dorsal and ventral region of wildtype (C) &(D) Dorsal and ventral region of cBdnf ko, (E) & (F) Dorsal and ventral region of wildtype, (G) &(H) Dorsal and ventral region of cBdnf ko. Under control condition, the wildtype expresses BDNF in dorsal and ventral hippocampus whereas the cBdnf ko has high reduction in BDNF expression. Under EE, the wildtype does not seem to have visibly clear increase in BDNF level but cBdnf ko shows increased BDNF level in comparison to the ko under control condition. Scale bar, (A), (C), (E), (G) - 200 μm, (B), (D), (F), (G) - 50 μm.

3.8 Adult-born granule neurons are affected in mossy fiber-specific BDNF KO mice

Recent data showed that the integrity of adult-born dentate gyrus granule neurons and the functional impact of newborn neurons in the dentate gyrus depends on BDNF/TrkB signalling. In these experiments, genetic deletion of either TrkB or BDNF from dividing neural progenitors in the adult-born neuron lineage affected the dendritic complexity of adult-born granule neurons, indicating that cell-autonomous deletion of the receptor and its ligand changes the fundamental structure of the same cell. However, these studies did not exclude the possibility that microcircuit effects by local BDNF signalling would also affect the development or maturation of adult-born neurons in a non-cell autonomous fashion.

To answer this question, the number of DCX+ immature neurons was counted in the dorsal and ventral hippocampus of *cBdnf* KO mice. As BDNF as well as the CNTF-Cre expression pattern is age-dependent, mice of an age of two, three and six months were investigated. Wildtype littermates served as control. For this free floating vibratome sections of the hippocampus were labelled with anti-DCX, and were imaged by confocal microscopy. Then the number of DCX+ neurons was counted manually in maximum intensity projection images (9 μm in z) with the help of the ImageJ software. In case of the two-month-old animals, for each animal, one section representing the dorsal and one section representing the ventral hippocampus were analyzed according to the stereotactic coordinates (data are shown in Fig. 20). At this age, no change in the number of DCX+ cells was found in the dorsal and ventral hippocampus.

In case of the three or six-month-old animals, for each animal, three sections representing the dorsal and two sections representing the ventral hippocampus were analyzed from three animals (data are shown in Fig. 21,22). DCX+ cells were found to be increased in the ventral hippocampus of three-months-old CNTF-Cre; $Bdnf^{fl/fl}$ mice (Fig. 21). No significant difference was observed for the dorsal hippocampus, neither at the age of three month nor at the age of six months (Fig. 21,22). This indicates a region-specific and age-dependent effect of granule neuron-specific deletion of on the neurogenesis.

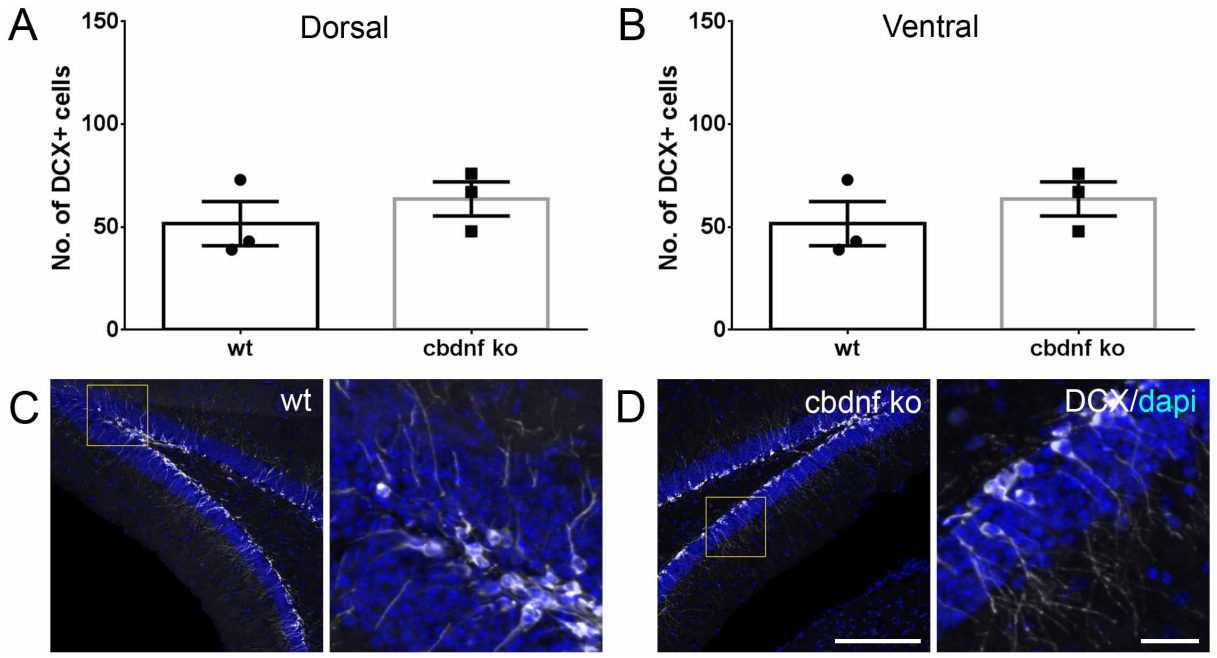

Figure 20 The number of DCX-positive immature neurons is not changed in two-month-old granule cell specific BDNF knockouts.

A, B) *The number of DCX + immature neurons is not different in the dorsal and ventral hippocampus of cBdnf KO mice in comparison to wildtype control animals. Each data point reflects the result obtained from an individual animal. Unpaired t-test, p = 0.4285 (dorsal), p = 0.8374 (ventral).* ***C, D)*** *Representative overview images and high-resolution images of DCX+ neurons in the dentate gyrus of the hippocampus. Dapi was used as counterstain. Scale bar 200 µm and 20µm. Shown are the mean values of the number (No.) of DCX+ cells per section ± S.E.M.*

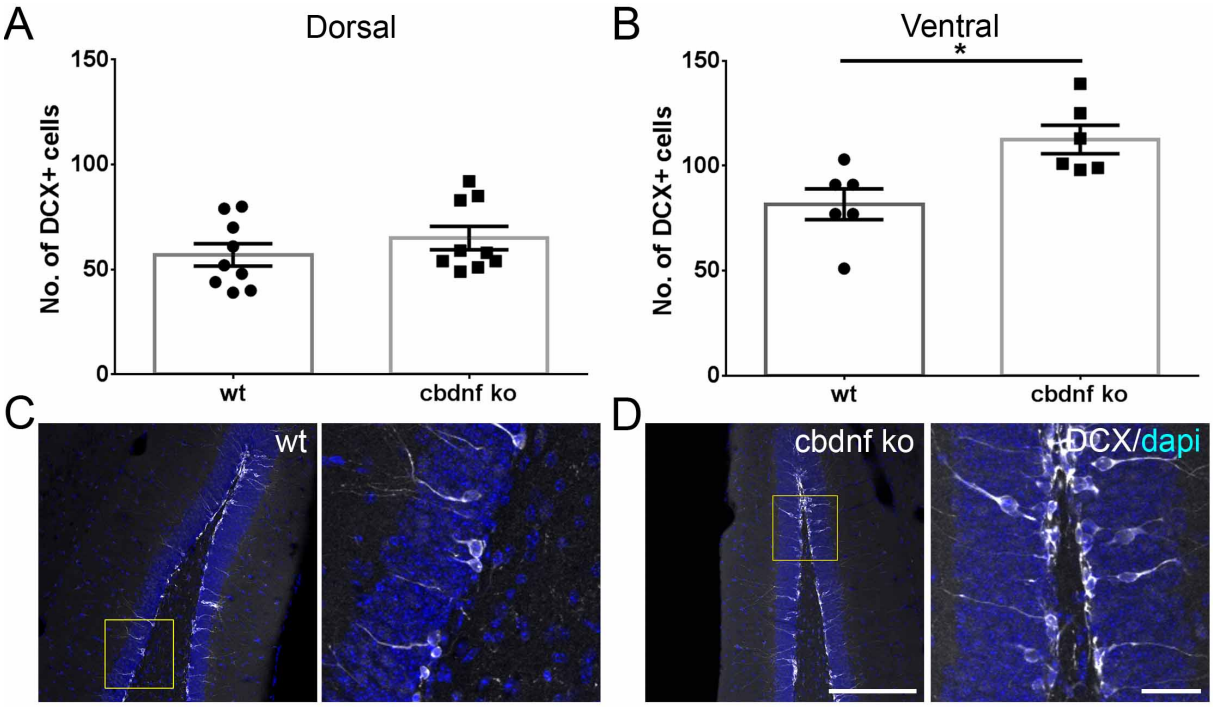

Figure 21 The number of DCX-positive immature neurons is increased in the ventral hippocampus of three-month-old granule cell-specific BDNF knockouts.

*A, B) The number of DCX+ immature neurons was determined in comparison to wildtype control animals. Each data point reflects the total number (No.) of DCX-positive cells per image. Data was obtained from three (dorsal) and two (ventral) microscopy images per animal. Three animals per genotype was used. Unpaired t-test, p = 0.317 (dorsal), p = 0.0116 (ventral). C, D) Representative overview images and high-resolution images of DCX+ neurons in the dentate gyrus of the hippocampus. Dapi was used as counterstain. Scale bar 200 µm and 20µm. Shown are mean values ± S.E.M.*p< 0.05.*

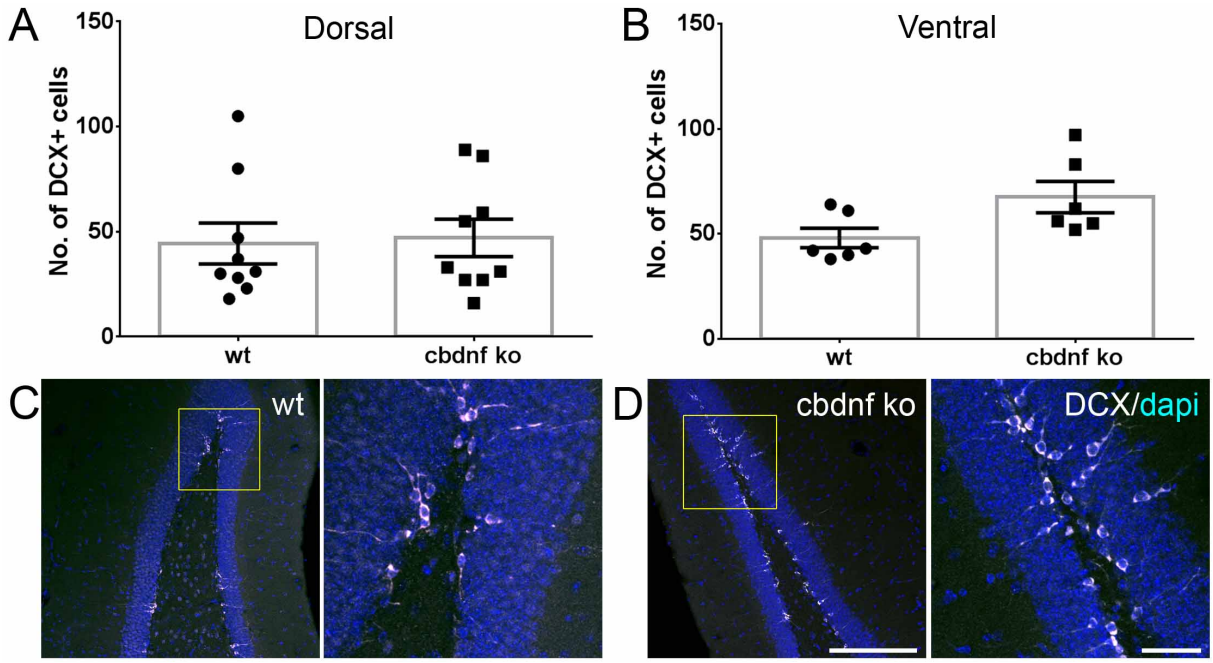

Figure 22 The number of DCX-positive immature neurons is normal in the ventral hippocampus of six-month-old granule cell-specific BDNF knockouts.

A, B) The number (No.) of DCX+ immature neurons was determined in comparison to wildtype control animals. Each data point reflects the total number (No.) of DCX-positive cells per image. Data was obtained from three (dorsal) and two (ventral) microscopy images per animal. Three animals per genotype was used. Unpaired t-test, p = 0,8423 (dorsal), p= (ventral) Unpaired t-test, p = 0.317 (dorsal), p = 0.0116 (ventral). C, D) Representative overview images and high-resolution images of DCX+ neurons in the dentate gyrus of the hippocampus. Dapi was used as counterstain. Scale bar 200 µm and 20µm. Shown are mean values ± S.E.M.

The phenomenon of adult neurogenesis in the hippocampus is age-dependent in the mouse. Therefore, it was checked whether a decline in the number of DCX+ neurons is observed in older compared to younger mice. In the dorsal hippocampus, in both wildtype and *cBdnf* KO there was just a slight tendency of a reduced number of DCX+ cells in six-month-old compared to three-month-old animals (Fig. 23A). In the ventral hippocampus, in both wildtype and *cBdnf* KO mice, there was a significant reduction in the number of DCX+ cells in six-month-old compared to three-month-old animals (Fig. 23B). This experiment supports the view that the increased

number of DCX+ positive cells in *cBdnf* KO mice is due to the genetic state of the animals and might reflect a delay in the maturation of adultborn neurons.

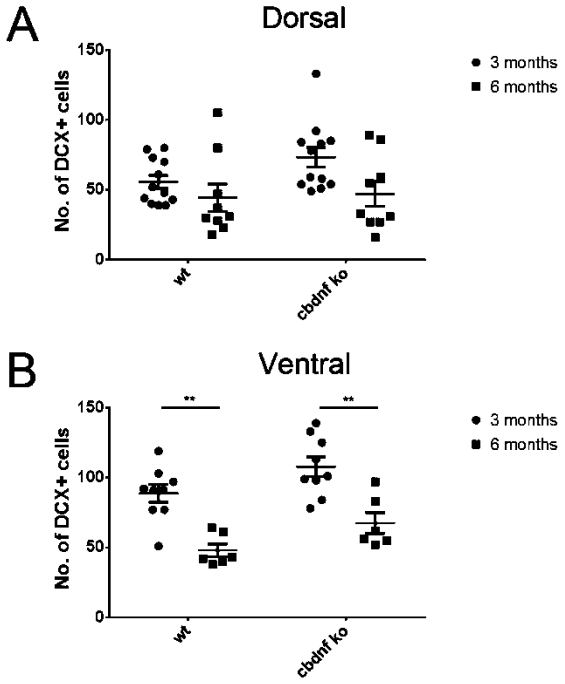

Figure 23 Age-dependent decline in the number of DCX-positive immature neurons in the ventral hippocampus of wildtype and cBdnf KO mice.

*The number (No.) of DCX+ immature neurons was determined in confocal images of the dorsal and ventral hippocampus. The total number (No.) of DCX-positive cells per image was determined from three (dorsal) or two (ventral) microscopy images per animal. Three animals per genotype was used. Shown are mean values ± S.E.M. A) Dorsal hippocampus, Two way ANOVA, p- value of Interaction = 0.8897, Genotype = 0.3798, Age = 0.3159. B) Ventral hippocampus, Two way ANOVA, p- value of Interaction = 0.2607, Genotype = 0.0953, Age = 0.0024. **p< 0.01.*

3.9 More stage III adult-born granule neurons in mossy fiber-specific BDNF KO mice

An increased number of DCX+ cells at a specific age raised the question which type of DCX+ cells is more often found in three-month-old *cBDNF* KO mice. The developmental stage of DCX+ adult-born neurons can be classified according to the pattern of dendritic arborization of the immature neuron, on base of the DCX immunolabel (Deusser et al., 2015). Early DCX+ cells (stage I) have no or short processes, intermediate DCX+ cells (stage II) have processes within the GCL, and late DCX+ cells (stage III) are present with dendritic branches reaching into the molecular layer. DCX+-neuron staging in three-month-old mice showed that more DCX+ cells in the ventral hippocampus of *cBdnf* KO belong to stage 2 and stage 3 (Fig. 24). At an age of six month, the *cBdnf* KO had significantly more DCX+ cells in all three stages (Fig. 24 E-G). The analysis of DCX+ cells in the hippocampus of *cBdnf* KO mice confirms a fundamental

neurobiological consequence of BDNF deletion from adult granule neurons on the hippocampal system.

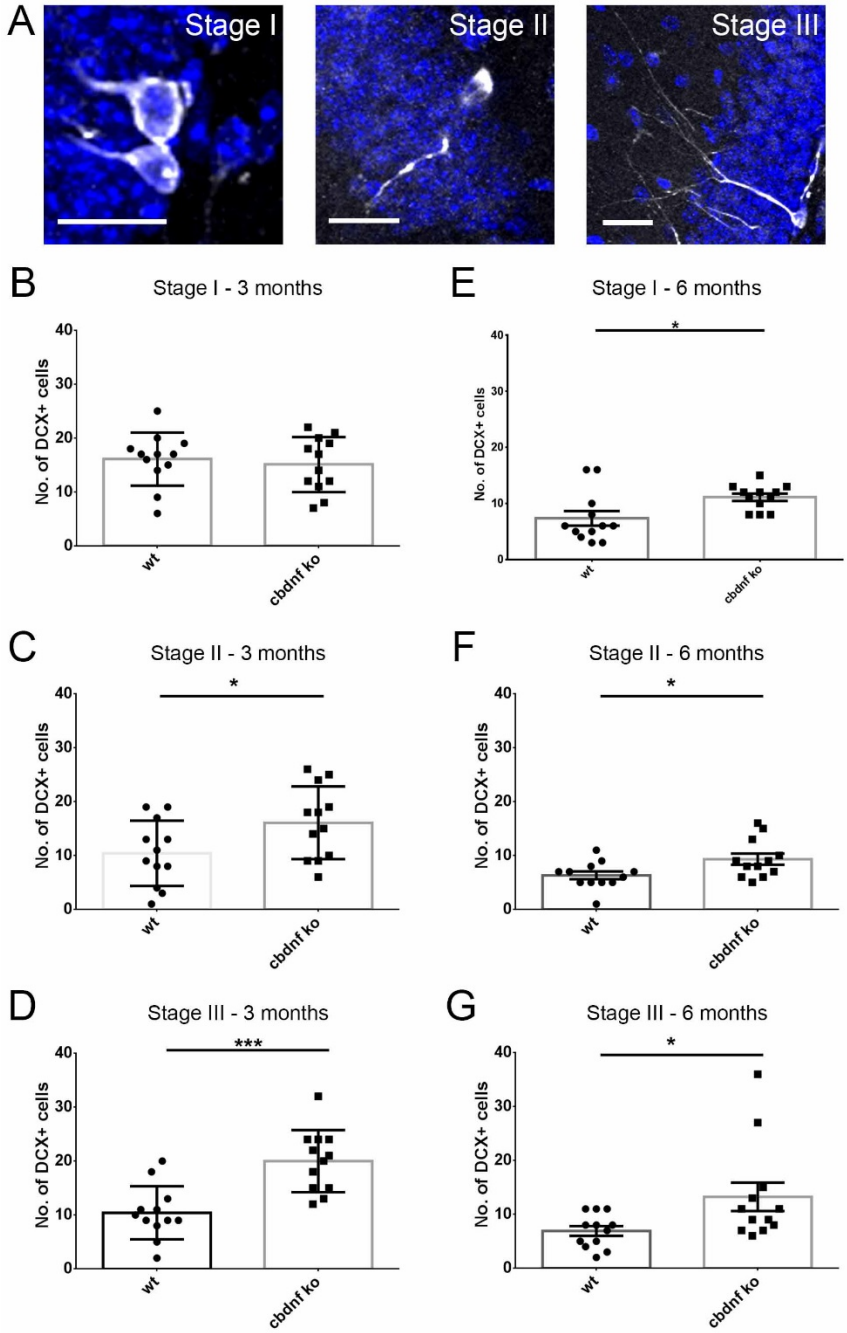

Figure 24 Immature neuron staging in granule cell-specific BDNF knockouts.

A) Representative images indicating different developmental stages (stage I - III) of DCX + immature neurons in the subgranular zone of the hippocampus. All scale bar represents 20 um. Each data point reflects the total number (No.) of DCX-positive cells of respective stage per image. Data was obtained from four ventral microscopy images per animal. Three animals per genotype was used. B - G) Number (No.) of DCX+ neurons in different developmental stages at indicated age and genotype. Compared are wildtype and cBdnf KO mice. Statistics, Unpaired t-test: p = 0.6302 (B), p = 0.0416 (C), p = 0.0003 (D). E-G) In all the three stages, there was a significant increase in number of DCX positive cells in cBdnf ko in comparison to wt. Statistics, Unpaired t-test, p = 0.0198 (E), p =

*0.0274 (F), p = 0.0397 (G). Statistical significance *p< 0.05, ***p<0.001. Shown are mean values ± S.E.M.*

3.10 The dendritic branching is disturbed in adult-born DCX+ neurons of granule cell-specific BDNF knockouts

Changes in the developmental profile of DCX+ neurons of *cBdnf* KO mice let me ask whether the dendritic branching of stage III DCX+ neurons is also affected in these animals. To analyze the dendrites of adult-born neurons, confocal images covering the dendritic tree of DCX+ neurons (z-stack covering 20-30 μm, resolution of 207 nm per pixel) were assembled in the software Imaris. With the help of a tracing tool, the length of the primary dendrite, the total length and the branching and arborization of DCX+ dendrites was determined in x,y-z image stacks. The analysis showed no change in the length of the primary dendrite at different ages (Fig. 25). Nevertheless, the total dendritic length was slightly, but significantly reduced in the *cBdnf* KO mice compared to their wildtype littermates (Fig. 25 D,E). The dendrite branching from soma was considered as the primary dendrite. The branches formed from the primary dendrite was counted as secondary, in general all the primary branches only split into two secondary branching. The dendritic branching pattern per se, was not changed between the wildtype and *cBdnf* KO mice, as indicated by the same number of tertiary dendritic branches. (Fig. 25 F,G).

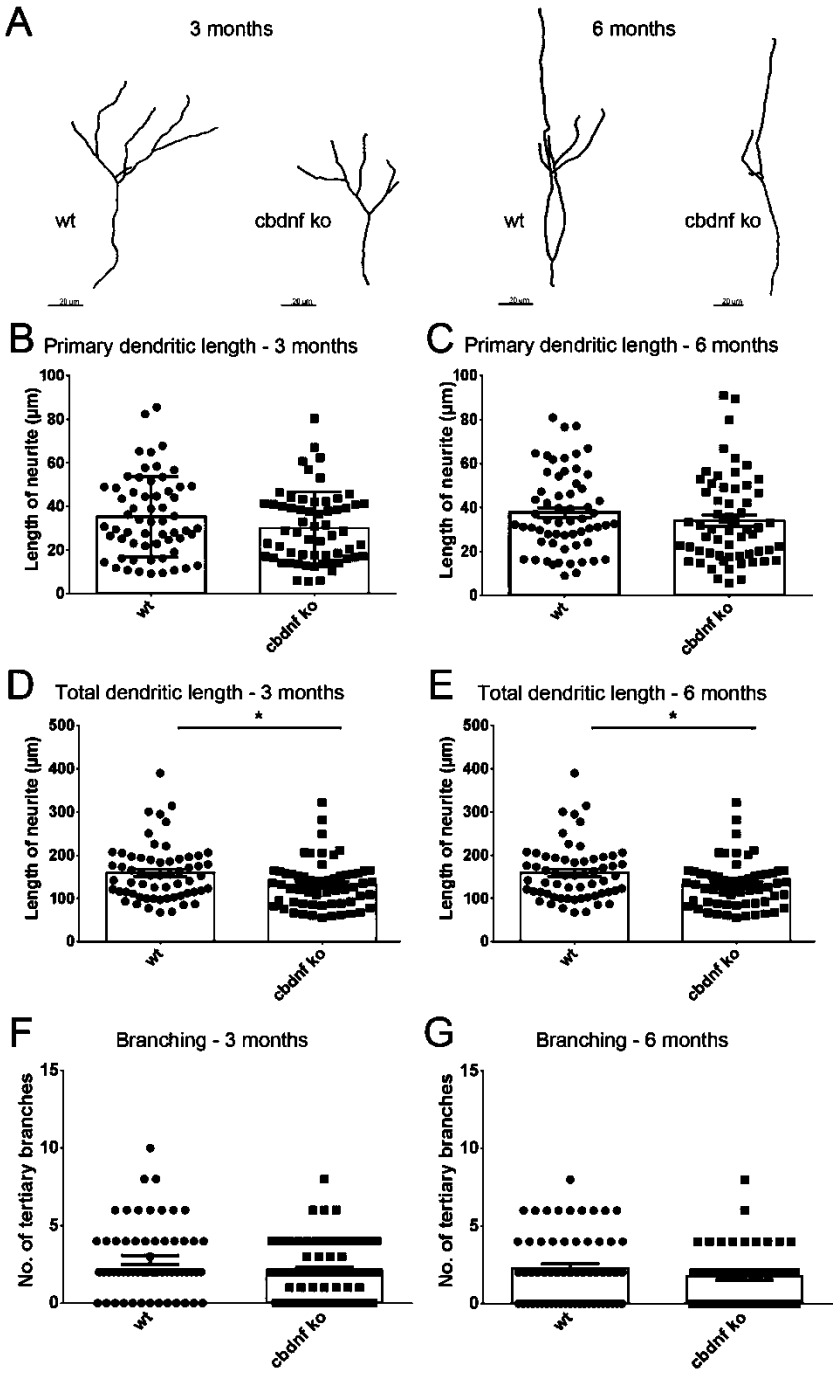

Figure 25 Morphological analysis of DCX+ neurons in granule-cell specific Bdnf KO mice.
*A) Morphology of representative neurons after dendrite reconstitution in wildtype (wt) and cBdnf KO mice of an age of three or six months. B), C) Primary dendritic length was similar between wt and cBdnf KO mice. Unpaired t-test, p = 0.1165 (3 months), p = 0.2928 (6 months) D - E) Total dendritic length was significantly shorter in cBdnf KO mice in comparison to wt littermates. Mann Whitney t-test, p = 0,048 (3 months), 0.0156 (6 months), *p< 0.05. F - G) The number of branching points were of equal number in wt and cBdnf ko in both 3 and 6 months old mice. Mann Whitney t-test, p = 0,1032 (3 months), 0,3217 (6 months). Each data point represents primary or total neuronal length or branches from one single neuron. Twenty neurons were measured from each animal. Three animals per genotype was used. Shown are mean values ± S.E.M.*

3.11 The gross size of the mossy fiber synapse area is not changed in cBdnf KO mice

It has been discussed whether an increase or decrease in BDNF availability in the mossy fiber region causes mossy fiber sprouting or a decrease in the size of the Stratum lucidum, due to a reduced number of mossy fiber synapses (Buckmaster, 2012; Scharfman et al., 1999). Therefore, the size of the mossy fiber area was measured on base of confocal images showing anti-Zinc transporter 3 (ZnT3) immunolabels of the hippocampus. ZnT3 is highly expressed in mossy fiber synapses and therefore anti-ZnT3 immunolabels are often used to lable the mossy fiber synapse field. The analysis showed that the gross morphology of the Stratum lucidum area with mossy fiber synapses is not changed between wildtype and *cBdnf* KO mice at the age of 3 months (Fig. 26), meaning at an age, when the DCX+ neurons in the dentate gyrus are already affected by the local BDNF deletion.

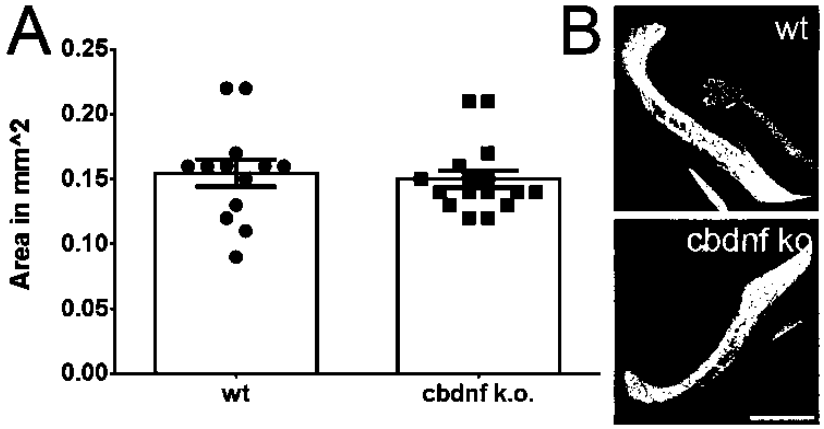

Figure 26 The size of the mossy fiber area is not changed after Cre-mediated deletion of BDNF from granule neurons.

A) Every 10th section from the dorsal hippocampus was stained for ZnT3. Four sections per animal was measured and three animals per genotype was used. The ZnT3 labels the complete field with mossy fiber synapses. ZnT3 area, an exclusive mossy fiber label, was measured, there was no change between the wt and cBdnf ko. The ZnT3 label-positive area was marked in ImageJ software and the area positive for ZnT3 immunoreactivity was measured. Each data point was area from individual section. Mann Whitney t-test, p = 0.3766. B) Representative images of ZnT3 area of wildrtype and cBdnf ko, post-labeled with ZnT3. Scale bar 200 µm.

3.12 The number of Parvalbumin-positive interneurons is not changed in cBdnf KO mice

Parvalbumin-positive (Parv+) interneurons belong to one of the most important GABAergic population in the hippocampal circuit (Kosaka et al., 1987). These inhibitory neurons form pre-synaptic connection with CA3 pyramidal neurons and importantly receive pre-synaptic connections from glutamatergic mossy cells and granule neurons via filopodia from mossy fiber

bouton synapses (Bischofberger et al., 2006a; Nicoll and Schmitz, 2005). The Parv+ interneurons contribute to the process of memory precision, contextual memory retrieval and pattern separation functions of the hippocampus. Parv+ interneurons regulate the output of CA3 pyramidal neurons via feed-forward inhibition (Danzer and McNamara, 2004; Hashimotodani et al., 2017). It is known that reducing axonal BDNF can affect the number of Parv+ interneurons in target tissues (Altar et al., 1997). Hence, the number of Parv+ interneurons in along the blade of the CA3 region and stratum lucidum was manually counted in three-month-old mice. Neither in dorsal, nor in the ventral hippocampus, a difference in the number of Parv+ interneurons was observed (Fig. 27).

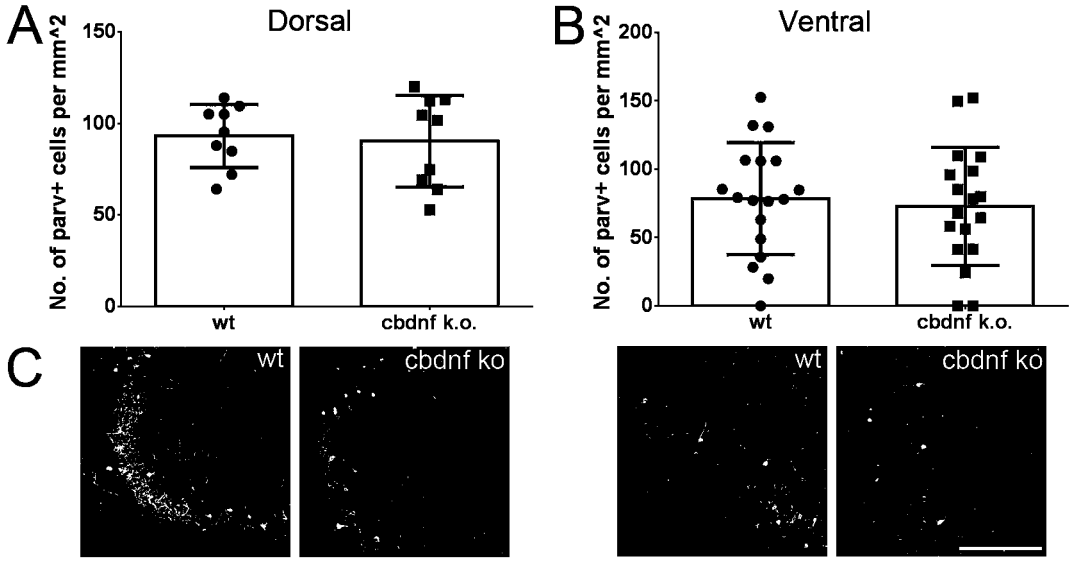

Figure 27 Number of Parvalbumin-positive interneurons is not changed in the mossy fiber area of granule-cell specific Bdnf KO animals.

A - B) In the dorsal and ventral hippocampus, the number of Parv+ interneurons in 3 month old wildtype and cBdnf KO animals was counted. Statistics, Unpaired t-test, p = 0.7831 (dorsal), 0.698 (ventral). Each data point was total number of parv+ cell from individual section, three sections from dorsal and six sections from ventral hippocampus was used. Three animals per genotype was used. C) Representative confocal images showing Parv+ interneurons in the dorsal and ventral hippocampus of wildtype and of cBdnf KO animals. Scale bar 200 µm.

3.13 Structural tracing of mossy fiber synapses in granule-cell specific *Bdnf* KO mice

Recent studies showed that anti-BDNF immunoreactivity is not only present in the corpus of the mossy fiber bouton, but is also seen in small mossy fiber synapse filopodia that project to local Parv+ interneurons. This indicates that anterograde BDNF secretion may regulate hippocampal function by feed forward inhibition mechanisms (Danzer and McNamara, 2004). As BDNF is known to be a major factor for structural plasticity at synapses, we wanted to find out whether

presynaptic deletion of BDNF would also affect the structural parameters in mossy fiber terminals.

To analyze the structure of mossy fiber terminals in *cBdnf* KO mice, GFP reporter mice were bred into CNTF-Cre mice and into the corresponding *cBdnf* KO mice. Then mossy fiber synapses were labeled against GFP, BDNF and vGlut. Anti-GFP labels were used to visualize the Cre-positive, GFP positive mossy fiber synapses. Anti-BDNF labels were used to verify the Cre-mediated deletion of BDNF in the presynapse, and anti-vGlut1 was used as a presynaptic counterstain. High-resolution confocal analysis showed that indeed GFP-positive mossy fiber boutons showed almost no anti-BDNF immunoreactivity, thus again confirming the presynaptic origin of the BDNF label, but the GFP signal was not sufficiently present in the small mossy fiber filopodia (Fig. 28). Therefore, it was necessary to develop a new strategy to trace mossy fiber synapses.

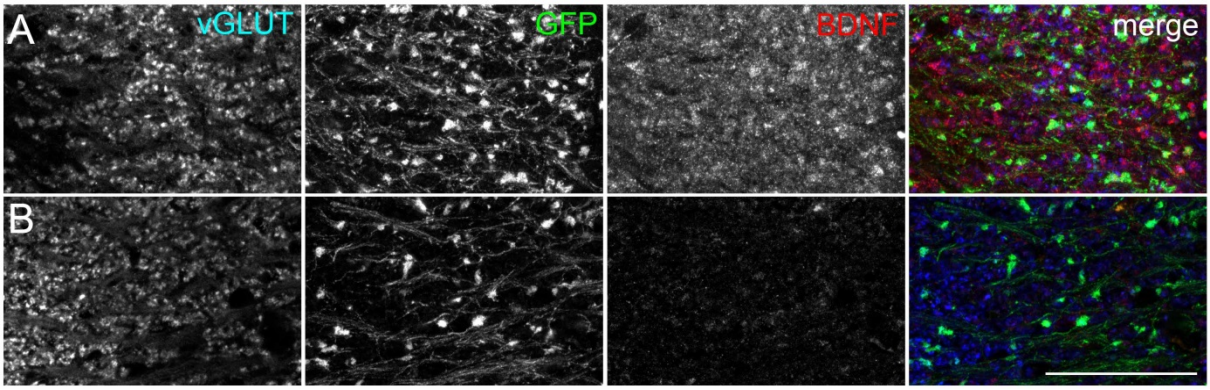

Figure 28 High-resolution confocal analysis of Cre-mediated GFP expression in mossy fiber terminals of granule cell-specific BDNF knockouts.

Shown are immmunofluorescence stainings in the Stratum lucidum of the hippocampus against GFP, BDNF (mab#9) and vesicular glutamate transporter (vGlut). A) Corresponding staining in wildtype mice (CNTF::Cre tg/+ BDNF +/+ CAGeGFP tg/+ mice). B) Corresponding staining in granule cell specific Bdnf KO mice (CNTF::Cre tg/+ Bdnf$^{fl/fl}$ CAGeGFP tg/+). After Cre-mediated BDNF deletion, GFP-positive mossy fiber boutons become BDNF immuno-negative. Cre-induced GFP labels could well mark mossy fiber boutons, however, the typical filopodia of mossy fiber synapses remained invisible. Scale bar 25 µm.

GFP is a soluble protein in the cytosol and can often not enter fine structures of cells, such as filopodia or microdomains. For this reason, a viral construct was cloned that contained two fluorescent proteins, Tandem tomato and GFP, with a LCK myristoylation/palmitoylation consensus sequence at the aminoterminal end.

The construct consists of an artificial Kozak sequence followed by a short aminoterminal sequence encoding the LCK myristoylation / palmitoylation consensus sequence (MGCVCSSNPEDD) (Kabouridis et al., 1997; Rathod et al., 2012) followed by a 5 amino acid linker sequence (GGSGG) coupled to eGFP with a deleted start ATG.

Myristoylation is the covalent attachment of myristic acid to an aminoterminal glycine residue of a protein substrate through an amide bond (Boutin, 1997). Palmitoylation is a covalent

attachment of fatty acids, mostly to cysteine residues of proteins. Both posttranslational modifications enhance the hydrophobicity of a protein and improve the targeting and binding of proteins to the membrane (Resh, 1999). When coupled to fluorescent proteins, membrane-targeted fluorescent proteins are able to outline the plasma membranes of spines and filopodia and enable the visualization of structural plasticity events (De Paola et al., 2003).
To enable a tracing system that is under Cre control, we designed lentiviral vectors (Fig. 29) with the following components:

- Myristoylation and palmitoylation sequence (MGCVCSSNPEDD) preceding a TdTomato gene sequence with a double stop. A short linker sequence (GGSGGSGG) was placed between the membrane targeting sequence and the fluorescent protein.
- The MyrLCK-TdTomato sequence was flanked by *Lox2272* sites, a modified *LoxP* sequence (2272 feature – GGATACTT).
- Downstream of TdTomato, a MyrLCK-linker-GFP sequence was introduced.

The linker was found to be a vital part to ensure the plasma membrane targeting of the fusion protein. The *Lox2272* was used instead of the traditional Lox P site. A traditional LoxP site would create an artifical start ATG site upstream of the expected start ATG in the GFP, after Cre-mediated recombination. This unwished ATG site would create a frame shift in the expression of the MyrGFP. To avoid this problem, the *Lox2272* site was used.
In the cloning strategy, the Lox-2272 flanked MyrTdtomato was designed and synthesised. Then, the MyrTdtomato was cloned into a lentiviral vector (pLV-CAG; appendix - vector map 4) via a blunt EcoRV site. The vector pLV-CAG is a traditional self-inactivating lentiviral expression vector (third generation) with an intrinsic chicken-beta actin promoter (CAG). In a next step, the MyrGFP sequence (Map 2) was cloned downstream of the floxed MyrTdTomato gene cassette (Fig. 29).

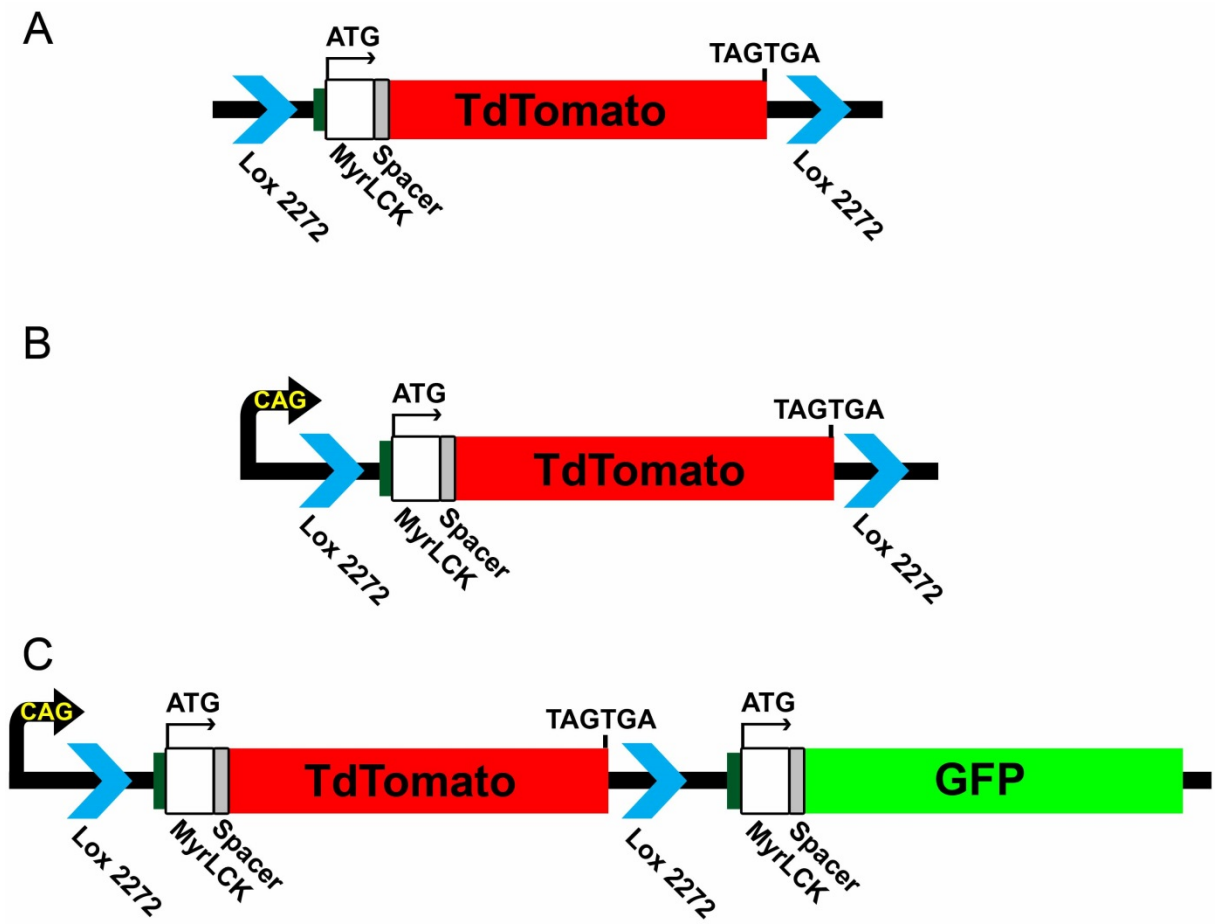

Figure 29 Cre-dependent myristoylation construct.
A) A construct containing Myr-Tdtomato was flanked by Lox2272 sites. B) The flanked Myr-Tdtomato was cloned under a CAG promoter in a self-inactivating lentiviral expression vector. C) A myristoylated and palmitoylated GFP sequence was finally introduced downstream of the second Lox2272 sequence to obtain the vector LV-CAG-floxed Myr-TDtomato/Myr-GFP.

The tracing vector was verified by DNA sequencing and the lentiviral vectors were produced according to standard methods. The viral titre was tested by infecting HEK cells for 48-72 hours. Cells were fixed and labeled with anti-RFP (TDtomato) and anti-GFP. Confocal imaging confirmed a clear membrane localization of the TdTomato protein (Fig. 30). However, few cells with Myr-GFP expression were observed, indicating that a certain amount of the viral vectors did not contain the TDtomato gene cassette, most likely due to recombination between the Lox2272 sites before viral packaging (Fig. 30).

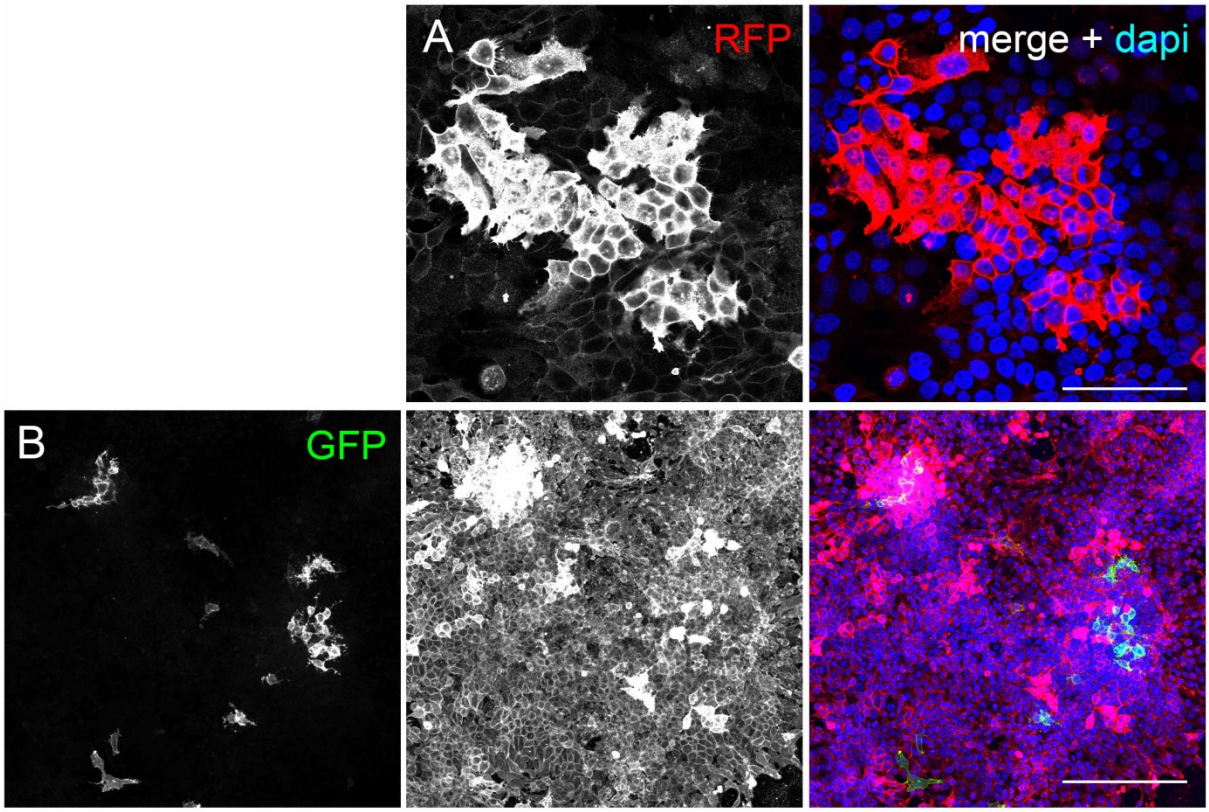

Figure 30 A Lentiviral tracing vector (LV-CAG-floxed Myr-TDtomato/Myr-GFP) expressed in HEK293 cells.

A) HEK cells were infected with the corresponding lentiviral construct. At 5dpi, the cells were fixed and labelled with dapi, RFP, and GFP. Shown is a confocal image indicating the targeting of virally expressed TdTomato to the plasma membrane. Scale bar 100 µm. B) Overview image (confocal) shows a preferential expression of Myr-TDtomato in most cells. However, single cell clones also show membrane-bound GFP, indicating Cre-independent GFP expression. Scale bar 200 µm.

In collaboration with the group of Prof. Philip Tovote in our institute, the virus was unilaterally injected into the dorsal dentate gyrus of two CNTF-Cre deleter mice (Fig 29A) (Tovote et al., 2016). At 7 day post infection (DPI), one animal was prepared for immunohistochemistry, while the second animal was investigated at DPI 14.

Vibratome sections (40 μm thick) were directly embedded and imaged with confocal microscopy. Notably, GFP expression was easy to see in the cell membrane of granule neurons, mossy fibers and some single astrocytes along the hippocampal fissure. In the mossy fiber and in the hilus, the Myr-GFP signal labeled *en passant* boutons, large mossy fiber terminals and even the fine mossy fiber filopodia at the axon terminals (Fig. 31-32). In the granule cell layer, the vector enabled the tracing of single dendritic spines (Fig. 32).

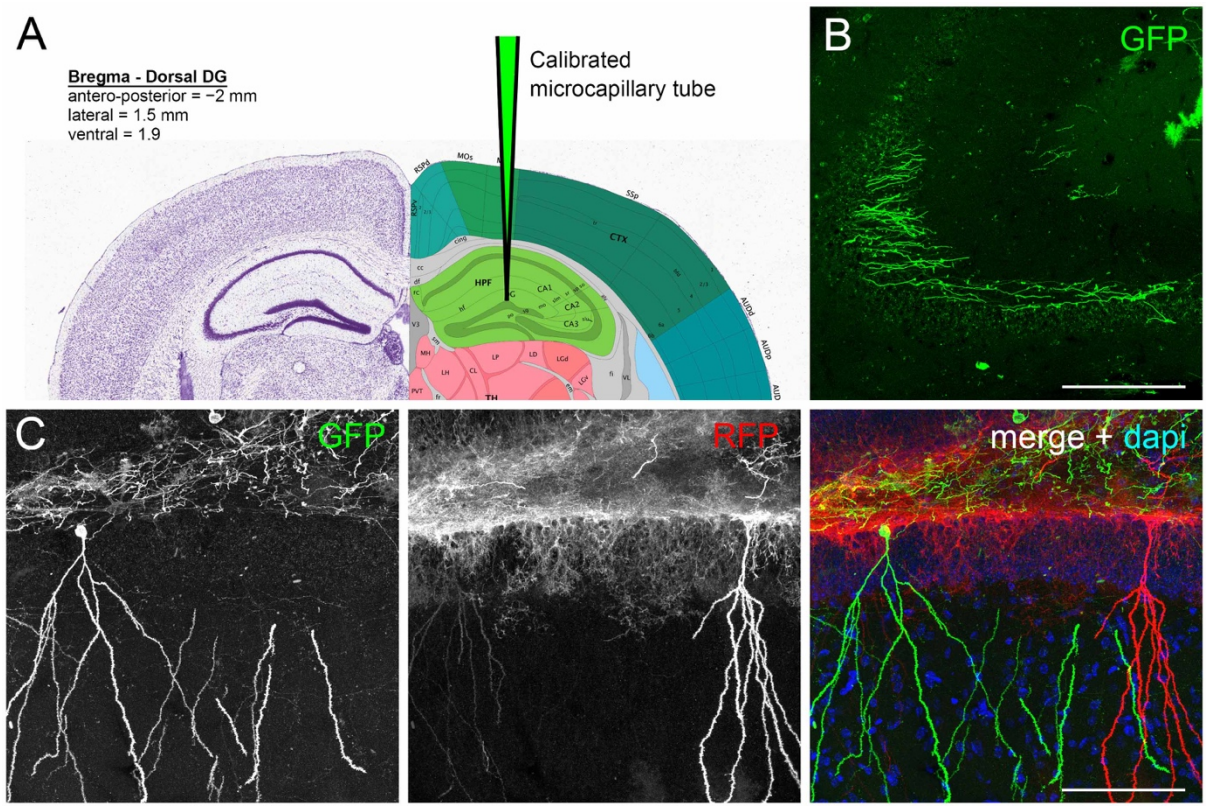

Figure 31 In vivo tracing of dentate gyrus granule neurons, dendrites and mossy fiber projections.

A) Schematic image depicting the location of viral injection in the hippocampus according to Bregma coordinates. 100 nl of the lentivirus was injected into the dorsal hippocampus of CNTF::Cre tg/+ Bdnf $^{fl/fl}$ mice. B) At 7dpi, the brain was fixed and fresh cut vibratome slices were imaged by confocal microscopy. The overview image shows the vector-based tracing of mossy fibers and the corresponding mossy fiber boutons. Scale bar 200 µm. C) Vibratome sections were labelled with dapi, GFP and RFP. Confocal imaging verified the dense expression of Myr-TDtomato and Myr-GFP in dendrites of granule neurons. Co-existence of GFP-labels and TDtomato labels indicates Cre-mediated excision of the TDtomato gene cassette in individual mature granule neurons. Scale bar 100 µm.

Confocal image of the mossy fiber-CA3 terminal showed the Myr-GFP expression along the mossy fiber axons (Fig. 32A). At higher resolution, the large mossy fiber boutons were seen at the stratum lucidum, the myristoylated GFP clearly showed the complete volume of the boutons and as well labelled whole length of filopodias (Fig. 32B). Also, the dendritic spines of dentate gyrus neurons are densely labelled by lentiviral Myr-GFP and Myr-TDtomato (Fig 29 C-E). This was further confirmed by imaging under super resolution microscopy, which showed the ability of MyrGFP expression from the Cre-dependent vector to effectively label dendritic spine heads. In subsequent experiments, it was tested to which extend the lentiviral construct was infecting neurons along the septo-temporal axis (Fig. 33). Coronal sections were collected from bregma 42 until bregma 56, as described in (Franklin and Paxinos, 2008). Every sixth section from bregma 42 were post-labelled with anti-GFP and anti-RFP and it was observed that the injected

virus diffused around 900 um that would be approximately from bregam 42-50 (-1.34 mm - -2.30 mm).

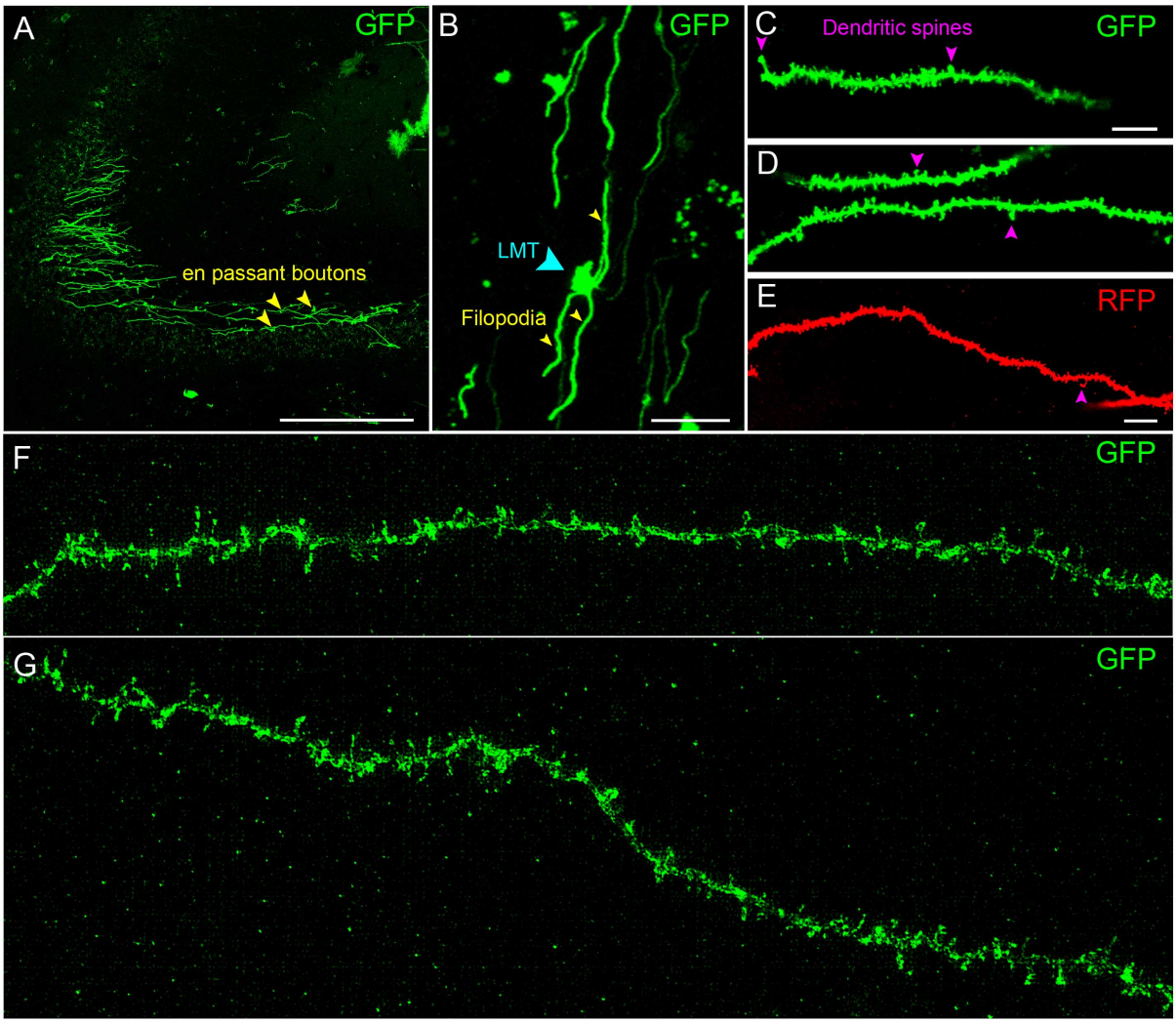

Figure 32 Lentiviral tracing of synaptic structures of adult granule neurons in the hippocampus.

A) Confocal image showing Myr-GFP expression in mossy fiber axons (image also used in Fig. 29B). En passant mossy fiber boutons are indicated by yellow arrows. Scale bar 200µm. B) High-resolution maximum intensity projection image showing axonal mossy fibers and a single large mossy fiber terminal (LMT). Synaptic filopodia are indicated. Scale bar 20µm. C - E) Dendritic spines of dentate gyrus neurons are densely labelled by lentiviral Myr-GFP or Myr-TDtomato. Shown is the endogenous GFP signal (in C, D). TDtomato was post-labeled with anti-RFP (in E). Scale bar 10 um. F - G) Super-resolution image (SIM microscopy, in collaboration with Prof. M. Sauer, University of Würzburg) of Myr-GFP expressed by single dentate gyrus granule neurons. The GFP protein was post-labelled with anti-GFP / Alexa488. Shown is a maximum intensity projection of 2 um. Scale bar 10 um.

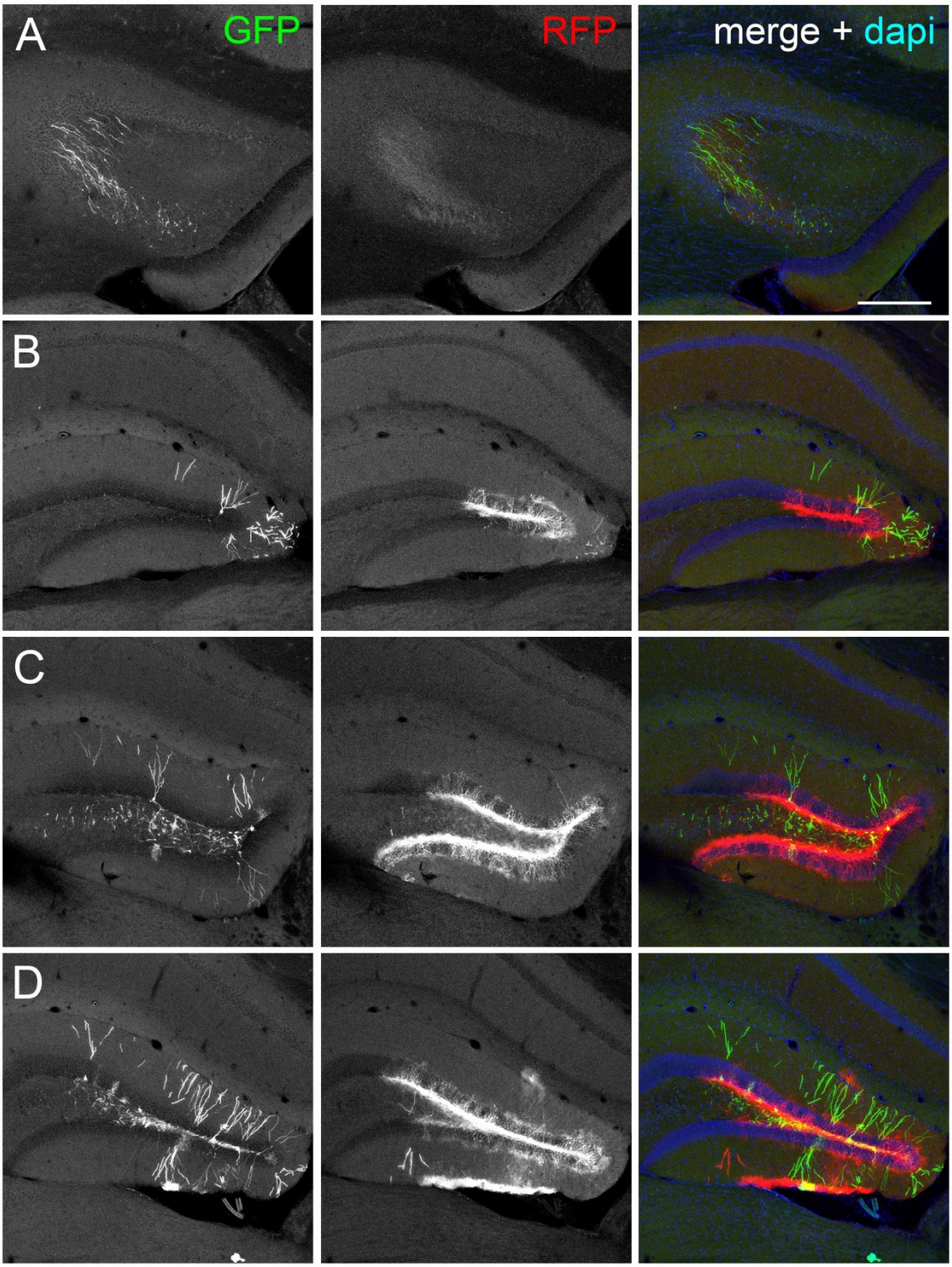

Figure 33 Dispersion of lentiviral vectors after local injection.

The figure shows the expression pattern of the vector LV-CAG-floxed Myr-TDtomato/Myr-GFP at day 14 post-infection. Coronal hippocampal sections from cBdnf KO mice were immunolabeled against GFP and RFP. Dapi was used as nuclear counterstain. The images show the expression pattern of lentiviral Myr-GFP and Myr-TDtomato along the septo-temporal axis. A - D) Starting at position Bregma 42, every 6th section (40µm thick) of the dorsal hippocampus was labelled and imaged by confocal microscopy. The images confirm that the viral infection with a volume of about

100 nl, is sufficient to label single granule neurons over a distance of approximately 900 µm in the septo-temporal direction. Scale bar 200 µm.

3.14 Cre-independent expression of Myr-GFP by lentiviral vectors

Cell culture experiments indicated that the lentiviral vector LV-CAG-floxed Myr-TDtomato/Myr-GFP can cause an unwished Cre-independent expression of Myr-GFP (Fig. 34). To find out whether Myr-GFP signals after in vivo expression might be Cre-independent, the corresponding tracing virus was injected into the dorsal dentate gyrus of 8-week-old wildtype mice. At day 7 after infection, mice were perfused and vibratome sections were post-labelled with anti-RFP and anti-GFP. Notably, confocal imaging confirmed a considerable Myr-GFP expression in the Cre-negative granule neurons (Fig. 34), most likely due to unavoidable plasmid recombination in the course of the vector production process.
For this reason, other strategies for Cre-dependent tracing of granule neuron synapses needed to be tested.

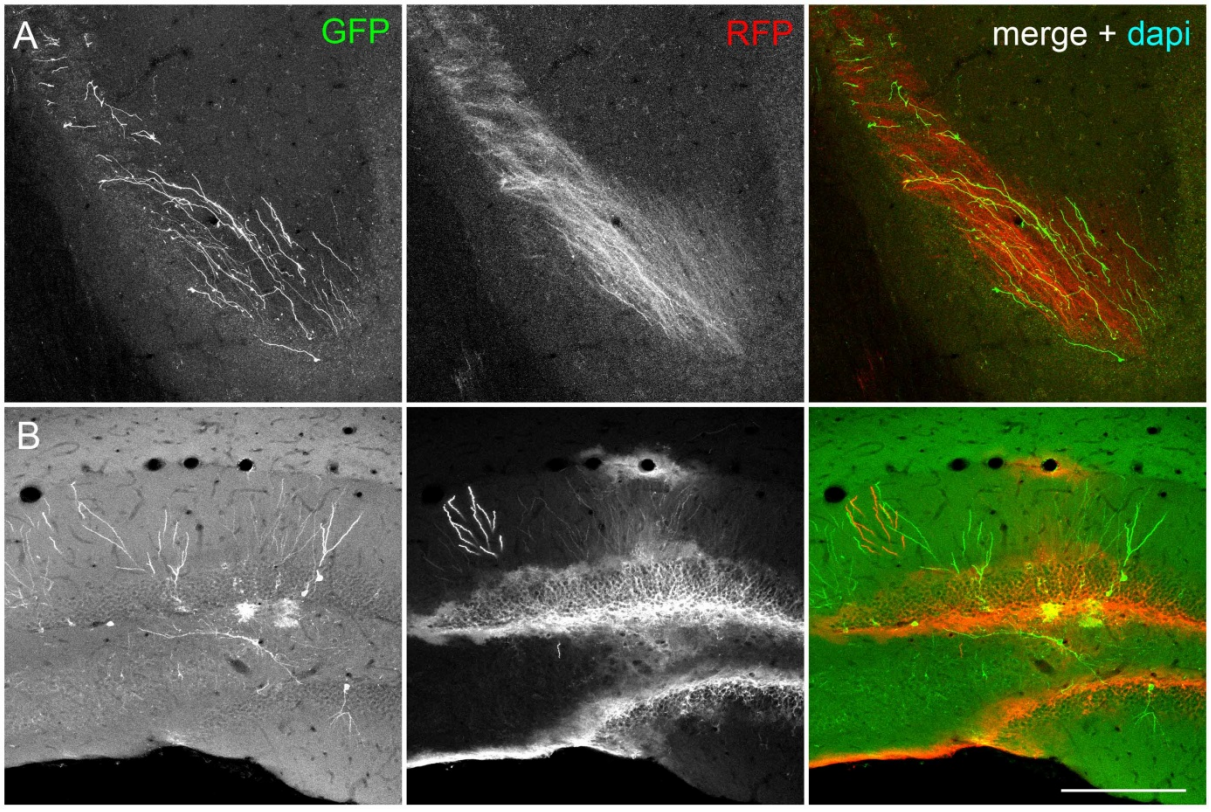

Figure 34 Cre-independent Myr-GFP expression from LV-CAG-floxed Myr-TDtomato/Myr-GFP vectors.

Wildtype brains were infected with lentiviral CAG-floxed Myr-TDtomato/Myr-GFP vectors. Coronal sections were investigated at DPI 14. Shown are confocal images. Both fluorescent proteins were immunolabeled against GFP and RFP. Dapi served as counterstain. A, B) GFP-positive immunosignals indicate Cre-independent expression of GFP in mosy fibers (in A) and granule neurons (in B). Scale bar 200 µm.

3.15 Cre-positive tracing vector to label granule cell synapses

In order to obtain the possibility to trace of mossy fiber synapses and granule cell spines, a tracing was designed that expresses the Myr-GFP, but also a Cre under control of an internal ribosomal entry site (IRES). The vector was cloned under the pLV-CAG backbone (appendix, vector map 4). An IRES Cre sequence was cloned downstream of the Myr-GFP to obtain the vector pLV-CAG-Myr-GFP-^{IRES}Cre (Fig. 35). The clone was verified by DNA sequencing and lentiviral particles were produced according to standard methods. The viral titre was tested by infecting HEK cells for 4 days. The cells showed a clear membrane localization of the GFP protein and Cre recombinase expression in GFP+ cells. Then hippocampal neurons (day in vitro 14) were infected with the corresponding LV-CAG-Myr-GFP-^{IRES}GFP virus. Cells were fixed and post-labelled at DIV21. Confocal imaging verified the strong expression of the vector in hippocampal neurons and verified the efficient targeting of the protein to plasma membranes and spines (Fig. 36).

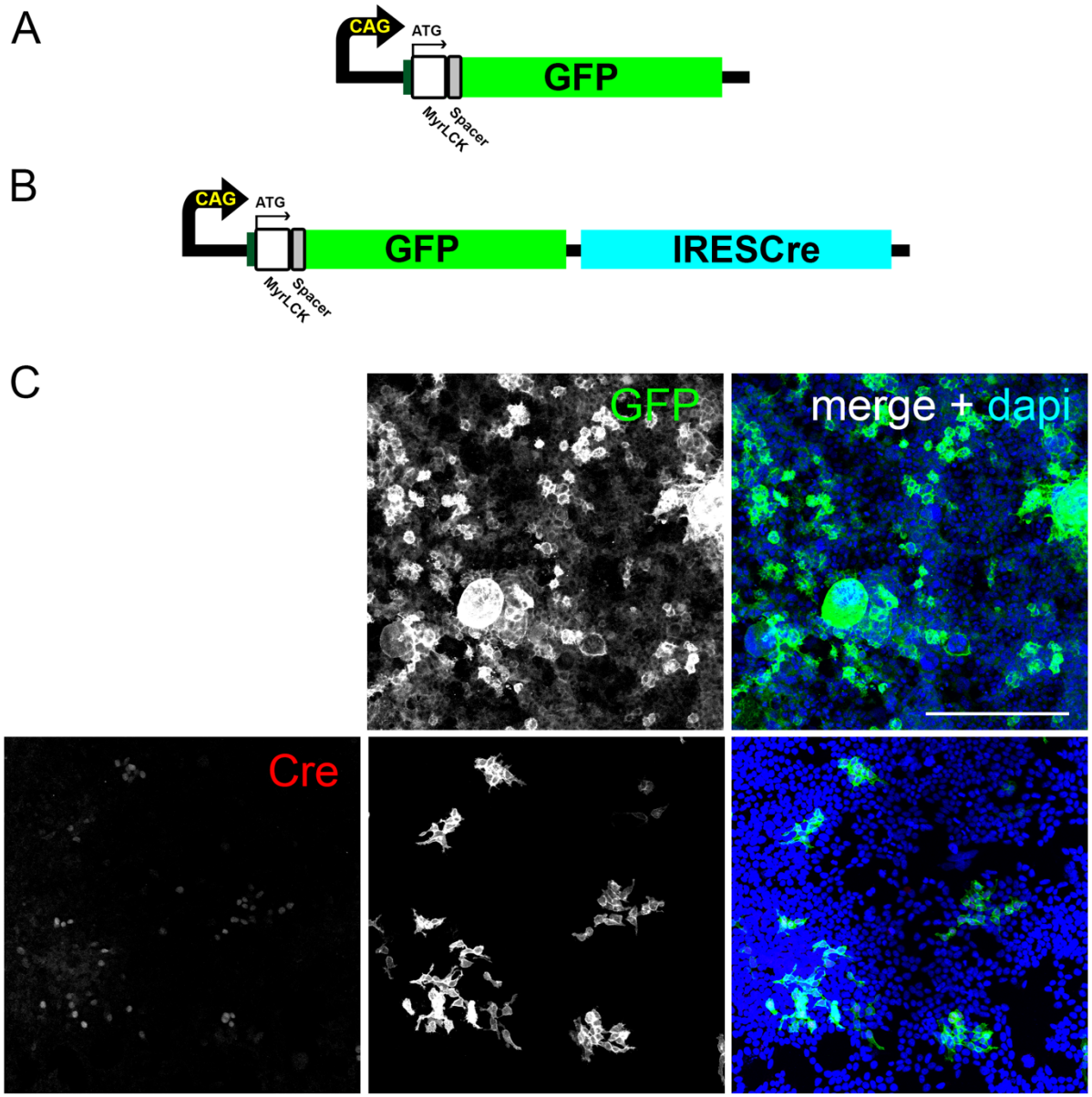

Figure 35 pLV-CAG-Myr-GFP-IRESCre, a biscistronic vector to express Myr-GFP and Cre. *A) Myr-GFP was cloned under control of the CAG promoter. B) An IRES-Cre sequence was introduced downstream of the CAG-MyrGFP construct. C) Confocal image showing HEK cells after infection with LV-CAG-Myr-GFP-^{IRES}GFP vectors. At DPI 4, the cells show the specific expression of Myr-GFP and Cre recombinase. Scale bar 200 µm.*

To better visualize the plasma membrane targeting of Myr-GFP and to better visualize how Myr-GFP can outline the neuronal spine morphology, super resolution imaging (SIM) was performed (Fig. 36). As shown in Fig. 36B, Myr-GFP is lining out the plasma membrane of neuronal dendrites, thus indicating that the label can be used as a cell surface counterstain. Images were reconstructed using IMARIS and show that the high signal intensity given by Myr-GFP can outline the spine volume (Fig. 36C). These experiments show that LV-CAG-Myr-GFP-^{IRES}Cre vectors are suited to label synaptic structures and are also able to delete floxed genes due to the bicistronic expression of Cre from the same vector.

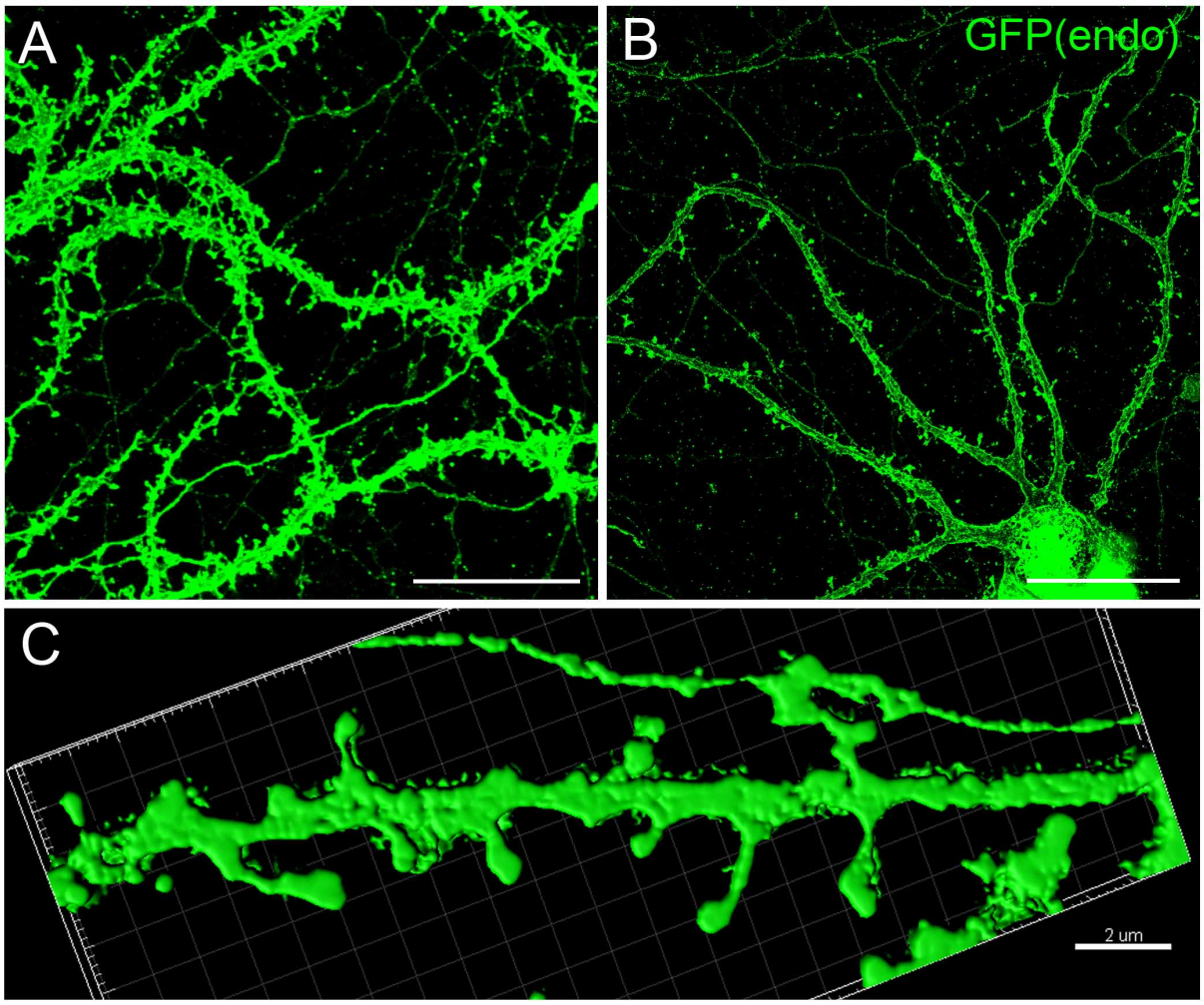

Figure 36 Hippocampal neurons expressing LV-CAG-Myr-GFP-IRESCre vectors.

Hippocampal neurons were infected with CAG-Myr-GFP-IRESCre lentivirus. A) Confocal image showing the endogenous expression of Myr-GFP in dendritic spines of mature hippocampal neurons at DPI 5. B) SIM microscopy image of endogenous Myr-GFP in dendritic spines of mature hippocampal neurons (DIV 24) at DPI 5. Scale bar 20 um. C) Reconstruction image of Myr-GFP signals in dendritic spines. Scale bar: 2 µm. Myr-GFP outlines the complete volume of the dendritic spines.

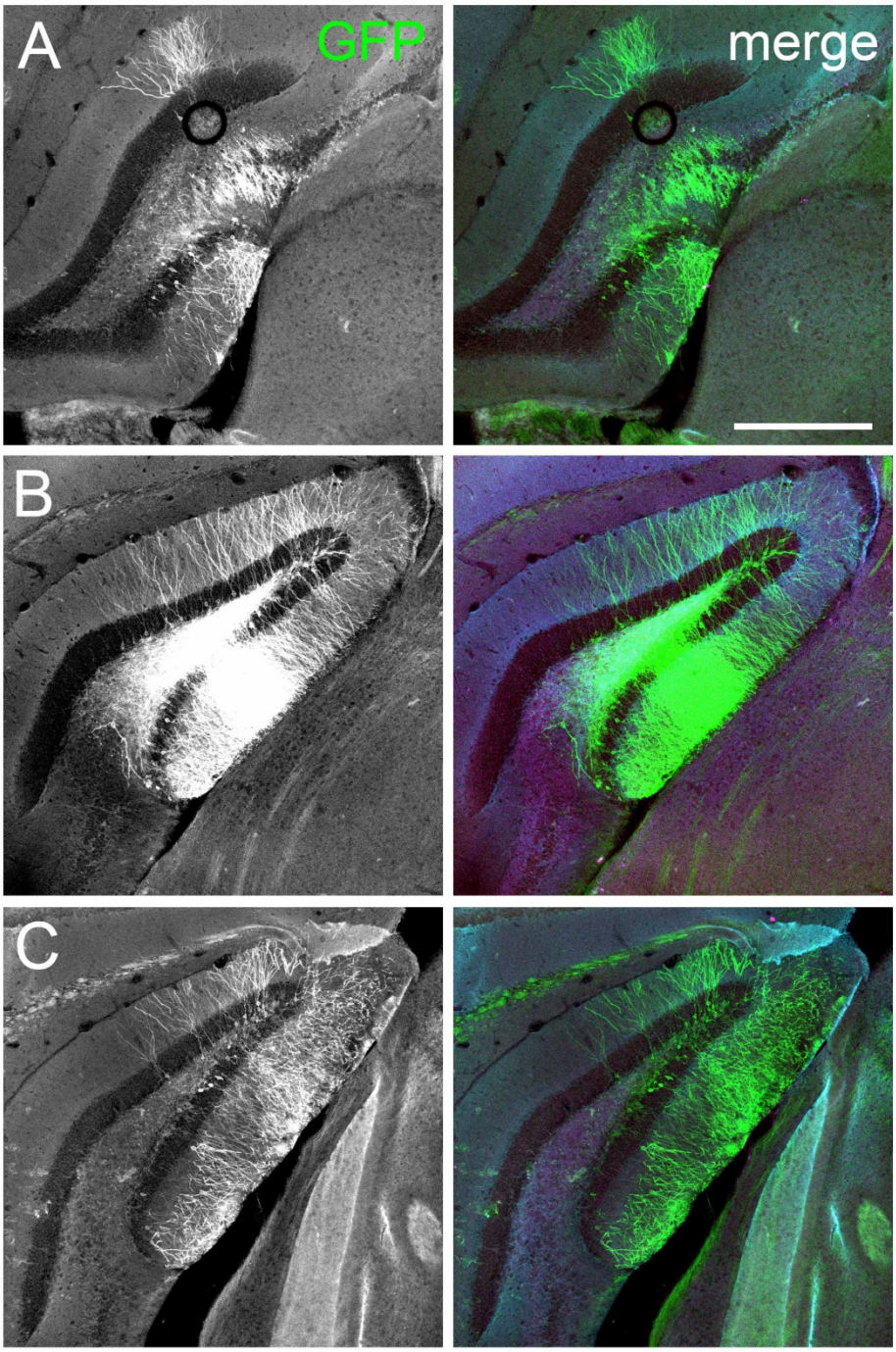

Figure 37 In vivo expression of LV-CAG-Myr-GFP-IRESCre vectors.

100 nl of the LV was injected into the dorsal hippocampus of wildtype animals (as shown in Fig. 29A). The images represent localization of Myr-GFP in three different animals. A - C), At DPI 14, the brain was fixed, and the sections were post-labelled with anti-GFP and dapi. The overview images (confocal) show the strong expression of the corresponding construct in granule neurons. Scale bar 200 µm.

3.16 Lentiviral flip-excision (FLEx) vector for Cre-dependent granule cell tracing:

Bicistronic expression of Myr-GFP and IRES-Cre is suited to be used in mice with floxed genes. However, to further test whether it is possible to distinguish Cre-positive granule neurons from Cre-negative granule neurons in CNTF-Cre deleter mice, we wanted to exploit a dual colour FLEx system for lentiviral vectors. In the FLEx system, a Cre-mediated switch allows to bring open reading frames under control of an intrinsic promoter (Schnutgen et al., 2003). The vector system was designed as follows (Fig. 38).

- The Myr-TdTomato sequence was flanked by the *Lox2272 and LoxP* sequence.
- Downstream of TdTomato, a Myr-GFP was put in a reverse orientation.
- HindIII, EcoRV, EcoRI sites were introduced in between the sense TdTomato sequence and anti-sense GFP sequence
- And the whole sequence was flanked with XhoI site

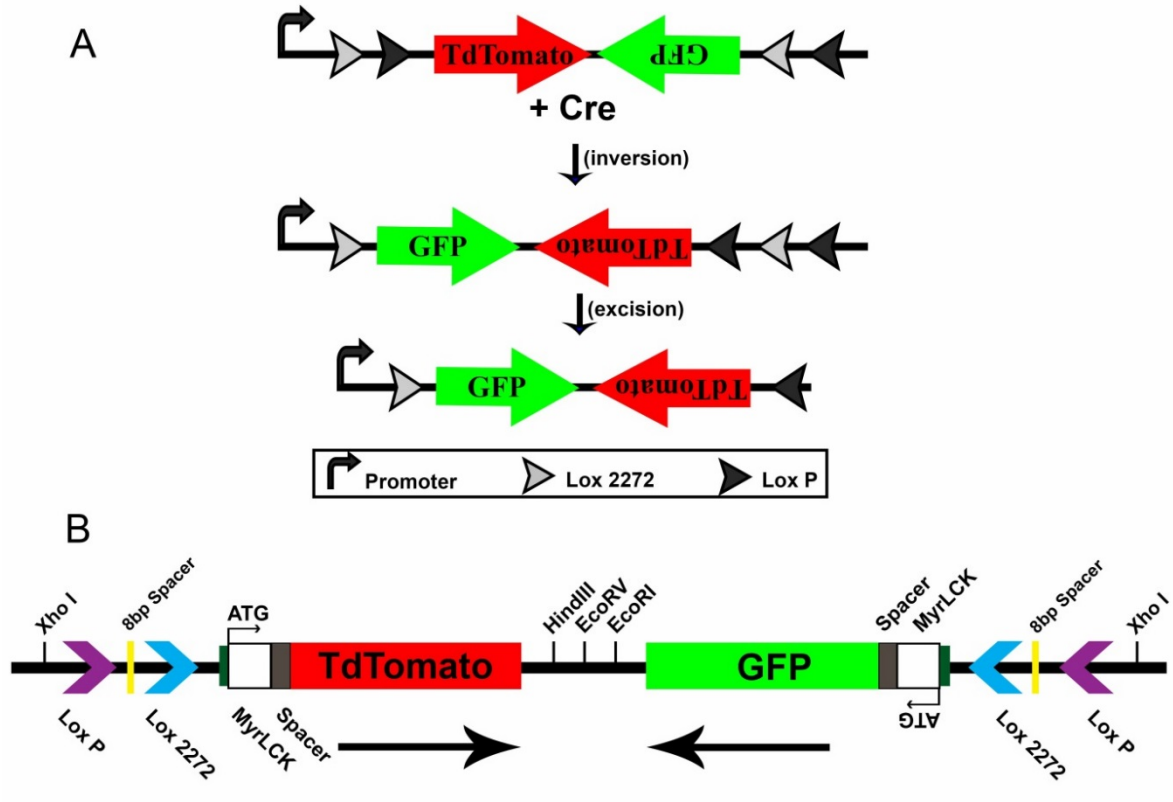

Figure 38 Lentiviral dual colour FLEx system.

A) The FLEx switch is Cre-dependent. Cre-activity brings an inverted GFP open reading frame under control of a CAG promoter. Subsequent excision of the LoxP sites stabilizes the sense orientation of the construct. B) Outline of pLV-CAG FLEx Myr-TdTomato/Myr-GFP. The Myr-TdTomato and reverse Myr-GFP sequence are flanked by Lox2272 and LoxP.

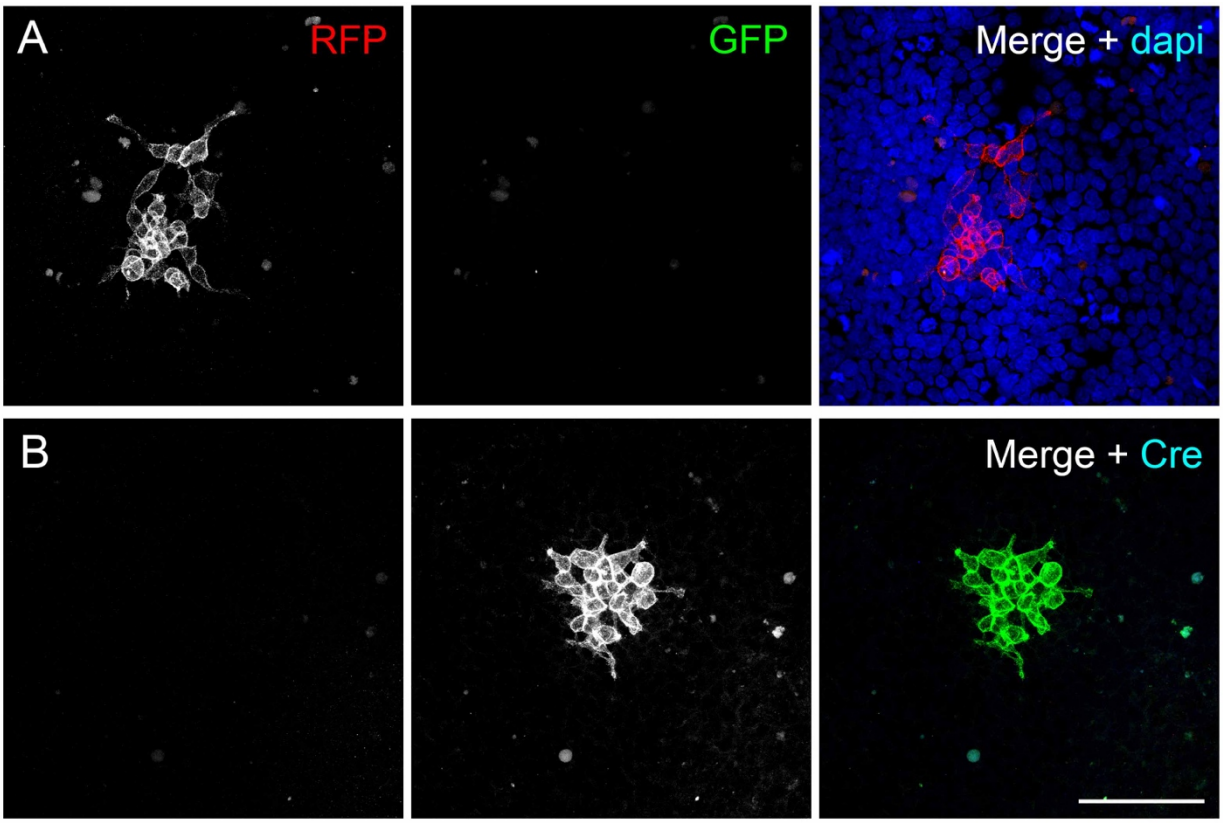

Figure 39 Lentivrial FLEx vector expression in HEK293 cells

A) HEK cells were infected with the pLV-CAG-FLEx lentiviral construct. At 5dpi, the cells were fixed and labelled with dapi, RFP and GFP. Shown is a confocal image indicating the targeting of virally expressed TdTomato to the plasma membrane. B) HEK cells were infected with the pLV-CAG-FLEx lentiviral construct. At 5dpi, the cells were seeded in a fresh plate and transfected with pmc-Cre. 72 hours after transfection, the cells were fixed and labelled with dapi, RFP and GFP. Shown is a confocal image virally expressed GFP to the plasma membrane indicating that the Cre can effectively flip the expression cassette. Scale bar 100 µm.

The entire vector insert sequence was designed in silico and cloned under pLV-CAG. The pLV-CAG-FLEx vector was verified via digestion and sequencing and was packaged. The lentiviral expressing FLEx vector was tested by infecting HEK293 cells. After 5dpi, the HEK cells expressed only red fluorescent protein (Fig 39A), confirming that there wasn't any leaky GFP expression. The transduced HEK cells were passaged and transfected with pmc-Cre. The transfected pmc-Cre cells were immunolabelled with dapi, GFP, RFP and Cre. The confocal images showed GFP+ cells co-labelled with Cre indicating the working efficiency of the flip the cassette (Fig 39B). The FLEx vector cloned here can effectively be used in CNTF::Cre BDNF fl mouse model to outline the BDNF- Cre+ cells and BDNF+ Cre- cells. This would make an effective tool to analyse the effect of BDNF on structural modification at the MFT.

4 Discussion:

BDNF (brain-derived neurotrophic factor), one of the most extensively studied neurotrophic factor since it's discovery in 1982 is involved in diverse functions in the central and peripheral nervous system of rodents and particularly in higher order mammals (Barde, 1994; Barde et al., 1982; Egan et al., 2003; Lu et al., 2013). In the CNS, BDNF regulates the differentiation of certain types of neurons by binding to its receptor TrkB. Once released at synaptic locations, BDNF acts only locally (Horch and Katz, 2002; Horch et al., 1999; Sasi et al., 2017). Synaptic release of BDNF activates (Bramham and Messaoudi, 2005) many signalling cascades downstream of TrkB that regulate synaptic transmission, synaptic stability, plasticity and dendritogenesis (Altar et al., 1997; Bath et al., 2012b; Harward et al., 2016; Hedrick et al., 2016; Korte et al., 1995; Li et al., 2012; Lohof et al., 1993; Patterson et al., 1996; Pattwell et al., 2012). Moreover, BDNF/TrkB signalling modulates synaptic plasticity events such as LTP, synaptic scaling and structural plasticity (Harward et al., 2016; Hedrick et al., 2016; Korte et al., 1995; Rutherford et al., 1998; Sasi et al., 2017; Turrigiano et al., 1998). Although, the synaptic effects of BDNF are well understood, it is still not clear whether BDNF is primarily released from pre- or postsynaptic sites. Moreover, in case BDNF is secreted via both directions, it is not well understood if it will act in paracrine or in autocrine fashion or in both ways (Conner et al., 1997; Dieni et al., 2012; Kolarow et al., 2007; Lessmann and Brigadski, 2009; Sasi et al., 2017).

This study verifies that anti-BDNF immunoreactivity in the presynaptic mossy fiber terminal in the hippocampus is primarily produced by the corresponding dentate gyrus granule neuron. Deletion of BDNF from individual granule neurons alters the local microcircuit properties, as shown by a modulatory effect on neurogenesis in the dentate gyrus. Tracing techniques, developed in here to target the mossy fiber structures, will help to investigate the function of presynaptic mossy fiber BDNF in functional and structural synaptic plasticity.

4.1 BDNF localization at subcellular level

BDNF secretion is a highly debated topic in the field of neurotrophic factor research. One of the fundamental questions being from which subcellular vesicle is BDNF is released at the synapses (Edelmann et al., 2014; Park and Poo, 2013; Sasi et al., 2017). The classical concept of neurotrophins being target-derived factors argued for an almost exclusive release of BDNF from postsynaptic sites (Levi-Montalcini, 1987; Thoenen, 1995). The theory of postsynaptic secretion argues for a vesicular particle that will release BDNF either from the postsynaptic spine or from dendrites directly. On the other hand, the conception of presynaptic location of BDNF argues for dense core vesicles in or close to the synapse as BDNF release occurs via vesicles (Brigadski et al., 2005; Danzer and McNamara, 2004; Dieni et al., 2012; Hartmann et al., 2001; Harward et al., 2016; Leschik et al., 2019; Matsumoto et al., 2008). In accordance with these two contradictory assumptions, BDNF must localize in vesicle-like structures either in the dendrite

or close to the postsynapse or in the presynaptic terminal or varicosity (Edelmann et al., 2014; Sasi et al., 2017).

Early studies on BDNF localization already suggested that BDNF is synthetized in cell body and transported subsequently to its release site in an anterograde manner (Altar et al., 1997; Conner et al., 1997). Furthermore, it was shown that a high amount of BDNF immunoreactivity is found in the mossy fiber of the hippocampus, in fibers projecting to the BNST and the central amygdala (Conner et al., 1997). Recent data looking at immunoreactivity against endogenous, and not to overexpressed BDNF, used electron microscopy techniques or super-resolution microscopy and found that most of the BDNF is preferentially found at presynaptic sites (Andreska et al., 2014; Dieni et al., 2012; Sasi et al., 2017).

A very recent publication showed that knocking in a BDNF-GFP construct to the BDNF-encoding exon of mice leads to a specific expression of BDNF-GFP in CA3 pyramidal neurons and almost no BDNF-GFP label in presynaptic mossy fiber terminals (Leschik et al., 2019). However, immunolabeling of BDNF gives the strongest anti-BDNF immunoreactivity in presynaptic mossy fiber terminals that project to CA3 pyramidal neurons (Conner et al., 1997; Danzer and McNamara, 2004; Dieni et al., 2012; Sasi et al., 2017). Hence, expression of BDNF-GFP in CA3 pyramidal neurons, and absence of BDNF in mossy fibers of dentate gyrus granule neurons questions presynaptic storage of BDNF at synapses (Leschik et al., 2019).

This study shows, however, that BDNF is highly abundant in mossy fiber terminals, as shown by different antibodies against BDNF. Furthermore, it also demonstrates that specific deletion of the *Bdnf* gene from dentate gyrus granule neurons also reduces the BDNF immunoreactivity in the mossy fiber of the hippocampus. An important experiment would be to co-label endogenous BDNF and BDNF-GFP in corresponding heterozygous BDNF-GFP knockin mice (Leschik et al., 2019) to find out whether anti-BDNF immunoreactivity and BDNF-GFP immunoreactivity overlap or not.

4.2 Cre-mediated deletion of BDNF from the mossy fiber terminal

4.2.1 Morphological characterization of the cBDNF ko

To better understand the effect of anterograde BDNF signalling at the MFT, a Cre-deleter mouse model was needed that allows the specific deletion of BDNF from adult granule neurons. Here, we found that a Cre recombinase under the control of the endogenous CNTF promoter exhibited an exclusive activity in the mature dentate gyrus granule neurons. The Cre-mediated recombination starts early in adulthood and occurs almost exclusively in adult granule neurons, at least in the central nervous system. Cre-deleter activity was also seen in some single neurons in CA1, in the basolateral amygdala and in single non-neuronal cells along capillaries. In the peripheral nervous system, Cre-reporter activity was found in Schwann cells. The Cre activity in granule neurons was age-dependent but did not occur in the cell lineage undergoing adult neurogenesis. When the CNTF::Cre mouse line was crossed with a *Bdnf* $^{fl/fl}$ mouse model (Rauskolb et al., 2010) to get a BDNF deletion exclusively in dentate gyrus granule neurons, BDNF immunoreactivity was specifically lost from mossy fiber terminals.

We analysed if genetic deletion of BDNF from adult granule neurons had an effect on neurogenesis, due to a local network effect, as BDNF was shown to be directly associated to induce adult neurogenesis in subgranular zone (Bath et al., 2012a; Castren and Rantamaki, 2010; Obernier et al., 2018; Quesseveur et al., 2013). The analysis of Doublecortin-positive (DCX+) immature neurons in the cBdnf ko showed an increased number of DCX-positive cells and more cells with a well-arborized dendritic tree (stage III DCX+ neurons). As BDNF is a factor for synapse maturation, the effect could be best explained as a delay in maturation. Alternatively, BDNF deletion might induce increased local neuronal activity and therefore trigger neurogenesis by inducing DCX+ cells expression. Indeed, BDNF/TrkB signalling has already been shown to stimulate differentiation and dendritic morphogenesis in the hippocampus (Wang et al., 2015). Here, more DCX+ attributes in the hippocampus might be caused by circuit effects on neurogenesis.

BDNF is rather a differentiation factor and not a survival factor for neurons in the central nervous system (Rauskolb et al., 2010). Here, no evidence for a reduced survival of Cre-positive, BDNF-negative neurons was found, as indicated by an indistinguishable gross morphology of dentate granule neurons in GFP-reporter-positive, cBdnf knockout mice. This is in accordance with a study showing almost no effect on the morphology of CA1 pyramidal neurons after global BDNF deletion from all neurons (Rauskolb et al., 2010). Here, the size of the mossy fiber terminal region was not affected in the cBdnf ko. It needs to be noted that BDNF overexpression with the help of a strong neuronal promoter can lead to an increased mossy fiber terminal region (Isgor et al., 2015).

Early studies indicated that BDNF might serve as a survival factor for parvalbumin-positive neurons, at least in the striatum (Altar et al., 1997). For this reason, it was determined whether genetic deletion of BDNF from granule neurons affects the local number of parvalbumin-positive

interneurons, one of the most prominent GABAergic population in the hippocampal circuit (Kosaka et al., 1987). The MFT terminal forms filopodial connections with these interneurons, which in turn forms inhibitory connections on to the CA3 pyramidal neurons (Bischofberger et al., 2006a; Nicoll and Schmitz, 2005). The parv+ interneuron population in the stratum lucidum is vital for memory precision and participates in the pattern separation functions of the hippocampus via feed-forward inhibition (Danzer and McNamara, 2004; Hashimotodani et al., 2017; Ruediger et al., 2011). It has also been shown that the glutamatergic filopodial connections from the DG granule neurons carry BDNF and might release it upon activity onto the post-synaptic GABAergic interneurons (Danzer and McNamara, 2004). Here, we did not observe any changes in the number of the Parv+ interneuron population in the cBdnf ko, but we cannot exclude yet if there are functional or ultrastructural deficits in the MFT-interneuron connection, or not.

4.3 Labeling presynaptic mossy fiber terminal filopodia

BDNF can affect the connection between synapses by multiple mechanisms, including functional and structural plasticity (Sasi et al., 2017). In structural plasticity, mostly postsynaptic spines were shown to increase in volume in a coincidence mechanism combining presynaptic induction of glutamate release and local BDNF availability (Harward et al., 2016; Hedrick et al., 2016; Tanaka et al., 2008). Already there is considerable knowledge about BDNF function in structural plasticity regarding the postsynaptic spine in CA1, while its function in presynaptic structural plasticity is entirely unclear. A mouse model with specific deletion of BDNF from granule neurons, as it is described here, offers the unique opportunity to investigate whether and how presynaptic BDNF release affects the structural plasticity at the local synapse itself. For two reasons, the mossy fiber synapse is a well-suited model synapse to answer this important research question. First, as described above, it expresses high amounts of BDNF and affects structural plasticity onto the mossy fiber region (Danzer and McNamara, 2004; Dieni et al., 2012; Isgor et al., 2015; Sasi et al., 2017). Second, the mossy fiber synapse undergoes massive learning-related structural remodelling as indicated by changes in the length and number of mossy fiber filopodia after learning events (Galimberti et al., 2006; Ruediger et al., 2011).

Here, the cBdnf ko animals showed site-specific deletion of BDNF at the MFT in both dorsal and ventral hippocampus, thus offering the possibility to combine Cre-dependent structural tracing of mossy fiber filopodia with changes in structural plasticity. Initially, we decided to induce plasticity by introducing the animals to enriched environment, which can bring cellular and structural plasticity to the mossy fiber synapse (Caroni et al., 2012; Galimberti et al., 2006; Kempermann et al., 1997; Ruediger et al., 2011; Toni et al., 2008). In addition, exercise or enriched environment increases neurogenesis rates and stimulates plasticity events in the dentate gyrus – mossy fiber – CA3 system (Kheirbek et al., 2012; Malberg et al., 2000; Mongiat and Schinder, 2014; Revest et al., 2009; Sahay and Hen, 2007; Santarelli et al., 2003). However,

while our enriched environment situation was well suited to increase the number of DCX+ parameters in the dentate gyrus, it was not easily possible to trace mossy fiber terminals with the help of a Cre-dependent reporter crossed to the cBdnf KO mice. In here, we developed a triple transgenic mouse line wherein we crossed the CNTF::Cre BDNF flfl animal with a GFP reporter, which enabled the mossy fiber boutons to be well labelled by GFP. Yet due to unknown reasons, the GFP could not enter the filopodia of MFTs and therefore it was not possible to trace presynaptic structural plasticity in the corresponding cBdnfKO mice. Therefore, it was essential to develop a new approach for structural tracing of MF boutons.

4.4 Structural tracing vectors to evaluate the cBdnf ko effect on pre-synaptic mossy fiber terminal

Cytosolic green fluorescent protein (GFP) has widely been used to trace neuronal structures such as spines, axons or growth cones; not only in *in vitro*, but also in *in vivo* experiments (Deshpande et al., 2013; Michaelsen et al., 2010; Toni et al., 2008; Vivar et al., 2012; Zagrebelsky and Korte, 2014). Chicken-beta actin (CAG) promoter driven GFP expression was used for visualization of the mossy fiber synapse (Toni et al., 2008). However, here, chicken-beta actin promoter driven GFP expression was not sufficient to outline the structure of the MFB.

However, membrane-targeted fluorescent proteins have been exploited to outline the plasma membranes of spines, filopodia and growth cones to enable the visualization of structural plasticity events (De Paola et al., 2003; Kabouridis et al., 1997; Rathod et al., 2012). For membrane targeting, aminoterminal myristoylation and palmitoylation sequence motifs (Kabouridis et al., 1997) were shown to efficiently outline the neuronal membrane from inside the cell (De Paola et al., 2003; Galimberti et al., 2006; Ruediger et al., 2011).

To identify a strategy that enables the investigation of BDNF-dependent structural plasticity at the MFT, a Cre-dependent tracing system was developed. Initially, it was tested whether Cre-activity in *cBdnf* KO animals would enable us to visualize the Cre+ BDNF- neurons in green, by expressing a membrane-targeted GFP (Myr-GFP), and Cre- BDNF+ neurons in red, by labelling corresponding wildtypic neurons with Myr-tandem tomato (Myr-TDtomato). As the corresponding viral vector insert has a certain length, a lentiviral system with a CAG promoter was chosen. It was found that the system was very efficient in labelling the complete volume of large mossy fiber boutons and could even label the whole length of the filopodial extensions. Even the dense dendritic spine bodies of the DG granule neurons were distinctly labelled by the lentiviral tracing vector. The lentiviral particle showed a diffusion distance of over 900 μm and was therefore well suited to label many individual mossy fiber boutons. However, the lentiviral vectors showed pronounced recombination during DNA preparation of the corresponding expression vectors and therefore the vector produced a strong Cre-independent tracing signal.

To surmount this problem, we developed a Cre-independent system and introduced an IRES Cre downstream of the Myr-GFP. Thereby, GFP+ cells would also be Cre +, thus enabling the use

of the vector in floxed animals in absence of a Cre. However, these vectors were not easy to titrate and therefore these vectors are not fully suited to answer the research question of mossy fiber BDNF in structural plasticity.
Therefore, we used lentiviral vectors in combination with a flip-excision strategy (Schnutgen et al., 2003). In here, the two fluorescent proteins are in reverse directions and could be flipped by flanking them with compatible LoxP-sites, here Lox2272 and LoxP sequences were used. With this system, our initial plan to distinguish Cre+ and Cre- granule neurons could be achieved.
We employed super-resolution microscopy to image the myristoylated GFP+ neurons to see whether such a vector system can outline the fine structure of synapses. Applying these modern viral vectors to the here described granule-cell specific cBdnfKO animal will help to find out whether presynaptic release of BDNF is involved in autocrine, presynaptic structural plasticity. In addition, it will also help to find out how target-structures of MF boutons are affected if BDNF is deleted from the presynapse.

4.5 Conclusion

This study favours the concept that BDNF is stored and released from presynaptic mossy fiber boutons in the hippocampus. The vast amount of mossy fiber BDNF is synthetized by adult granule neurons, and not, as indicated by other studies, by postsynaptic CA3 pyramidal neurons. Mossy fiber BDNF plays a role in local neural circuit functions as indicated by changes in neurogenesis parameters in the dentate gyrus. Future studies with the help of the novel lentiviral tracing tools developed in this study will allow us to find out how presynaptic BDNF is involved in functional and structural plasticity at the mossy fiber synapse, a model synapse to investigate learning and memory from molecule to behaviour.

5 Supplementary

Sup. Table 1. Statistical data of t-test

Normally distributed samples – Unpaired t-test

Not normally distributed samples^{+} – Mann Whitney t-test

Statistical significance *p< 0.05, **p<0.01, ***p<0.001

Fig. 20 The number of DCX-positive immature neurons in two-month-old granule cell specific BDNF knockouts.	**P value**	**t**	**df**
Fig. 20 A) dHippo	0.4285	0.8865	3.753
Fig. 20 B) vHippo	0.8374	0.2246	2.862
Fig. 21. The number of DCX-positive immature neurons in three-month-old granule cell-specific BDNF knockouts	**P value**	**t**	**df**
Fig. 21 A) dHippo	0.317	1.033	15.98
Fig. 21 B) vHippo	0.0116	3.085	9.942
Fig. 22. The number of DCX-positive immature neurons in six-month-old granule cell-specific BDNF knockouts	**P value**	**t**	**df**
Fig. 22 A) dHippo	0.8423	0.2022	15.88
Fig. 22 B) vHippo	0.0559	2.218	8.381
Fig. 24. Immature neuron staging in granule cell-specific BDNF knockouts	**P value**	**t**	**df**
Fig. 24 B) Stage I - 3 months	0.6302	0.4882	21.97
Fig. 24 C) Stage II - 3 months	0.0416	2.166	21.74
Fig. 24 D) Stage III - 3 months	0.0003	4.377	21.51
Fig. 24 E) Stage I - 6 months	0.0198	2.586	16.11
Fig. 24 F) Stage II - 6 months	0.0274	2.382	19.67
Fig. 24 G) Stage III - 6 months	0.0397	2.275	13.58
Fig. 25. Morphological analysis of DCX+ neurons in granule-cell specific Bdnf KO mice	**P value**	**t**	**df**
Fig. 25 B) Primary dendritic length - 3 months	0.1165	1.581	116.4
Fig. 25 C) Primary dendritic length - 6 months	0.2928	1.057	117.2
Fig. 25 D) Total dendritic length - 3 months	0.0698	1.830	112.0
Fig. 25 E) Total dendritic length - 6 months	0.0153	2.463	114.6
Fig. 25 F) Branching - 3 months	0.0733	1.808	114.4
Fig. 25 G) Branching - 6 months	0.1711	1.378	109.9
Fig. 27. Number of Parvalbumin-positive interneurons in the mossy fiber area of cBdnf ko	**P value**	**t**	**df**
Fig. 27 A) dHippo	0.7831	0.2799	16
Fig. 27 B) vHippo	0.698	0.3914	34
Fig. 26. The size of the mossy fiber area in cBdnf ko	**P value**	**Mann Whitney U**	
Fig. 26 A) Area of MF^{+}	0.3766	83.5	

P value – probability value t – Test statistic value, df – degrees of freedom

Sup. Table 2. Statistical data of Two-way ANOVA test
Statistical significance *p< 0.05, **p<0.01, ***p<0.001

Fig. 23 A) Age-dependent decline in the number of DCX+ neurons - dHippo			
Source of Variation	**% of total variation**	**P value**	**F (DFn, DFd)**
Interaction	8.231	0.1368	F (2, 36) = 2.103
Genotype	10.77	0.0246	F (2, 36) = 2.103
Age	16.5	0.0227	F (2, 36) = 2.103

Fig. 23 B) Age-dependent decline in the number of DCX+ neurons - vHippo			
Source of Variation	**% of total variation**	**P value**	**F (DFn, DFd)**
Interaction	5.284	0.1619	F (2, 24) = 1.966
Genotype	6.779	0.0342	F (2, 24) = 1.966
Age	50.58	0.0001	F (2, 24) = 18.82

P value – probability value, F - (Fisher–Snedecor distribution) ratio, DF – degrees of freedom

Sup. Table 3. Statistical data of Bonferroni Multiple Comparison Test

Fig. 23 A) Age-dependent decline in the number of DCX+ neurons - dHippo	**Mean diff.**	**95% CI of diff.**	**Adjusted P Value**
wt:3 months vs. wt:6 months	11.33	-18.14 to 40.81	> 0.9999
cbdnf ko:3 months vs. cbdnf ko:6 months	26.33	-3.140 to 55.81	0.1044
Fig. 23 B) Age-dependent decline in the number of DCX+ neurons - vHippo	**Mean diff.**	**95% CI of diff.**	**Adjusted P Value**
wt:3 months vs. wt:6 months	40.67	12.93 to 68.41	0.0017
cbdnf ko:3 months vs. cbdnf ko:6 months	40.28	12.54 to 68.02	0.0019

CHAPTER -II

An open source tool for automatic spatiotemporal assessment of calcium transients and local 'signal-close-to-noise' activity in calcium imaging data

1. Introduction:

In the course of this study and in collaboration with Thomas Seidenbecher, Institute of Physiologie, University of Münster, our group found that presynaptic lack of BDNF caused increased excitability in the hippocampal network. Increased excitability of arborized neurons cannot easily be detected by electrophysiological analysis of neuronal cell bodies. For this major reason, calcium imaging became prominent to analyse functions like cellular excitability, neurotransmitter release, and activity-dependent synaptic plasticity. However, calcium transients caused by excitability changes may be difficult to analyse as they normally appear in an unpredictable temporal and spatial pattern. This is accordingly expected for BDNF signalling that is linked to excitability effects at axonal or postsynaptic sites.

Therefore, when we saw that presynaptic BDNF seem to serve as excitability regulator, we asked whether it would be possible to extract excitability effects from calcium imaging data. As calcium imaging is based on analysis of fluorescence signals, there is not ultimate definition whether a calcium event is an event or not (binary yes/no-decision). The main reasons regarding the lack of studies on binary definition of excitability events by calcium imaging could be due to the following:

1.) Calcium transients could localize at very distinct locations.

2.) Functional diversity of the neuronal proteins involved in the excitation can cause very different signal signatures.

3.) Neuronal calcium signals may be spontaneous, local or very small, meaning close to noise.

Usually, calcium signals are analysed by regions-of-interests (ROIs) that are selected manually or in a semi-automated manner. In most cases, this is quite time consuming and in case of excitability analysis impossible to perform, because one cannot predict where and when an activity event occurs. There are several computational tools developed to support the analysis of calcium imaging data sets. These tools use complex arithmetic to read out the calcium signals from existing raw data. Each of the methods has its pros and cons (Broussard et al., 2018; Deneux et al., 2016; Mukamel et al., 2009). However, all available tools did not allow deciding whether a local calcium signal or changes in the signal fluctuation are signals or just noise.

In our study, we have developed a computational tool that would identify activity close to the noise level.

To enable the development of computational strategies for excitability analysis, calcium imaging experiments were performed. Aim was to separate homeostatic versus signal-close-to-noise activity events from induced activity events. The approach led to the development of a new computational tool, called NA_3 (spoken: NA cubic). The biocomputation was done by Dr. Juan Prada and Thomas Dandekar, Department of Bioinformatics, University of Würzburg. All test data, manuals, codes and other important information can be found at: https://www.biozentrum.uni-wuerzburg.de/bioinfo/computing/neuralactivitycubic/

The computational tool is a Continuous Wavelet Transform (CWT) based algorithm which pinpoints the activity over an x,y-t imaging data set. The open source tool consists of around 800 lines of code and the core functionality is about 140 lines long. The activity events are calculated on `R' (https://www.r-project.org). Image J and R are embedded in the Bio7 environment, an open platform (http://bio7.org/). The tool itself is available on: https://github.com/jpits30/NeuronActivityTool. The tool containing the ROI feature is available at: https://github.com/jpits30/NeuronActivityTool_ROI.

In the tool, the pixel intensities are analysed to detect the peaks that relate to the neuronal activity. Our algorithm sums the information obtained from matching the calcium activity peak with several scaled versions of a mother wavelet and decides based on that whether that part of the trace contains a peak of activity or not. The tool facilitates the fast and unbiased analysis of changes in fluorescence in imaging data. Furthermore, the tool allows reading out or even identifying noise-like, spontaneous activity patterns from large imaging data sets. The tool tries to find activity and disagrees with the ‘concept of noise’.

Here, in the result section, calcium imaging data are analysed with a final version of the computer tool NA3.

2. Materials & Methods:

2.1. Materials:

Refer section 2.1 of chapter I.

2.2. Methods:

2.2.1. Cell Culture

2.2.1.1. Coating cover glass

Cover glass (10 mm, Marienfeld) was either placed in 4-wells or in 24-well plates. 100 µl of 0.1% PLL was added to each cover glass and incubated at 4°C overnight. The PLL was removed and the cover glasses were washed thrice with HBSS. In case of transfection or lentiviral transduction of HEK293 cells, the cells were added immediately upon HBSS removal. In case of primary hippocampal neurons, the HBSS was replaced with maintenance medium and equilibrated for few hours in a cell culture incubator (37°C, 5% CO_2).

2.2.1.2. Primary hippocampal neurons

Hippocampi from both hemispheres were prepared from five E19 C57Bl/6J mice or CD1 mice. The hippocampi were washed twice with dissection medium and 500 µl 2.5% trypsin was added and incubated at 37°C, 5% CO_2 for 20 min. 500 µl DNase was added to the trypsinated hippocampal cells and incubated at 37°C, 5% CO_2 for 5 min. The cells were washed twice with dissection medium. 500 µl trypsin-inhibitor (TI) was added to stop the trypsinization. The cells in dissection medium with TI were triturated with a 1ml pipette tip and were pelleted by centrifugation at 1400 × g for 3 min. The trituration step was repeated once more. The pelleted cells were re-suspended in maintenance medium (with 1% serum) and were triturated with yellow pipette tip. Cells were counted using a Neubauer chamber and 20,000 cells per cover glass were plated on 0.1% PLL-coated cover glasses. The cells were flooded with maintenance medium (with 1% serum) to a final volume of 2 ml. Cells were cultured at 37°C, 5% CO_2. Half of the medium was exchanged on day in vitro (DIV) 5 and once more on DIV 10 with serum-free maintenance medium.

2.2.1.3. Calcium Imaging

2.2.1.3.1. Preparation of the Imaging solution:

Artificial cerebral spinal fluid (ACSF) containing 135 mM NaCl, 6 mM KCl, 2 mM CaCl2, 1 mM MgCl2, 5.5 mM D-Glucose and 10 mM HEPES was prepared. The chemical LTP solution containing 128 mM NaCl, 13 mM KCl, 3 mM CaCl2, 5.5 mM D-Glucose and 10 mM HEPES and 0.1 mM Glycine was prepared and the calcium-free ACSF contained 0.1 mM EGTA. The pH of all the buffers were adjusted to 7.4.

2.2.1.3.2. Dye loading of the neurons:

5mM stock solution of Oregon Green 488 BAPTA-1, AM (OGB) was prepared by diluting in 8.9µl of 20% Pluronic F-27 in DMSO. The OGB was mixed thoroughly using a water-bath sonicator for 10 min. And 0.5µl aliquots of the stock were prepared. 500 µl of the pre-warmed ACSF was used to resuspend 1 aliquot of OGB and the volume was transferred to a 4-well plate.

A coverslip with the hippocampal neurons was placed carefully into the 4-well containing the dye. The labelling of the neurons was done by incubating the cells in the dye for 15 min at 37°C and 5% CO2.

2.2.1.3.3. Preparation of the live imaging set up:

The solutions were pre-warmed to room temperature. The epifluorescences microscope, camera set up and all the computer programs were started. The inline solution heater, imaging chamber in the microscope stage were prewarmed. A high vacuum grease was applied to the imaging chamber for 10-12 mm coverslip using a paint brush. The live imaging set up was build up and the continuous perfusion system was tested on a dummy run to ensure constant flow and no leakage.

2.2.1.3.4. Live cell calcium imaging:

The labelled coverslip was carefully placed into the heated imaging chamber. The imaging was performed under continuous perfusion with the ACSF. The region of interest was focussed with a 40X objective. The images (8-bit) were recorded at high scan rates 5-10 Hz speed in a stream approach manner under continuous illumination with a 470nm LED light source. The calcium dynamics were monitored in a x,y-t scale under the specific experimental conditions.

3. Results

3.1. Spontaneous calcium activity:

First it was tested, whether the wavelet algorithm is able to detect spontaneous synaptic activity in hippocampal neurons.

For this, primary hippocampal neurons labelled with OGB were imaged at 10 Hz speed under low intensity fluorescence condition with constant ACSF flow (Fig. 1A). The neurons exhibited spontaneous spiking behaviour. The tool NA[3] quite efficiently detected the global activity events that were localized in distant axons. Later, the neurons were blocked acutely with tetrodotoxin (TTX), the antagonist of TTX-sensitive sodium channels and 6-cyano-7-nitroquinoxaline-2,3-dione (CNQX), an antagonist of some ionotropic glutamate receptors. The tool could compute a more than 10-fold decrease (total activity 790 to 60) in the overall spiking behaviour after activity blockade. This experiment demonstrates the ability of the tool to identify the global activity across varied spiking behaviour patterns and shows its ability to detect and count calcium spikes.

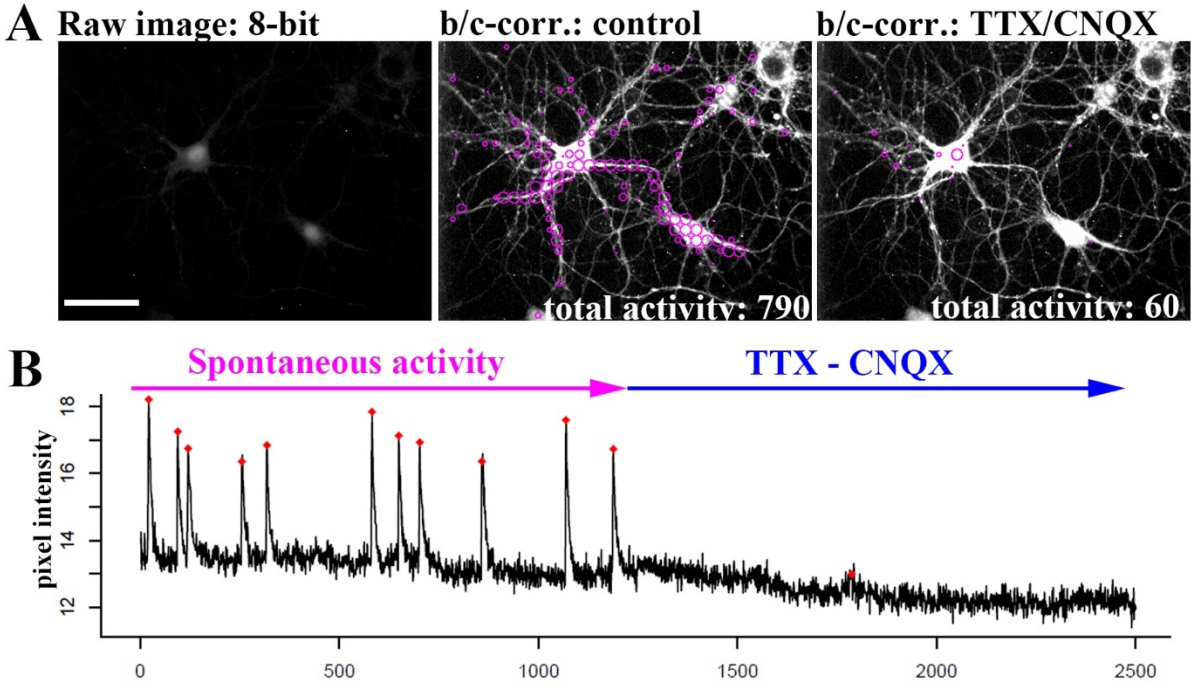

Fig 1 Analysis of spontaneous spiking behaviour of hippocampal neurons.
(A) Hippocampal neurons were imaged under low intensity. Pink circles show the activity detected by the NA[3] tool. Spontaneous spiking behaviour under control condition and respective cells under TTX/CNQX blockade are depicted. (B) Graph, the pixel-intensity intensity values are plotted against the frame number showing that the TTX/CNQX effectively blocks the spontaneous activity. Scale bar 50 μm.

3.2. Neuronal activity under chemical LTP induction:

Next, it was asked how the wavelet-based analysis in NA[3] computes increased excitability. Calcium imaging with hippocampal neurons was performed under constant perfusion and neuronal activity was stimulated via chemical LTP solution. This solution contained glycine to increase the open probability of NMDA receptors and increased extracellular potassium to pre-

depolarize neurons, thus triggering increased calcium responses in neurons. The heat map of activity shows the increased activity after cLTP stimulation. NA3 finds highly diverse signals on somata and complex pattern of local signals on distant neurites (Fig. 2A). In Fig. 2B, the red circle's diameter is directly proportional to the calcium signal intensity in the respective ROIs. The computed image shows high activity patterns in the neuronal peripheries. We further observed synchronous spiking activity in these distant axonal regions after the increased activity (Fig. 2C). The tool recognised small events that on the initial observation show a noise-like characteristics and it calculated an increased number of events (Fig. 2C).

3.3. Analysing activity events under spike blockade:

To verify if the tool detects high number false-positive events, we measured calcium activity under spike blockade conditions. Spontaneously firing neurons (Fig. 3A) were blocked with TTX and with the antagonist of ionotropic glutamate receptors CNQX and APV (D-2-amino-5-phosphonovalerate). Under control condition, the tool computed a high number of activities including multiple small, non-spikes like calcium activities. After perfusion with the inhibitor mix, the classical calcium spike activity decreased (Fig. 3B), but few small signals were computed in the periphery of the neurons. These small, non-spike like activities were majorly localized in the periphery and mostly not shaped as a typical calcium spike like event with a fast onset and a slow decay.

3.4. Measurement of 'signal-close-to-noise':

An ultimate test of whether a computational tool can see signal-close-to-noise activity is the computation of homeostatic calcium fluxes. These fluxes become visible when neuronal activity is ultimately blocked. In such an experimental situation, calcium leaks out of the endoplasmic reticulum (ER), the major intracellular calcium and this calcium leaves the cell via the plasma membrane(Samtleben et al., 2015). To compensate this calcium loss, neurons have a resting store-operated calcium entry (SOCE)(Alzoubi et al., 2013; Samtleben et al., 2013; Samtleben et al., 2015). To compute the homeostatic calcium fluxes between the ER and the extracellular space, we performed wash-out experiments wherein we removed the extracellular calcium for 3 minutes and re-introduced it back. To fully block neuronal activity, we added the following blockers to the extracellular media: tetrodotoxin (TTX), the antagonist of TTX-sensitive sodium channels and 6-cyano-7-nitroquinoxaline-2,3-dione (CNQX), APV (D-2-amino-5-phosphonovalerate), the antagonist of ionotropic glutamate receptors. As shown in the Fig. 4A, both in individual pixel-wise (Fig. 4B) and the whole optical view-wise (Fig. 4C) the calcium activity drops down upon extracellular calcium removal. The re-introduction of calcium resorted the cytosolic calcium signals and as well more global activity was computed. We further summed up the activity events (results not shown here) and computed the variance area for all the grid windows. The results show that the activity computed by NA^3 could be regarded as a biological phenomenon and represents 'signal-close-to-noise' activity. Thus, the tool enables the visualization of signal-close-to-noise activities in an unbiased manner.

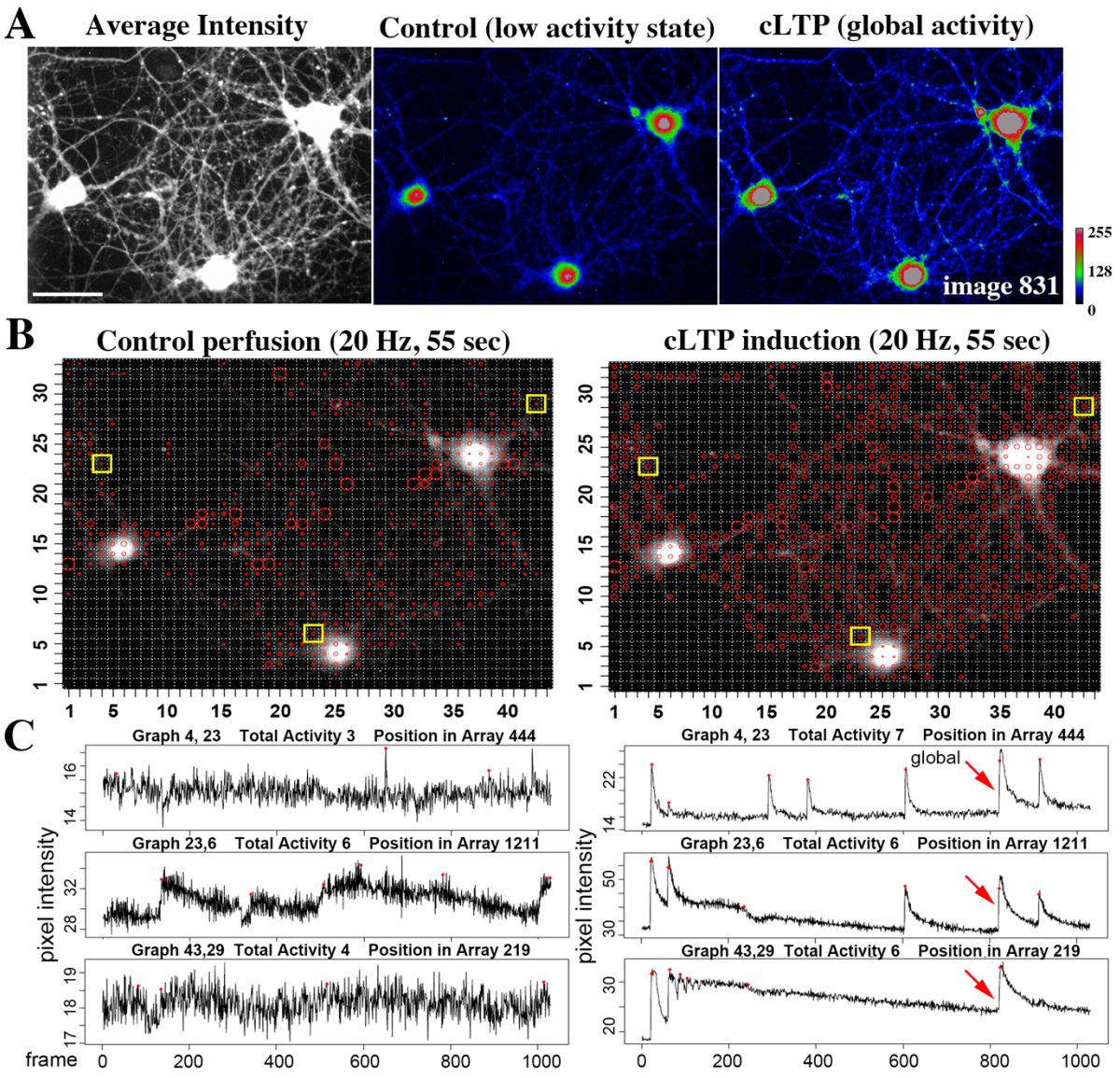

Fig 2 cLTP stimulation of hippocampal neurons.

(A) Average intensity of the hippocampal neurons labelled with calcium indicator. Control condition of the neurons exhibiting low activity and followed by stimulation with cLTP. (B) Imaging data computed with NA3 tool outputs the activity distribution pattern. The diameter of the circle is proportional to the intensity of the signal. The cLTP increased the total activity. (C) Graph, the intensity plotted against the frame number. Activity close to base level are observed under control conditions. After cLTP induction, local and global calcium events are observed.

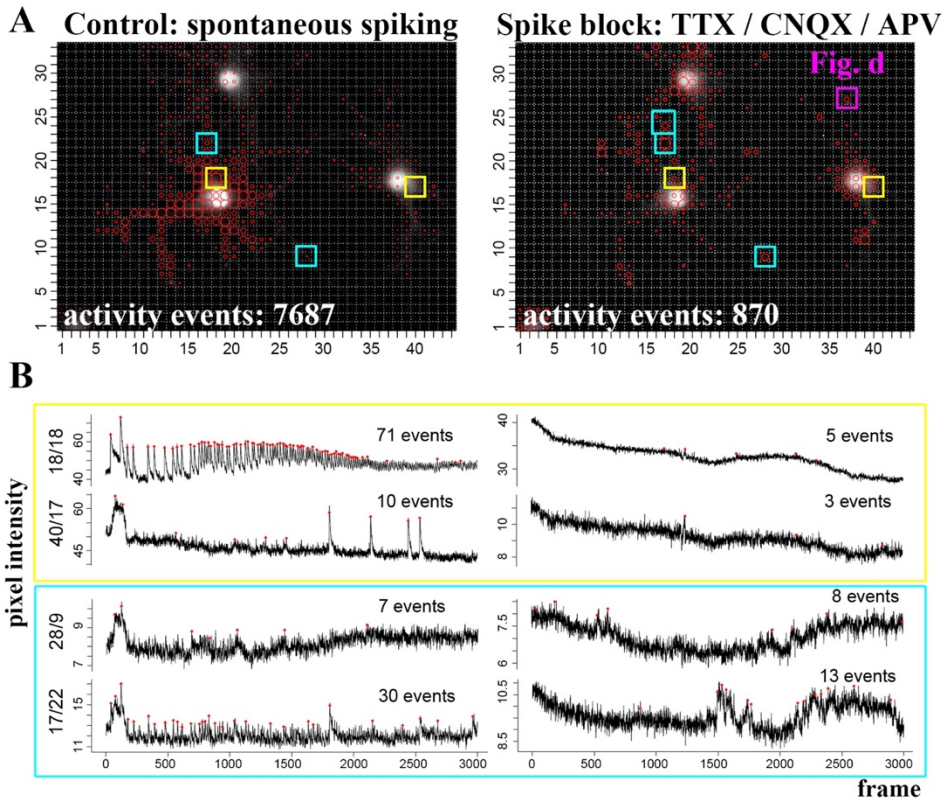

Fig 3 Neuronal activity under spike block.

A) Computed data, neuronal activity from an imaging plane under control conditions and respective cells showing intense decrease in total activity under spike bloke condition. Under control conditions, one neuron, the lower left shows a high spiking activity, as indicated by the activity pattern (red circles in the grid windows). After acute treatment with an inhibitor cocktail (TTX, CNQX, APV), spiking behavior is blocked (yellow squares; traces in B), non-spike-like activity events become visible on the soma and in the periphery. B) Graph, pixel intensity plotted against frame number clearly showing the spiking pattern before and after spike block. Shape and number of residual activity signals are quite diverse (bright blue squares; traces in B). Grid window-specific signal traces with the corresponding activity marks (red) as indicated in A.

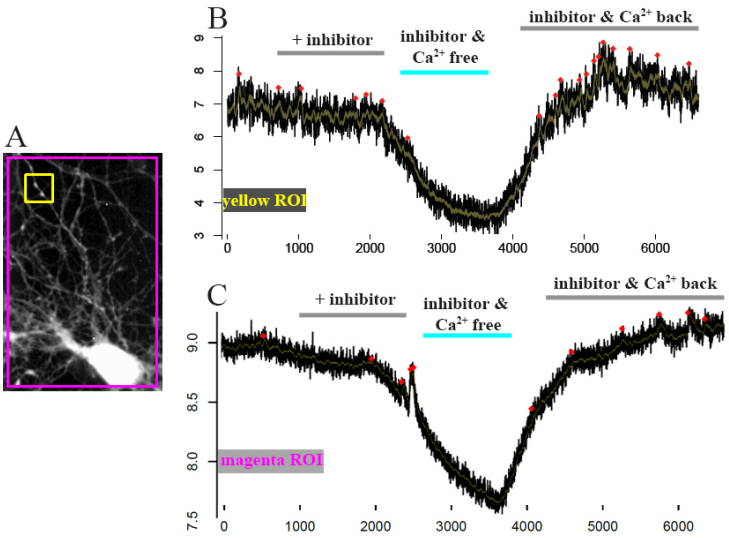

Fig 4 Computing signal-close-to-noise'.
(A) Single hippocampal neuron loaded with calcium indicator, in which two ROIs were indicated. Calcium activity in B) showed the calcium activity in the distant neurite (yellow ROI) and C) showed the calcium traces in Magenta ROI, In B) and C) , there is a removal of extracellular calcium caused a decline in the calcium indicator signal. This correlates with a overall reduced number of computed activity events (red dots).

4. Discussion:

In the recent years, there has been an extensive interest in comprehending the neural circuitry correlations to defined behaviors in freely behaving rodents (Grienberger and Konnerth, 2012; O'Keefe, 1976; Seidenbecher et al., 2003). Understanding the calcium dynamics have been proving to be an essential strategy to investigate these mechanisms correlated with synaptic function and spine plasticity at a single-cell level (Bock et al., 2011; Grienberger and Konnerth, 2012). Two-photon microscopy in head-fixed animals under respective behavioral paradigms has become a feasible and a promising approach for imaging calcium transients (Cheng et al., 2011a; Grienberger and Konnerth, 2012; Matsuzaki et al., 2011). Furthermore, in parallel there is extensive research in improving the optogenetic methods which is used in correlation with the calcium transient recordings to achieve a targeted system and additionally control over the function of the cells of interest (Broussard et al., 2018). Hence, a growing number of applications for calcium imaging has been developed to study signalling mechanisms in disease mouse models for preclinical research (Busche et al., 2015; Grienberger and Konnerth, 2012; Rochefort et al., 2011).

This brought us to the point to ask for computational tools suited to analyze calcium imaging data automatically and to test whether computational tools can see small and local excitability events, and not only calcium spikes.

Calcium imaging raw data contain much information, which needs to be analyzed systematically and meticulously. Although, there are many straight-forward bioinformatical tools utilizing de-noising and spike analysis (Mukamel et al., 2009; Patel et al., 2015; Pnevmatikakis et al., 2016), such tools, in general ignore small activity patterns close to noise and occurring at distant localization from somata (Prada et al., 2018). Many of these small, non-spike-like transients do carry relevant information and the function of subthreshold excitability is not well understood (Prada et al., 2018).

In our study (Prada et al., 2018), we have presented a tool that focuses on spatiotemporal calcium signalling in neurons. It computes the typical spike-like activity events nevertheless also the non-spike like signals that are close to noise. It computes the overall data irrespective of spike detection and specific ROIs that enables the user to have complete outlook of the total calcium activity pattern. This makes the tool an unbiased approach to analyze calcium imaging data in x,y-t direction. The tool processes the data in ImageJ and the signal extraction is done via “R”. The tool itself is embedded in BIO7 that provides the user accessibility to further ‘n’ number of image processing plugins. Furthermore, it is available as an open source tool and does not require any license purchase. The tool is easily operated by Windows, Mac and Linux computers and the user manual for the tool is available in our publication (Prada et al., 2018).

Thus, the NA3 tool gives us the unique possibility to analyze BDNF-mediated excitability effects in the living mouse, in future experiments.

I. Abbreviations

Bdnf	Brain derived neurotrophic factor gene
°C	Degree Celsius
*Bam*HI	*Bacillus amyloli*
BDNF	Brain derived neurotrophic factor
BGH	Bovine growth hormone
bp	Base pair
CA	*Cornu Ammonis*
CAG	Cyclomegalovirus (CMV) early enhancer element and chicken beta-actin
CAT	Chloramphenicol acetyltransferase
CNTF	Ciliary Neurotrophic factor
DAPI	4',6-diamidino-2-phenylindol
DCX	Doublecortin
DEPC	Diethylpyrocarbonate
dHippo	Dorsal hippocampus
DG	Dentate gyrus
dH2O	Distilled water
DNA	Deoxyribonucleic acid
dNTP	Deoxyribonucleotide
E. coli	*Escherichia coli*
*Eco*RI	Escherichia coli R-factor I
EDTA	Ethylenediaminetetraacetic acid
eGFP	Enhanced green fluorescent protein
EtOH	Ethanol
g	Grams
GFP	Green fluorescent protein
HCl	Hydrochloric acid
hr	Hour
K_2HPO_4	Di-potassium hydrogen phosphate
KCl	Potassium chloride
kg	Kilograms
KH_2PO_4	Potassium di-hydrogen phosphate
L	Litre
LB	*Luria-Bertani*
M	Molar
mg	Milligram
$MgCl_2$	Magnesium chloride
$MgSO_4$	Magnesium sulphate
min	Minute
ml	Millilitre
mM	Millimolar
mm	Millimetre
Na_2PO_4	Di-sodium hydrogen phosphate
NaCl	Sodium chloride
NaH_2PO_4	Sodium di-hydrogen phosphate
NaOH	Sodium hydroxide
NeuN	Neuronal nuclei marker
nm	Nanometre

nt	Nucleotides
P	Postnatal
PBS	Phosphate buffered saline
PCR	Polymerase chain reaction
PFA	Paraformaldehyde
Pfu	*Pyrococcus furiosus*
pmol	Picomole
RNA	Ribonucleic acid
rpm	Rotation/revolution per minute
RT	Room temperature
s	Seconds
SDS	Sodium dodecyl sulphate
SGZ	Sub granular zone
SVZ	Sub ventricular zone
TAE	Tris- Acetate EDTA
Taq	*Thermus aquaticus*
tdTomato	Tandem dimer Tomato
TE	Tris EDTA
tg	Transgenic
U	Units
V	Volts
vHippo	Ventral hippocampus
wt	Wild type
XhoI	*Xanthomonas holcicola* I
µg	Microgram
µl	Microliter

II. List of Tables

III. List of Figures

CHAPTER -II

IV. References

Aarse, J., S. Herlitze, and D. Manahan-Vaughan. 2016. The requirement of BDNF for hippocampal synaptic plasticity is experience-dependent. *Hippocampus*. 26:739-751.

Adachi, N., M. Oyasu, T. Taniguchi, Y. Yamaguchi, R. Takenaka, Y. Shirai, and N. Saito. 2005. Immunocytochemical localization of a neuron-specific diacylglycerol kinase beta and gamma in the developing rat brain. *Brain Res Mol Brain Res*. 139:288-299.

Aid, T., A. Kazantseva, M. Piirsoo, K. Palm, and T. Timmusk. 2007. Mouse and rat BDNF gene structure and expression revisited. *J Neurosci Res*. 85:525-535.

Altar, C.A., N. Cai, T. Bliven, M. Juhasz, J.M. Conner, A.L. Acheson, R.M. Lindsay, and S.J. Wiegand. 1997. Anterograde transport of brain-derived neurotrophic factor and its role in the brain. *Nature*. 389:856-860.

Alzoubi, K.H., O.F. Khabour, I.A. Alhaidar, A.M. Aleisa, and K.A. Alkadhi. 2013. Diabetes impairs synaptic plasticity in the superior cervical ganglion: possible role for BDNF and oxidative stress. *J Mol Neurosci*. 51:763-770.

Amaral, D.G., H.E. Scharfman, and P. Lavenex. 2007. The dentate gyrus: fundamental neuroanatomical organization (dentate gyrus for dummies). *Progress in brain research*. 163:3-22.

An, J.J., K. Gharami, G.Y. Liao, N.H. Woo, A.G. Lau, F. Vanevski, E.R. Torre, K.R. Jones, Y. Feng, B. Lu, and B. Xu. 2008. Distinct role of long 3' UTR BDNF mRNA in spine morphology and synaptic plasticity in hippocampal neurons. *Cell*. 134:175-187.

Anastasia, A., K. Deinhardt, M.V. Chao, N.E. Will, K. Irmady, F.S. Lee, B.L. Hempstead, and C. Bracken. 2013. Val66Met polymorphism of BDNF alters prodomain structure to induce neuronal growth cone retraction. *Nat Commun*. 4:2490.

Andreska, T., S. Aufmkolk, M. Sauer, and R. Blum. 2014. High abundance of BDNF within glutamatergic presynapses of cultured hippocampal neurons. *Frontiers in cellular neuroscience*. 8:107.

Autry, A.E., and L.M. Monteggia. 2012. Brain-derived neurotrophic factor and neuropsychiatric disorders. *Pharmacological reviews*. 64:238-258.

Balkowiec, A., and D.M. Katz. 2002. Cellular mechanisms regulating activity-dependent release of native brain-derived neurotrophic factor from hippocampal neurons. *The Journal of neuroscience : the official journal of the Society for Neuroscience*. 22:10399-10407.

Bannerman, D.M., J.N. Rawlins, S.B. McHugh, R.M. Deacon, B.K. Yee, T. Bast, W.N. Zhang, H.H. Pothuizen, and J. Feldon. 2004. Regional dissociations within the hippocampus--memory and anxiety. *Neurosci Biobehav Rev*. 28:273-283.

Barde, Y.A. 1994. Neurotrophins: a family of proteins supporting the survival of neurons. *Progress in clinical and biological research*. 390:45-56.

Barde, Y.A. 2002. Neurobiology: neurotrophin channels excitement. *Nature*. 419:683-684.

Barde, Y.A., D. Edgar, and H. Thoenen. 1982. Purification of a new neurotrophic factor from mammalian brain. *EMBO J*. 1:549-553.

Bath, K.G., M.R. Akins, and F.S. Lee. 2012a. BDNF control of adult SVZ neurogenesis. *Developmental psychobiology*. 54:578-589.

Bath, K.G., D.Q. Jing, I. Dincheva, C.C. Neeb, S.S. Pattwell, M.V. Chao, F.S. Lee, and I. Ninan. 2012b. BDNF Val66Met impairs fluoxetine-induced enhancement of adult hippocampus plasticity. *Neuropsychopharmacology : official publication of the American College of Neuropsychopharmacology*. 37:1297-1304.

Benarroch, E.E. 2015. Brain-derived neurotrophic factor: Regulation, effects, and potential clinical relevance. *Neurology*. 84:1693-1704.

Bergami, M., G. Masserdotti, S.G. Temprana, E. Motori, T.M. Eriksson, J. Gobel, S.M. Yang, K.K. Conzelmann, A.F. Schinder, M. Gotz, and B. Berninger. 2015. A critical period for experience-dependent remodeling of adult-born neuron connectivity. *Neuron*. 85:710-717.

Bergami, M., S. Santi, E. Formaggio, C. Cagnoli, C. Verderio, R. Blum, B. Berninger, M. Matteoli, and M. Canossa. 2008. Uptake and recycling of pro-BDNF for transmitter-induced secretion by cortical astrocytes. *The Journal of cell biology*. 183:213-221.

Bischofberger, J., D. Engel, M. Frotscher, and P. Jonas. 2006a. Timing and efficacy of transmitter release at mossy fiber synapses in the hippocampal network. *Pflugers Archiv : European journal of physiology*. 453:361-372.

Bischofberger, J., D. Engel, L. Li, J.R. Geiger, and P. Jonas. 2006b. Patch-clamp recording from mossy fiber terminals in hippocampal slices. *Nature protocols*. 1:2075-2081.

Bliss, T.V., and G.L. Collingridge. 1993. A synaptic model of memory: long-term potentiation in the hippocampus. *Nature*. 361:31-39.

Bliss, T.V., and T. Lomo. 1973. Long-lasting potentiation of synaptic transmission in the dentate area of the anaesthetized rabbit following stimulation of the perforant path. *The Journal of physiology*. 232:331-356.

Blum, R., K.W. Kafitz, and A. Konnerth. 2002. Neurotrophin-evoked depolarization requires the sodium channel $Na_V1.9$. *Nature*. 419:687-693.

Blum, R., and A. Konnerth. 2005. Neurotrophin-mediated rapid signaling in the central nervous system: mechanisms and functions. *Physiology (Bethesda)*. 20:70-78.

Bock, D.D., W.C. Lee, A.M. Kerlin, M.L. Andermann, G. Hood, A.W. Wetzel, S. Yurgenson, E.R. Soucy, H.S. Kim, and R.C. Reid. 2011. Network anatomy and in vivo physiology of visual cortical neurons. *Nature*. 471:177-182.

Boutin, J.A. 1997. Myristoylation. *Cellular signalling*. 9:15-35.

Bramham, C.R., and E. Messaoudi. 2005. BDNF function in adult synaptic plasticity: the synaptic consolidation hypothesis. *Prog Neurobiol*. 76:99-125.

Brigadski, T., M. Hartmann, and V. Lessmann. 2005. Differential vesicular targeting and time course of synaptic secretion of the mammalian neurotrophins. *The Journal of neuroscience : the official journal of the Society for Neuroscience*. 25:7601-7614.

Broussard, G.J., Y. Liang, M. Fridman, E.K. Unger, G. Meng, X. Xiao, N. Ji, L. Petreanu, and L. Tian. 2018. In vivo measurement of afferent activity with axon-specific calcium imaging. *Nature neuroscience*. 21:1272-1280.

Buckmaster, P.S. 2012. Mossy Fiber Sprouting in the Dentate Gyrus. *In* Jasper's Basic Mechanisms of the Epilepsies. th, J.L. Noebels, M. Avoli, M.A. Rogawski, R.W. Olsen, and A.V. Delgado-Escueta, editors, Bethesda (MD).

Busche, M.A., M. Kekus, H. Adelsberger, T. Noda, H. Forstl, I. Nelken, and A. Konnerth. 2015. Rescue of long-range circuit dysfunction in Alzheimer's disease models. *Nature neuroscience*. 18:1623-1630.

Canossa, M., A. Gartner, G. Campana, N. Inagaki, and H. Thoenen. 2001. Regulated secretion of neurotrophins by metabotropic glutamate group I (mGluRI) and Trk receptor activation is mediated via phospholipase C signalling pathways. *The EMBO journal*. 20:1640-1650.

Caroni, P., F. Donato, and D. Muller. 2012. Structural plasticity upon learning: regulation and functions. *Nature reviews. Neuroscience*. 13:478-490.

Castren, E., and T. Rantamaki. 2010. The role of BDNF and its receptors in depression and antidepressant drug action: Reactivation of developmental plasticity. *Developmental neurobiology*. 70:289-297.

Chao, M.V. 2003. Neurotrophins and their receptors: a convergence point for many signalling pathways. *Nat Rev Neurosci*. 4:299-309.

Chen, F., M. Ardalan, B. Elfving, G. Wegener, T.M. Madsen, and J.R. Nyengaard. 2018. Mitochondria Are Critical for BDNF-Mediated Synaptic and Vascular Plasticity of Hippocampus following Repeated Electroconvulsive Seizures. *Int J Neuropsychopharmacol*. 21:291-304.

Chen, Z.Y., A. Ieraci, H. Teng, H. Dall, C.X. Meng, D.G. Herrera, A. Nykjaer, B.L. Hempstead, and F.S. Lee. 2005. Sortilin controls intracellular sorting of brain-derived neurotrophic factor to the regulated secretory pathway. *The Journal of neuroscience : the official journal of the Society for Neuroscience*. 25:6156-6166.

Chen, Z.Y., P.D. Patel, G. Sant, C.X. Meng, K.K. Teng, B.L. Hempstead, and F.S. Lee. 2004. Variant brain-derived neurotrophic factor (BDNF) (Met66) alters the intracellular trafficking and activity-dependent secretion of wild-type BDNF in neurosecretory cells and cortical neurons. *The Journal of neuroscience : the official journal of the Society for Neuroscience*. 24:4401-4411.

Cheng, A., J.T. Goncalves, P. Golshani, K. Arisaka, and C. Portera-Cailliau. 2011a. Simultaneous two-photon calcium imaging at different depths with spatiotemporal multiplexing. *Nat Methods*. 8:139-142.

Cheng, P.L., A.H. Song, Y.H. Wong, S. Wang, X. Zhang, and M.M. Poo. 2011b. Self-amplifying autocrine actions of BDNF in axon development. *Proceedings of the National Academy of Sciences of the United States of America*. 108:18430-18435.

Chiaruttini, C., M. Sonego, G. Baj, M. Simonato, and E. Tongiorgi. 2008. BDNF mRNA splice variants display activity-dependent targeting to distinct hippocampal laminae. *Mol Cell Neurosci*. 37:11-19.

Chicurel, M.E., and K.M. Harris. 1992. Three-dimensional analysis of the structure and composition of CA3 branched dendritic spines and their synaptic relationships with mossy fiber boutons in the rat hippocampus. *The Journal of comparative neurology*. 325:169-182.

Cohen, S., R. Levi-Montalcini, and V. Hamburger. 1954. A Nerve Growth-Stimulating Factor Isolated from Sarcom as 37 and 180. *Proceedings of the National Academy of Sciences of the United States of America*. 40:1014-1018.

Collingridge, G.L., and T.V. Bliss. 1995. Memories of NMDA receptors and LTP. *Trends in neurosciences*. 18:54-56.

Conner, J.M., J.C. Lauterborn, Q. Yan, C.M. Gall, and S. Varon. 1997. Distribution of brain-derived neurotrophic factor (BDNF) protein and mRNA in the normal adult rat CNS: evidence for anterograde axonal transport. *The Journal of neuroscience : the official journal of the Society for Neuroscience*. 17:2295-2313.

Danzer, S.C., and J.O. McNamara. 2004. Localization of brain-derived neurotrophic factor to distinct terminals of mossy fiber axons implies regulation of both excitation and feedforward inhibition of CA3 pyramidal cells. *The Journal of neuroscience : the official journal of the Society for Neuroscience*. 24:11346-11355.

De Paola, V., S. Arber, and P. Caroni. 2003. AMPA receptors regulate dynamic equilibrium of presynaptic terminals in mature hippocampal networks. *Nature neuroscience*. 6:491-500.

Dean, C., H. Liu, F.M. Dunning, P.Y. Chang, M.B. Jackson, and E.R. Chapman. 2009. Synaptotagmin-IV modulates synaptic function and long-term potentiation by regulating BDNF release. *Nature neuroscience*. 12:767-776.

Deneux, T., A. Kaszas, G. Szalay, G. Katona, T. Lakner, A. Grinvald, B. Rozsa, and I. Vanzetta. 2016. Accurate spike estimation from noisy calcium signals for ultrafast three-dimensional imaging of large neuronal populations in vivo. *Nat Commun*. 7:12190.

Deshpande, A., M. Bergami, A. Ghanem, K.K. Conzelmann, A. Lepier, M. Gotz, and B. Berninger. 2013. Retrograde monosynaptic tracing reveals the temporal evolution of inputs onto new neurons in the adult dentate gyrus and olfactory bulb. *Proceedings of the National Academy of Sciences of the United States of America*. 110:E1152-1161.

Deusser, J., S. Schmidt, B. Ettle, S. Plotz, S. Huber, C.P. Muller, E. Masliah, J. Winkler, and Z. Kohl. 2015. Serotonergic dysfunction in the A53T alpha-synuclein mouse model of Parkinson's disease. *J Neurochem*. 135:589-597.

Dieni, S., T. Matsumoto, M. Dekkers, S. Rauskolb, M.S. Ionescu, R. Deogracias, E.D. Gundelfinger, M. Kojima, S. Nestel, M. Frotscher, and Y.A. Barde. 2012. BDNF and its pro-peptide are stored in presynaptic dense core vesicles in brain neurons. *The Journal of cell biology*. 196:775-788.

Edelmann, E., E. Cepeda-Prado, M. Franck, P. Lichtenecker, T. Brigadski, and V. Lessmann. 2015. Theta Burst Firing Recruits BDNF Release and Signaling in Postsynaptic CA1 Neurons in Spike-Timing-Dependent LTP. *Neuron*. 86:1041-1054.

Edelmann, E., V. Lessmann, and T. Brigadski. 2014. Pre- and postsynaptic twists in BDNF secretion and action in synaptic plasticity. *Neuropharmacology*. 76 Pt C:610-627.

Egan, M.F., M. Kojima, J.H. Callicott, T.E. Goldberg, B.S. Kolachana, A. Bertolino, E. Zaitsev, B. Gold, D. Goldman, M. Dean, B. Lu, and D.R. Weinberger. 2003. The BDNF val66met polymorphism affects activity-dependent secretion of BDNF and human memory and hippocampal function. *Cell*. 112:257-269.

Fan, D., J. Li, B. Zheng, L. Hua, and Z. Zuo. 2016. Enriched Environment Attenuates Surgery-Induced Impairment of Learning, Memory, and Neurogenesis Possibly by Preserving BDNF Expression. *Molecular neurobiology*. 53:344-354.

Feng, L., Z. Puyang, H. Chen, P. Liang, J.B. Troy, and X. Liu. 2017. Overexpression of Brain-Derived Neurotrophic Factor Protects Large Retinal Ganglion Cells After Optic Nerve Crush in Mice. *eNeuro*. 4.

Figurov, A., L.D. Pozzo-Miller, P. Olafsson, T. Wang, and B. Lu. 1996. Regulation of synaptic responses to high-frequency stimulation and LTP by neurotrophins in the hippocampus. *Nature*. 381:706-709.

Franklin, K., and G. Paxinos. 2008. The Mouse Brain in Stereotaxic Coordinates. 256 pp.

Galimberti, I., N. Gogolla, S. Alberi, A.F. Santos, D. Muller, and P. Caroni. 2006. Long-term rearrangements of hippocampal mossy fiber terminal connectivity in the adult regulated by experience. *Neuron*. 50:749-763.

Gärtner, A., and V. Staiger. 2002. Neurotrophin secretion from hippocampal neurons evoked by long-term-potentiation-inducing electrical stimulation patterns. *Proceedings of the National Academy of Sciences of the United States of America*. 99:6386-6391.

Gogolla, N., I. Galimberti, and P. Caroni. 2007. Structural plasticity of axon terminals in the adult. *Current opinion in neurobiology*. 17:516-524.

Gomez-Palacio-Schjetnan, A., and M.L. Escobar. 2008. In vivo BDNF modulation of adult functional and morphological synaptic plasticity at hippocampal mossy fibers. *Neuroscience letters*. 445:62-67.

Gooney, M., E. Messaoudi, F.O. Maher, C.R. Bramham, and M.A. Lynch. 2004. BDNF-induced LTP in dentate gyrus is impaired with age: analysis of changes in cell signaling events. *Neurobiol Aging*. 25:1323-1331.

Grienberger, C., and A. Konnerth. 2012. Imaging calcium in neurons. *Neuron*. 73:862-885.

Hartmann, M., R. Heumann, and V. Lessmann. 2001. Synaptic secretion of BDNF after high-frequency stimulation of glutamatergic synapses. *EMBO J*. 20:5887-5897.

Harward, S.C., N.G. Hedrick, C.E. Hall, P. Parra-Bueno, T.A. Milner, E. Pan, T. Laviv, B.L. Hempstead, R. Yasuda, and J.O. McNamara. 2016. Autocrine BDNF-TrkB signalling within a single dendritic spine. *Nature*. 538:99-103.

Hashimotodani, Y., K. Nasrallah, K.R. Jensen, A.E. Chavez, D. Carrera, and P.E. Castillo. 2017. LTP at Hilar Mossy Cell-Dentate Granule Cell Synapses Modulates Dentate Gyrus Output by Increasing Excitation/Inhibition Balance. *Neuron*. 95:928-943 e923.

Hedrick, N.G., S.C. Harward, C.E. Hall, H. Murakoshi, J.O. McNamara, and R. Yasuda. 2016. Rho GTPase complementation underlies BDNF-dependent homo- and heterosynaptic plasticity. *Nature*. 538:104-108.

Hempstead, B.L. 2015. Brain-Derived Neurotrophic Factor: Three Ligands, Many Actions. *Trans Am Clin Climatol Assoc*. 126:9-19.

Horch, H.W., and L.C. Katz. 2002. BDNF release from single cells elicits local dendritic growth in nearby neurons. *Nat Neurosci*. 5:1177-1184.

Horch, H.W., A. Kruttgen, S.D. Portbury, and L.C. Katz. 1999. Destabilization of cortical dendrites and spines by BDNF. *Neuron*. 23:353-364.

Huang, E.J., and L.F. Reichardt. 2003. Trk receptors: roles in neuronal signal transduction. *Annual review of biochemistry*. 72:609-642.

Huang, Y.Z., E. Pan, Z.Q. Xiong, and J.O. McNamara. 2008. Zinc-mediated transactivation of TrkB potentiates the hippocampal mossy fiber-CA3 pyramid synapse. *Neuron*. 57:546-558.

Isgor, C., C. Pare, B. McDole, P. Coombs, and K. Guthrie. 2015. Expansion of the dentate mossy fiber-CA3 projection in the brain-derived neurotrophic factor-enriched mouse hippocampus. *Neuroscience*. 288:10-23.

Ito, Y., S. Wiese, N. Funk, A. Chittka, W. Rossoll, H. Bommel, K. Watabe, M. Wegner, and M. Sendtner. 2006. Sox10 regulates ciliary neurotrophic factor gene expression in Schwann cells. *Proceedings of the National Academy of Sciences of the United States of America*. 103:7871-7876.

Jha, S., B.E. Dong, Y. Xue, D.F. Delotterie, M.G. Vail, and K. Sakata. 2016. Antidepressive and BDNF effects of enriched environment treatment across ages in mice lacking BDNF expression through promoter IV. *Translational psychiatry*. 6:e896.

Ji, J., and S. Maren. 2005. Electrolytic lesions of the dorsal hippocampus disrupt renewal of conditional fear after extinction. *Learn Mem*. 12:270-276.

Kabouridis, P.S., A.I. Magee, and S.C. Ley. 1997. S-acylation of LCK protein tyrosine kinase is essential for its signalling function in T lymphocytes. *EMBO J*. 16:4983-4998.

Kafitz, K.W., A. Lepier, H. Thoenen, and A. Konnerth. 2001. Saxitoxin-sensitivity of neurotrophin-induced rapid excitation and neurite growth. *Pflugers Archiv : European journal of physiology*. 441 Supplement:R125, O122-122.

Kempermann, G., H.G. Kuhn, and F.H. Gage. 1997. More hippocampal neurons in adult mice living in an enriched environment. *Nature*. 386:493-495.

Kjelstrup, K.G., F.A. Tuvnes, H.A. Steffenach, R. Murison, E.I. Moser, and M.B. Moser. 2002. Reduced fear expression after lesions of the ventral hippocampus. *Proceedings of the National Academy of Sciences of the United States of America*. 99:10825-10830.

Kohara, K., A. Kitamura, M. Morishima, and T. Tsumoto. 2001. Activity-dependent transfer of brain-derived neurotrophic factor to postsynaptic neurons. *Science*. 291:2419-2423.

Kolarow, R., T. Brigadski, and V. Lessmann. 2007. Postsynaptic secretion of BDNF and NT-3 from hippocampal neurons depends on calcium calmodulin kinase II signaling and proceeds via delayed fusion pore opening. *The Journal of neuroscience : the official journal of the Society for Neuroscience*. 27:10350-10364.

Kolbeck, R., I. Bartke, W. Eberle, and Y.A. Barde. 1999. Brain-derived neurotrophic factor levels in the nervous system of wild-type and neurotrophin gene mutant mice. *J Neurochem*. 72:1930-1938.

Korte, M., P. Carroll, E. Wolf, G. Brem, H. Thoenen, and T. Bonhoeffer. 1995. Hippocampal long-term potentiation is impaired in mice lacking brain-derived neurotrophic factor. *Proceedings of the National Academy of Sciences of the United States of America*. 92:8856-8860.

Kosaka, T., H. Katsumaru, K. Hama, J.Y. Wu, and C.W. Heizmann. 1987. GABAergic neurons containing the Ca2+-binding protein parvalbumin in the rat hippocampus and dentate gyrus. *Brain Res*. 419:119-130.

Kovalchuk, Y., E. Hanse, K.W. Kafitz, and A. Konnerth. 2002. Postsynaptic Induction of BDNF-Mediated Long-Term Potentiation. *Science*. 295:1729-1734.

Kowianski, P., G. Lietzau, E. Czuba, M. Waskow, A. Steliga, and J. Morys. 2018. BDNF: A Key Factor with Multipotent Impact on Brain Signaling and Synaptic Plasticity. *Cell Mol Neurobiol*. 38:579-593.

Kramar, E.A., L.Y. Chen, J.C. Lauterborn, D.A. Simmons, C.M. Gall, and G. Lynch. 2012. BDNF upregulation rescues synaptic plasticity in middle-aged ovariectomized rats. *Neurobiol Aging*. 33:708-719.

Lang, S.B., V. Stein, T. Bonhoeffer, and C. Lohmann. 2007. Endogenous brain-derived neurotrophic factor triggers fast calcium transients at synapses in developing dendrites. *The Journal of neuroscience : the official journal of the Society for Neuroscience*. 27:1097-1105.

Leal, G., C.R. Bramham, and C.B. Duarte. 2017. BDNF and Hippocampal Synaptic Plasticity. *Vitam Horm*. 104:153-195.

Lebow, M.A., and A. Chen. 2016. Overshadowed by the amygdala: the bed nucleus of the stria terminalis emerges as key to psychiatric disorders. *Mol Psychiatry*. 21:450-463.

Lee, R., P. Kermani, K.K. Teng, and B.L. Hempstead. 2001. Regulation of cell survival by secreted proneurotrophins. *Science*. 294:1945-1948.

Leibrock, J., F. Lottspeich, A. Hohn, M. Hofer, B. Hengerer, P. Masiakowski, H. Thoenen, and Y.A. Barde. 1989. Molecular cloning and expression of brain-derived neurotrophic factor. *Nature*. 341:149-152.

Leschik, J., R. Eckenstaler, T. Endres, T. Munsch, E. Edelmann, K. Richter, O. Kobler, K.D. Fischer, W. Zuschratter, T. Brigadski, B. Lutz, and V. Lessmann. 2019. Prominent Postsynaptic and Dendritic Exocytosis of Endogenous BDNF Vesicles in BDNF-GFP Knock-in Mice. *Molecular neurobiology*.

Lessmann, V., and T. Brigadski. 2009. Mechanisms, locations, and kinetics of synaptic BDNF secretion: an update. *Neurosci Res*. 65:11-22.

Levi-Montalcini, R. 1987. The nerve growth factor 35 years later. *Science*. 237:1154-1162.

Levi-Montalcini, R., H. Meyer, and V. Hamburger. 1954. In vitro experiments on the effects of mouse sarcomas 180 and 37 on the spinal and sympathetic ganglia of the chick embryo. *Cancer research*. 14:49-57.

Lewin, G.R., and Y.A. Barde. 1996. Physiology of the neurotrophins. *Annu Rev Neurosci*. 19:289-317.

Li, Y., D. Yui, B.W. Luikart, R.M. McKay, J.L. Rubenstein, and L.F. Parada. 2012. Conditional ablation of brain-derived neurotrophic factor-TrkB signaling impairs striatal neuron development. *Proceedings of the National Academy of Sciences of the United States of America*. 109:15491-15496.

Lisman, J., K. Cooper, M. Sehgal, and A.J. Silva. 2018. Memory formation depends on both synapse-specific modifications of synaptic strength and cell-specific increases in excitability. *Nature neuroscience*. 21:309-314.

Lohof, A.M., N.Y. Ip, and M.M. Poo. 1993. Potentiation of developing neuromuscular synapses by the neurotrophins NT-3 and BDNF. *Nature*. 363:350-353.

Lu, B., G. Nagappan, X. Guan, P.J. Nathan, and P. Wren. 2013. BDNF-based synaptic repair as a disease-modifying strategy for neurodegenerative diseases. *Nat Rev Neurosci*. 14:401-416.

Lu, H., H. Park, and M.M. Poo. 2014. Spike-timing-dependent BDNF secretion and synaptic plasticity. *Philos Trans R Soc Lond B Biol Sci*. 369:20130132.

Martin, E.A., D. Woodruff, R.L. Rawson, and M.E. Williams. 2017. Examining Hippocampal Mossy Fiber Synapses by 3D Electron Microscopy in Wildtype and Kirrel3 Knockout Mice. *eNeuro*. 4.

Martinowich, K., H. Manji, and B. Lu. 2007. New insights into BDNF function in depression and anxiety. *Nature neuroscience*. 10:1089-1093.

Matsuda, N., H. Lu, Y. Fukata, J. Noritake, H. Gao, S. Mukherjee, T. Nemoto, M. Fukata, and M.M. Poo. 2009. Differential activity-dependent secretion of brain-derived neurotrophic factor from axon and dendrite. *The Journal of neuroscience : the official journal of the Society for Neuroscience*. 29:14185-14198.

Matsumoto, T., S. Rauskolb, M. Polack, J. Klose, R. Kolbeck, M. Korte, and Y.A. Barde. 2008. Biosynthesis and processing of endogenous BDNF: CNS neurons store and secrete BDNF, not pro-BDNF. *Nature neuroscience*. 11:131-133.

Matsuzaki, M., G.C. Ellis-Davies, Y. Kanemoto, and H. Kasai. 2011. Simultaneous two-photon activation of presynaptic cells and calcium imaging in postsynaptic dendritic spines. *Neural Syst Circuits*. 1:2.

Maynard, K.R., J.W. Hobbs, M. Sukumar, A.S. Kardian, D.V. Jimenez, R.J. Schloesser, and K. Martinowich. 2017. Bdnf mRNA splice variants differentially impact CA1 and CA3 dendrite complexity and spine morphology in the hippocampus. *Brain Struct Funct*.

Meneghetti, E. 2010/11. Role of Ciliary Neurotrophic Factor (CNTF) in the development of the hippocampal network. *In* Facoltà di Scienze MM.FF.NN. Università delgi Studi di Padova, Padova, Italy.

Michaelsen, K., M. Zagrebelsky, J. Berndt-Huch, M. Polack, A. Buschler, M. Sendtner, and M. Korte. 2010. Neurotrophin receptors TrkB.T1 and p75NTR cooperate in modulating both functional and structural plasticity in mature hippocampal neurons. *Eur J Neurosci*. 32:1854-1865.

Middlemas, D.S., R.A. Lindberg, and T. Hunter. 1991. trkB, a neural receptor protein-tyrosine kinase: evidence for a full-length and two truncated receptors. *Molecular and cellular biology*. 11:143-153.

Morris, R.G., P. Garrud, J.N. Rawlins, and J. O'Keefe. 1982. Place navigation impaired in rats with hippocampal lesions. *Nature*. 297:681-683.

Mukamel, E.A., A. Nimmerjahn, and M.J. Schnitzer. 2009. Automated analysis of cellular signals from large-scale calcium imaging data. *Neuron*. 63:747-760.

Nakamura, T., M.C. Colbert, and J. Robbins. 2006. Neural crest cells retain multipotential characteristics in the developing valves and label the cardiac conduction system. *Circulation research*. 98:1547-1554.

Nicoll, R.A., and R.C. Malenka. 1995. Contrasting properties of two forms of long-term potentiation in the hippocampus. *Nature*. 377:115-118.

Nicoll, R.A., and D. Schmitz. 2005. Synaptic plasticity at hippocampal mossy fibre synapses. *Nat Rev Neurosci*. 6:863-876.

Novkovic, T., T. Mittmann, and D. Manahan-Vaughan. 2015. BDNF contributes to the facilitation of hippocampal synaptic plasticity and learning enabled by environmental enrichment. *Hippocampus*. 25:1-15.

O'Keefe, J. 1976. Place units in the hippocampus of the freely moving rat. *Exp Neurol*. 51:78-109.

Obernier, K., A. Cebrian-Silla, M. Thomson, J.I. Parraguez, R. Anderson, C. Guinto, J. Rodas Rodriguez, J.M. Garcia-Verdugo, and A. Alvarez-Buylla. 2018. Adult Neurogenesis Is Sustained by Symmetric Self-Renewal and Differentiation. *Cell Stem Cell*. 22:221-234 e228.

Pang, P.T., H.K. Teng, E. Zaitsev, N.T. Woo, K. Sakata, S. Zhen, K.K. Teng, W.H. Yung, B.L. Hempstead, and B. Lu. 2004. Cleavage of proBDNF by tPA/plasmin is essential for long-term hippocampal plasticity. *Science*. 306:487-491.

Park, H., and M.M. Poo. 2012. Neurotrophin regulation of neural circuit development and function. *Nat Rev Neurosci*. 14:7-23.

Park, H., and M.M. Poo. 2013. Neurotrophin regulation of neural circuit development and function. *Nat Rev Neurosci*. 14:7-23.

Patapoutian, A., and L.F. Reichardt. 2001. Trk receptors: mediators of neurotrophin action. *Current opinion in neurobiology*. 11:272-280.

Patel, T.P., K. Man, B.L. Firestein, and D.F. Meaney. 2015. Automated quantification of neuronal networks and single-cell calcium dynamics using calcium imaging. *J Neurosci Methods*. 243:26-38.

Patterson, S.L., T. Abel, T.A. Deuel, K.C. Martin, J.C. Rose, and E.R. Kandel. 1996. Recombinant BDNF rescues deficits in basal synaptic transmission and hippocampal LTP in BDNF knockout mice. *Neuron*. 16:1137-1145.

Pattwell, S.S., K.G. Bath, R. Perez-Castro, F.S. Lee, M.V. Chao, and I. Ninan. 2012. The BDNF Val66Met polymorphism impairs synaptic transmission and plasticity in the infralimbic medial prefrontal cortex. *The Journal of neuroscience : the official journal of the Society for Neuroscience*. 32:2410-2421.

Penn, A.C., C.L. Zhang, F. Georges, L. Royer, C. Breillat, E. Hosy, J.D. Petersen, Y. Humeau, and D. Choquet. 2017. Hippocampal LTP and contextual learning require surface diffusion of AMPA receptors. *Nature*. 549:384-388.

Petoukhov, E., S. Fernando, F. Mills, F. Shivji, D. Hunter, C. Krieger, M.A. Silverman, and S.X. Bamji. 2013. Activity-dependent secretion of progranulin from synapses. *J Cell Sci*. 126:5412-5421.

Pnevmatikakis, E.A., D. Soudry, Y. Gao, T.A. Machado, J. Merel, D. Pfau, T. Reardon, Y. Mu, C. Lacefield, W. Yang, M. Ahrens, R. Bruno, T.M. Jessell, D.S. Peterka, R. Yuste, and L. Paninski. 2016. Simultaneous Denoising, Deconvolution, and Demixing of Calcium Imaging Data. *Neuron*. 89:285-299.

Prada, J., M. Sasi, C. Martin, S. Jablonka, T. Dandekar, and R. Blum. 2018. An open source tool for automatic spatiotemporal assessment of calcium transients and local 'signal-close-to-noise' activity in calcium imaging data. *PLoS Comput Biol*. 14:e1006054.

Pruunsild, P., A. Kazantseva, T. Aid, K. Palm, and T. Timmusk. 2007. Dissecting the human BDNF locus: bidirectional transcription, complex splicing, and multiple promoters. *Genomics*. 90:397-406.

Quesseveur, G., D.J. David, M.C. Gaillard, P. Pla, M.V. Wu, H.T. Nguyen, V. Nicolas, G. Auregan, I. David, A. Dranovsky, P. Hantraye, R. Hen, A.M. Gardier, N. Deglon, and B.P. Guiard. 2013. BDNF overexpression in mouse hippocampal astrocytes promotes local neurogenesis and elicits anxiolytic-like activities. *Translational psychiatry*. 3:e253.

Rathod, R., S. Havlicek, N. Frank, R. Blum, and M. Sendtner. 2012. Laminin induced local axonal translation of beta-actin mRNA is impaired in SMN-deficient motoneurons. *Histochem Cell Biol*. 138:737-748.

Rauskolb, S., M. Zagrebelsky, A. Dreznjak, R. Deogracias, T. Matsumoto, S. Wiese, B. Erne, M. Sendtner, N. Schaeren-Wiemers, M. Korte, and Y.A. Barde. 2010. Global deprivation of brain-derived neurotrophic factor in the CNS reveals an area-specific requirement for dendritic growth. *The Journal of neuroscience : the official journal of the Society for Neuroscience*. 30:1739-1749.

Resh, M.D. 1999. Fatty acylation of proteins: new insights into membrane targeting of myristoylated and palmitoylated proteins. *Biochimica et biophysica acta*. 1451:1-16.

Rochefort, N.L., M. Narushima, C. Grienberger, N. Marandi, D.N. Hill, and A. Konnerth. 2011. Development of direction selectivity in mouse cortical neurons. *Neuron*. 71:425-432.

Rohrer, B., J.I. Korenbrot, M.M. LaVail, L.F. Reichardt, and B. Xu. 1999. Role of neurotrophin receptor TrkB in the maturation of rod photoreceptors and establishment of synaptic transmission to the inner retina. *The Journal of neuroscience : the official journal of the Society for Neuroscience*. 19:8919-8930.

Rose, C.R., R. Blum, B. Pichler, A. Lepier, K.W. Kafitz, and A. Konnerth. 2003. Truncated TrkB-T1 mediates neurotrophin-evoked calcium signalling in glia cells. *Nature*. 426:74-78.

Ruediger, S., C. Vittori, E. Bednarek, C. Genoud, P. Strata, B. Sacchetti, and P. Caroni. 2011. Learning-related feedforward inhibitory connectivity growth required for memory precision. *Nature*. 473:514-518.

Rutherford, L.C., S.B. Nelson, and G.G. Turrigiano. 1998. BDNF has opposite effects on the quantal amplitude of pyramidal neuron and interneuron excitatory synapses. *Neuron*. 21:521-530.

Sahay, A., and R. Hen. 2007. Adult hippocampal neurogenesis in depression. *Nature neuroscience*. 10:1110-1115.

Samtleben, S., J. Jaepel, C. Fecher, T. Andreska, M. Rehberg, and R. Blum. 2013. Direct imaging of ER calcium with targeted-esterase induced dye loading (TED). *J Vis Exp*:e50317.

Samtleben, S., B. Wachter, and R. Blum. 2015. Store-operated calcium entry compensates fast ER calcium loss in resting hippocampal neurons. *Cell Calcium*. 58:147-159.

Santi, S., S. Cappello, M. Riccio, M. Bergami, G. Aicardi, U. Schenk, M. Matteoli, and M. Canossa. 2006. Hippocampal neurons recycle BDNF for activity-dependent secretion and LTP maintenance. *EMBO J*. 25:4372-4380.

Sasi, M. 2014. Conditional removal of BDNF from mature granule neurons of the hippocampal dentate gyrus. *In* Institute for Clinical Neurobiolgy. Vol. MSc FOKUS Life Sciences. Julius-Maximilians Universität Würzburg, Würzburg.

Sasi, M., B. Vignoli, M. Canossa, and R. Blum. 2017. Neurobiology of local and intercellular BDNF signaling. *Pflugers Arch*. 469:593-610.

Scharfman, H.E., J.H. Goodman, and A.L. Sollas. 1999. Actions of brain-derived neurotrophic factor in slices from rats with spontaneous seizures and mossy fiber sprouting in the dentate gyrus. *The Journal of neuroscience : the official journal of the Society for Neuroscience*. 19:5619-5631.

Schjetnan, A.G., and M.L. Escobar. 2012. In vivo BDNF modulation of hippocampal mossy fiber plasticity induced by high frequency stimulation. *Hippocampus*. 22:1-8.

Schnutgen, F., N. Doerflinger, C. Calleja, O. Wendling, P. Chambon, and N.B. Ghyselinck. 2003. A directional strategy for monitoring Cre-mediated recombination at the cellular level in the mouse. *Nat Biotechnol*. 21:562-565.

Scoville, W.B., and B. Milner. 1957. Loss of recent memory after bilateral hippocampal lesions. *Journal of neurology, neurosurgery, and psychiatry*. 20:11-21.

Seidenbecher, T., T.R. Laxmi, O. Stork, and H.C. Pape. 2003. Amygdalar and hippocampal theta rhythm synchronization during fear memory retrieval. *Science*. 301:846-850.

Sendtner, M., B. Holtmann, R. Kolbeck, H. Thoenen, and Y.A. Barde. 1992. Brain-derived neurotrophic factor prevents the death of motoneurons in newborn rats after nerve section. *Nature*. 360:757-759.

Shimojo, M., J. Courchet, S. Pieraut, N. Torabi-Rander, R. Sando, 3rd, F. Polleux, and A. Maximov. 2015. SNAREs Controlling Vesicular Release of BDNF and Development of Callosal Axons. *Cell Rep*. 11:1054-1066.

Song, M., K. Martinowich, and F.S. Lee. 2017. BDNF at the synapse: why location matters. *Molecular psychiatry*. 22:1370-1375.

Tanaka, J., Y. Horiike, M. Matsuzaki, T. Miyazaki, G.C. Ellis-Davies, and H. Kasai. 2008. Protein synthesis and neurotrophin-dependent structural plasticity of single dendritic spines. *Science*. 319:1683-1687.

Teng, E., and L.R. Squire. 1999. Memory for places learned long ago is intact after hippocampal damage. *Nature*. 400:675-677.

Thoenen, H. 1995. Neurotrophins and neuronal plasticity. *Science*. 270:593-598.

Tongiorgi, E. 2008. Activity-dependent expression of brain-derived neurotrophic factor in dendrites: facts and open questions. *Neuroscience research*. 61:335-346.

Tongiorgi, E., M. Righi, and A. Cattaneo. 1997. Activity-dependent dendritic targeting of BDNF and TrkB mRNAs in hippocampal neurons. *The Journal of neuroscience : the official journal of the Society for Neuroscience*. 17:9492-9505.

Toni, N., D.A. Laplagne, C. Zhao, G. Lombardi, C.E. Ribak, F.H. Gage, and A.F. Schinder. 2008. Neurons born in the adult dentate gyrus form functional synapses with target cells. *Nature neuroscience*. 11:901-907.

Tovote, P., M.S. Esposito, P. Botta, F. Chaudun, J.P. Fadok, M. Markovic, S.B. Wolff, C. Ramakrishnan, L. Fenno, K. Deisseroth, C. Herry, S. Arber, and A. Luthi. 2016. Midbrain circuits for defensive behaviour. *Nature*. 534:206-212.

Tovote, P., J.P. Fadok, and A. Luthi. 2015. Neuronal circuits for fear and anxiety. *Nat Rev Neurosci*. 16:317-331.

Turrigiano, G.G., K.R. Leslie, N.S. Desai, L.C. Rutherford, and S.B. Nelson. 1998. Activity-dependent scaling of quantal amplitude in neocortical neurons. *Nature*. 391:892-896.

Vaynman, S., Z. Ying, and F. Gomez-Pinilla. 2004. Hippocampal BDNF mediates the efficacy of exercise on synaptic plasticity and cognition. *The European journal of neuroscience*. 20:2580-2590.

Vivar, C., M.C. Potter, J. Choi, J.Y. Lee, T.P. Stringer, E.M. Callaway, F.H. Gage, H. Suh, and H. van Praag. 2012. Monosynaptic inputs to new neurons in the dentate gyrus. *Nat Commun*. 3:1107.

Wang, L., X. Chang, L. She, D. Xu, W. Huang, and M.M. Poo. 2015. Autocrine action of BDNF on dendrite development of adult-born hippocampal neurons. *The Journal of neuroscience : the official journal of the Society for Neuroscience*. 35:8384-8393.

Wang, X.M., W. Pan, N. Xu, Z.Q. Zhou, G.F. Zhang, and J.C. Shen. 2018. Environmental enrichment improves long-term memory impairment and aberrant synaptic plasticity by BDNF/TrkB signaling in nerve-injured mice. *Neuroscience letters*. 694:93-98.

Wiera, G., and J.W. Mozrzymas. 2015. Extracellular proteolysis in structural and functional plasticity of mossy fiber synapses in hippocampus. *Front Cell Neurosci*. 9:427.

Will, T.J., G. Tushev, L. Kochen, B. Nassim-Assir, I.J. Cajigas, S. Tom Dieck, and E.M. Schuman. 2013. Deep sequencing and high-resolution imaging reveal compartment-specific localization of Bdnf mRNA in hippocampal neurons. *Sci Signal*. 6:rs16.

Winnubst, J., and C. Lohmann. 2017. Mapping Synaptic Inputs of Developing Neurons Using Calcium Imaging. *Methods Mol Biol*. 1538:341-352.

Yan, Q., R.D. Rosenfeld, C.R. Matheson, N. Hawkins, O.T. Lopez, L. Bennett, and A.A. Welcher. 1997. Expression of brain-derived neurotrophic factor protein in the adult rat central nervous system. *Neuroscience*. 78:431-448.

Yang, J., L.C. Harte-Hargrove, C.J. Siao, T. Marinic, R. Clarke, Q. Ma, D. Jing, J.J. Lafrancois, K.G. Bath, W. Mark, D. Ballon, F.S. Lee, H.E. Scharfman, and B.L. Hempstead. 2014. proBDNF negatively regulates neuronal remodeling, synaptic transmission, and synaptic plasticity in hippocampus. *Cell Rep*. 7:796-806.

Yang, J., C.J. Siao, G. Nagappan, T. Marinic, D. Jing, K. McGrath, Z.Y. Chen, W. Mark, L. Tessarollo, F.S. Lee, B. Lu, and B.L. Hempstead. 2009. Neuronal release of proBDNF. *Nat Neurosci*. 12:113-115.

Yeh, C.M., C.C. Huang, and K.S. Hsu. 2012. Prenatal stress alters hippocampal synaptic plasticity in young rat offspring through preventing the proteolytic conversion of pro-brain-derived neurotrophic factor (BDNF) to mature BDNF. *The Journal of physiology*. 590:991-1010.

Zagrebelsky, M., and M. Korte. 2014. Form follows function: BDNF and its involvement in sculpting the function and structure of synapses. *Neuropharmacology*. 76 Pt C:628-638.

V. ACKNOWLEDGEMENT:

First and foremost, I would like to give my sincere gratitude to Robert for being my mentor and supervisor for the last 5 years. I thank him for his guidance, teaching and encouragement throughout my doctoral work. And as well sharing his valuable thoughts and insights in guiding my career. I would like to acknowledge my thesis committee members Prof. Dr. Michael Sendtner, Prof. Dr. Chichung Lie and PD Dr. Angelika Schmitt for their valued input and advice for my project and for taking time out of their busy schedule to take part in my committee meetings. I would like to express my sincere acknowledgement to my collaborators, Dr. Juan Prada and Prof. Thomas Dandekar from Biozentrum, Universität Würzburg for their work in the calcium imaging NA3 tool paper and Dr. Thomas Seidenbecher, Universität Münster for his help in our SFB project. I am thankfully to Nina Scheffler and Prof. Dr. Philip Tovote for helping us with the in vivo injection of animals. And I would like to give my appreciation to Dr. Britta Wachter, for her supervision and training during my master work in all the techniques, experiments and for directing me to work with utmost diligence and precaution, which helped me in great deal during my PhD work.

I am highly grateful to Michi, for all her help with the animal injections, genotyping the animals and training me in the lab and for being one of the greatest colleagues ever. I would miss you a great deal, especially being your 'Little Chick'. And thank you Dennis, first for helping me with all the animal work and second for being a great colleague for all us. I would like to give my gratitude to all my past and present students and colleagues at the Institute for all their help during my work here. Also, thanks to Hilde for helping with the viral packages and the animal facility for all the animal breeding and maintenance.

I would like to thank my family and my friends for being a constant support and lifeline for me. I could not have done this and be here without you all.